

The cover features three large, overlapping blue circles in shades of light blue, medium blue, and dark blue. A thin blue line runs diagonally from the top left towards the bottom right, passing through the circles.

PHYSICO-CHEMICAL BEHAVIOUR OF IRRADIATED POLYIMIDE THIN FILMS

This Thesis Submitted in Fulfillment of The Requirements
For The Award of a Masters Degree (Applied Chemistry)

NURRA ALI KHELIL
Bachelor of Applied Science (Applied Chemistry) Honors (2002)

School of Applied Sciences
(Field of Study Nanotechnology)
RMIT University
August 2012

Declaration

I certify that except where due acknowledgement has been made, the work is that of the author alone; the work has not been submitted previously, in whole or in part, to qualify for any other academic award; the content of the thesis is the result of work which has been carried out since the official commencement date of the approved research program; and, any editorial work, paid or unpaid, carried out by a third party is acknowledged and guidelines have been followed.

Nurra Ali Khelil

28th of August 2012

Acknowledgements

My deepest gratitude goes to my supervisor, Dr. Julie Niere for the support and encouragement she has demonstrated especially throughout the later sections of my project. I also wish to acknowledge the encouragement offered by Professor David Mainwaring and his ongoing support and enthusiasm for the project. It has also been a privilege to work with my second supervisor, Dr. Pandiyan Murugaraj, his charitable willingness and enthusiasm to share his insightful knowledge of the subject area on many aspects of my project has benefited me immensely. My deepest gratitude to Associate Professor Colin Rix, for helping with the written part of this project. This research project was funded by the CRC for Microtechnology, Australia, to which I am immensely grateful for their trust in my capabilities and the great opportunity that I had to do fine science research with practical applications. I am also very grateful for the excellent technical support that was provided by the Departments of Applied Chemistry, Applied Physics and Engineering, RMIT University. I also wish to acknowledge the support and companionship of my research colleagues at RMIT University.

Last, but by no means least, I would like to thank my family for their support and encouragement and express my love for my beautiful baby daughter, for her noise, smile and endless patience with mummy.

Abstract

The effect of Cu^{3+} ion-beam irradiation on the microstructure of two polyimide (PI) films (PMDA-ODA, Kapton[®] and BTDA-ODA) was examined using ATR-FTIR and XPS spectroscopy. There were a number of significant changes in the FTIR spectra of the irradiated PI films which indicated the breakdown of the backbone linkages of the polymer, via cleavage of the nitrogen of the imide and elimination of hydrogen from the PI molecular structure, leading to the formation of crystallites containing graphite-like fused rings. These results were corroborated by XPS spectroscopy, where the development of carbon-rich regions with graphite-like properties were clearly identified.

The results also indicated modifications to the molecular structure of both films, with the major reaction arising from chain scission and the formation of an extended ring structure, similar to graphite. It was concluded that the ion-beam etched nanochannels in the polymer, and that they were lined with graphite-like aromatic fused rings, which formed along the full depth of the ion-beam, which corresponded to about 10% surface penetration.

ATR-FTIR spectroscopy was also used to examine the temperature dependent changes in the films after irradiation. Drying at 80 °C led to a reduction in the intensity of the water stretching band by approximately 90 to 95%. At higher "annealing" temperatures, 180 °C -280 °C, the water band was eliminated. The experimental results demonstrated the superior thermal resistance of PMDA-ODA films for high temperature applications, in preference to BTDA-ODA films.

The electrical conductivity of the irradiated PMDA-ODA films was found to increase as a function of increasing exposure to the ion-beam (fluence). A study of the temperature dependent electrical conductivity characteristics of the PMDA-ODA films, revealed that they behaved as typical semiconductor films. Thus, the theoretical treatment of the temperature dependence of the electrical conductivity of the irradiated PMDA-ODA films was based on a standard semiconductor relationship, which enabled calculation of the temperature exponent. The excellent linearity of this relationship suggests that while there were other mechanisms available for charge movement to occur through fluctuation-induced tunnelling, the dominant mechanism of direct current conduction in the irradiated PI films occurs via three dimensional thermally activated electron hopping from one site to the next. The resistance of the irradiated films was found to be inversely proportional to temperature, confirming their semiconducting behaviour with calculated thermally sensitive activation barriers in the range 0.4–2.3 eV.

In the present work it was found that Cu^{3+} ion-beam irradiation was directly responsible for the disruption of the main chain imidic groups in the polymer, and this affected the tensile strength of the PI films, as evidenced by changes in Young's Modulus, and they became slightly brittle at the highest levels of irradiation fluence. Thus, the degradation of PI films subjected to ion-beam irradiation consists of both chemical and physical modifications to the films. Hence, PI films, although appropriate for applications in lightweight, flexible structures, are subject to ion-beam degradation of their mechanical properties which will limit their applications.

The electromechanical properties of PMDA-ODA irradiated films were found to be consistent with those of semiconducting strain gauges. The "gauge factor" (GF) of a strain gauge indicates its strain sensitivity, which arises from changes in specific resistivity (or conductivity) of a material due to an applied strain. The PMDA-ODA irradiated films possessed GF values much higher than those of conventional composites and

an order of magnitude higher than any previously reported. Thus, the irradiated PI films are suitable as sensitive strain gauges with applications as strain sensors, provided they are protected from intense radiation sources.

Publications

1. Pandiyan Murugaraj, David Mainwaring, Nurra Ali Khelil, Ju Lin Peng, Rainer Siegele, Prashant Sawant. *The improved electromechanical sensitivity of polymer thin films containing carbon clusters produced in situ by irradiation with metal ions*. Carbon. 2010, 48 p:4230–4237.
2. Pandiyan Murugaraj, David Edward Mainwaring, Timur Jakubov, Nelson Eduardo Mora-Huertas, Nurra Ali Khelil, Rainer Siegele. *Electron transport in semiconducting nanoparticle and nanocluster carbon–polymer composites* Solid State Communications. 2006,137 p:422–426.
3. Pandiyan Murugaraja, David Mainwaring, Nurra Ali Khelil, Rainer Siegele, Lin Peng and Prashant Sawant. *On the High Electromechanical Sensitivity in Ion Beam Irradiated Polymer Thin Films*. 16th AINSE Conference on Nuclear and Complementary Techniques of Analysis (NCTA 2009), at Lucas Heights, Sydney25 - 27 November 2009.

TABLE OF CONTENTS

Declaration.....	I
Acknowledgements.....	II
Abstract.....	III
Publications.....	VI
Table of Contents.....	VI
List of Figures.....	XI
List of Tables.....	XVI
List of Equations.....	XVII

1 Introduction and Literature Review

1.1 Introduction.....	1
1.1.1 Rationale of Research Project.....	2
1.1.2 Objective.....	4
Background and Theory.....	5
1.1.3 Polyimide.....	5
1.1.4 Polyimide Composite.....	5
1.2 The Effects of Ion Beam Irradiation.....	7
1.2.1 Surface Morphology of Irradiated Polymeric Material.....	7
1.2.2 Attenuated Total Reflectance Fourier Transform Infrared Spectroscopy (ATR-FTIR).....	8
1.3 Electrical properties.....	10
1.3.1 Hopping and Tunnelling Conduction Processes.....	11
1.3.2 Temperature Dependent Electrical Conductivity.....	13
1.3.3 Electrical Conductivity of Polyimides.....	14
1.3.4 Electrical Conductivity of Irradiated Polyimides.....	15
1.4 Mechanical and Electromechanical Properties.....	17

1.4.1 Mechanical Properties of Irradiated Polymers.....	20
1.5 Summary of Chapter Topics.....	21
1.6.References.....	23
2 Materials and Methods	
2.1 Introduction.....	32
2.2 Materials.....	33
2.2.1 BTDA-ODA PI Thin Film Fabrication Process.....	35
2.2.2 Film Casting.....	37
2.2.3 Irradiation.....	38
2.3 Characterisation Techniques.....	43
2.3.1 Thermogravimetric Analysis.....	43
2.3.2 Thermal Stability Properties.....	44
2.3.3 Thermal Stability of Polyimide.....	44
2.3.4 Drying and Annealing For ATR-FTIR Analysis.....	45
2.3.5 Annealing Effect on Electrical Conductivity.....	47
2.3.6 Temperature Cell (Annealing).....	47
2.4.1 Fourier Transform Infrared Spectroscopy.....	48
2.5.1 Measurement of Electrical Resistance of Thin Films.....	51
2.5.2. Sample Preparation.....	51
2.5.3 Electrodes.....	51
2.5.4 DC Electrical Resistance Measurement.....	51
2.5.5 Current-Voltage Measurement.....	52
2.6.1 Mechanical Measurements.....	52
2.6.2 Dynamic Mechanical Measurements.....	56
2.6.3 Thermo Mechanical Measurement.....	61
2.6.4 Electromechanical Measurement.....	61
2.7 References.....	64

3 ATR-FTIR and XPS Spectroscopic Characterisation of Cu³⁺ Ion-Beam Irradiated Polyimide Films

3.1 Introduction.....	66
3.2 Sample Preparation and Characterisation.....	68
3.3 Irradiation Induced Molecular Change of Films.....	71
3.3.1 Molecular Characteristics of Pristine Polyimide.....	71
3.3.2 Ion-Beam Irradiation Induced Molecular Structure Changes in the Polyimide Films.....	76
3.3.3 Effect of Annealing on the Molecular Characteristics of Irradiated Polyimide Films.....	90
3.3.4 X-Ray Photon Spectroscopic Studies of the PI Films.....	91
3.5 Conclusion.....	104
3.6 References.....	107

4 Temperature Dependent Electrical Behaviour of Irradiated Polyimide Films

4.1 Introduction.....	111
4.2 Sample Preparation and Characterisation.....	114
4.3 Electrical Resistance Behaviour of Irradiated Films.....	115
4.3.1 Ambient Temperature Electrical Properties of Irradiated Polyimide Films.....	115
4.3.2 Temperature Dependent Electrical Properties of Irradiated Polyimide Films.....	117
4.3.3 Moisture Effect on Electrical Properties.....	124
4.4 Conclusion.....	126
4.5. References.....	128

5 Micromechanical and Electromechanical Behaviour of Irradiated Polyimide thin Films

5.1 Introduction.....	133
5.2 Sample Preparation and Characterisation.....	137
5.3.1 Room Temperature Mechanical Analysis.....	137
5.3.2 Temperature Dependent Mechanical Analysis.....	140
5.3.3 Temperature Dependent Dynamic Mechanical Analysis.....	143
5.4 Electromechanical Characterisation of PMDA-ODA	147
5.5 Conclusion.....	151
5.6.References.....	152
6 Summary.....	157

LIST OF FIGURES

Figure 1.1: The chemical structures of the polyimides, PMDA-ODA and BTDA-ODA.....	2
Figure 1.2: Illustration of film extension during application of mechanical stress-strain.....	18
Figure 2.1: The flow chart of BTDA-ODA film fabrication. The PAA viscosity was 3.5 Pa.s and BTDA-ODA concentration was 25% (w/w) in N-methyl pyrrolidinone (NMP).....	36
Figure 2.2: Shows a schematic of the time and temperature at which the free standing films were cured in a vacuum oven.....	37
Figure 2.3: shows the tandem accelerator used at ANSTO with its different units.....	39
Figure 2.4: Shows the films supported by the aluminium plates for irradiation.....	41
Figure 2.5: presents a schematic diagram of the irradiation process and storage sequence of the films after irradiation.....	42
Figure 2.6: Perkin Elmer TGA at RMIT University.....	43
Figure 2.7: (a) and (b) shows the weight loss percentage versus temperature and the derivative weight percentage vs. temperature of PMDA-ODA irradiated thin films.....	45
Figure 2.8: Schematic diagram of the drying and annealing process of the films.....	46
Figure 2.9: The step-by-step heating and cooling cycle of the films.....	47
Figure 2.10: Cell used for electrical conductance measurements of irradiated films, under an inert atmosphere, during thermal cycling of the films.....	48
Figure 2.11: ATR-FTIR spectrometer experimental setup. Diagram in this Figure is adapted from Hirata et al. [13] and [FTIR users' guide].....	49
Figure 2.12: Schematic outline of XPS instrumentation.....	50
Figure 2.13: The electrodes' contact and shaded area with Thickness, Length and Width.....	51

Figure 2.14: Schematic of the current-voltage circuit set-up used for the resistance vs. temperature measurements.....	53
Figure 2.15: Graph of polyimide-glassy carbon thin film composite. The resistance is observed to be decreasing with increasing temperature.....	53
Figure 2.16: An Arrhenius plot which was used to calculate the activation energy (AE) for the polyimide-glassy carbon thin film composite. AE was calculated to be 34.35 meV/K.	54
Figure 2.17: General stress-strain curve for polymeric materials adapted from Mernard et al.[16].....	55
Figure 2.18: The Perkin-Elmer DMA-7e.....	56
Figure 2.19: (a) shows the in-phase (elastic), (b) Out of phase (viscous) materials strain response to applied stress and (c) material between the viscous and elastic extremes [8].....	59
Figure 2.20: ϵ' In-phase, ϵ'' out-of -phase strain vectors, and ϵ^* the vector sum for materials behaving between viscous and elastic extremes [16].....	60
Figure 2.21: The Perkin-Elmer DMA-7e using the Mora-Huertas et al.[17] set up.....	62
Figure 3.1: Film contact with the single bounce transparent prism during ATR-FTIR analysis.....	69
Figure 3.2: (a) Molecular structure of 3',4',4'- benzophenonetetracarboxylic dianhydride; 4,4'- oxidianiline (BTDA-ODA), (b) Molecular structure of pyromellitic dianhydride-4,4'- oxidianiline (PMDA-ODA).....	71
Figure 3.3 (a): FTIR spectra of pristine PMDA-ODA and BTDA-ODA: range 4000-650 cm^{-1}	74
Figure 3.3 (b): FTIR spectra of pristine PMDA-ODA and BTDA-ODA: expanded view of the range 2000-650 cm^{-1}	75
Figure 3.4 (a): ATR-FTIR spectra region of 4000-650 cm^{-1} of pristine and irradiated PMDA-ODA (5×10^{14} ions cm^{-2}) films.....	81

Figure 3.4 (b): ATR-FTIR spectra region of 2000-650 cm^{-1} of pristine and irradiated PMDA-ODA (5×10^{14} ions cm^{-2}) films.....	82
Figure 3.5 (a): ATR-FTIR spectra region of 4000-650 cm^{-1} of pristine and irradiated BTDA-ODA (5×10^{14} ions cm^{-2}) films.....	86
Figure 3.5 (b): ATR-FTIR spectra region of 2000-650 cm^{-1} of pristine and irradiated BTDA-ODA (5×10^{14} ions cm^{-2}) films.....	87
Figure 3.6: Decomposition and formation of unsaturated bonds and the formation of free radicals such as H atoms, adapted from literature [7]. (a) PI film before ion beam irradiation, (b & c) PI during irradiation and (d) PI films after Irradiation.	88
Figure 3.7 (a): The ATR-FTIR spectra of irradiated, pristine, dried and annealed films, PMDA-ODA with fluence values of 3×10^{14} ions cm^{-2}	94
Figure 3.7 (b): The ATR-FTIR spectra of irradiated, pristine, dried and annealed films, BTDA, with fluence values of 3×10^{14} ions cm^{-2}	95
Figure 3.8 : XPS survey spectra of the pristine PMDA-ODA PI film and the film irradiated at a fluence of 5×10^{14} ions cm^{-1}	98
Figure 3.9: Molecular structure of pyromellitic dianhydride–4,4'-oxidianiline (PMDA-ODA). The numbers on the atoms in this structure refer to the numbers on the component peaks in Figure 3.10.....	98
Figure 3.10: XPS spectra of the non-irradiated pristine PI films after curve–fitting; each curve was assigned to a corresponding bond in the PMDA-ODA polyimide.....	99
Figure 3.11: presents the deconvoluted XPS spectra for the irradiated PI films, from which the data in Tables 3.4 and 3.5 have been compiled.....	101
Figure 4.1: Current-Voltage graph confirming ohmic behaviour of the irradiated PI film fluence 5×10^{14} ions cm^{-2}	116
Figure 4.2: Electrical resistivity variation with fluence of irradiated PMDA-ODA and BTDA-ODA PI nanocomposite films.....	117

Figure 4.3: Temperature dependent electrical resistivity of the irradiated PMDA-ODA films with fluence values ranging from 9×10^{13} to 5×10^{14} ion cm^{-2}	118
Figure 4.4: Variation in E_a for different fluences of the Cu^{3+} ion-beam irradiation of the PMDA-ODA films.....	120
Figure 4.5: Plots of the natural logarithm of the conductivity versus $1/T$, (a) PMDA-ODA PI film fluence 2×10^{14} ions cm^{-2} and (b) PMDA-ODA PI film fluence 5×10^{14} ions cm^{-2} , over the temperature range 25°C (298 K) to 55°C (328 K).....	122
Figure 4.6: (a) HRTEM of the cross sectional image of the irradiated films (b) The SAED diffraction pattern	123
Figure 4.7: Irradiated PMDA-ODA film fluence 5×10^{14} ions cm^{-2} resistance change over time, atmosphere and temperature.....	125
Figure 5.1: Initial mechanical analysis of unirradiated PMDA-ODA film, (a) static stress-strain measurements at room temperature, (b) storage and loss modulus, in frequency range 1 to 30 Hz and (c) storage and loss modulus, over temperature range 25 to 250°C	138
Figure 5.2: Stress Strain curves of unirradiated and irradiated PMDA-ODA films at ambient temperature	139
Figure 5.3: Temperature effect on the static mechanical analysis of PMDA-ODA films with fluence values of ; a) unirradiated, b) 1×10^{14} ions cm^{-2} , c) 3×10^{14} ions cm^{-2} , and d) 5×10^{14} ions cm^{-2}	141
Figure 5.4: DMTA of unirradiated and irradiated PI films (a) storage modulus, (b) loss modulus.....	146
Figure 5.4: DMTA of unirradiated and irradiated PI films (c) $\text{Tan } \delta$	147
Figure 5.5: (a) Change in resistance with applied tensile strain for fluence 5×10^{14} ions cm^{-2} ; (b) Relative change in resistance in response to the application of strain on a PI film irradiated at fluence values of 3×10^{14} and 5×10^{14} ions cm^{-2} at ambient temperature.....	149

LIST OF TABLES

Table 1.1: Representative Resistivity and Conductivity data.....	14
Table 2.1: Chemical structure and physical properties of each polyimide.....	34
Table 2.2: shows the various areas and the explanation of their operations.....	40
Table 2.3: The fluence values achieved and the exposure time and current density.....	41
Table 3.1: Band assignments of ATR-FTIR spectra of PMDA-ODA and BTDA-ODA films before ion-beam modification....	72
Table 3.2: Literature Infrared peak assignment for unirradiated kapton film [23]	73
Table 3.3: The elemental composition ratios of the PI, pristine PMDA-ODA film surface, the irradiated film surface, and graphite.....	97
Table 3.4: below, presents a summary of the deconvoluted XPS data for both the pristine and irradiated PMDA-ODA films.....	102
Table 3.5: The XPS component ratios for the C 1s, N 1s and O 1s binding energy bands for the theoretical PI, pristine PMDA-ODA film surface, the irradiated films, and graphite.....	102
Table 5.1. Young's Modulus of the irradiated PMDA-ODA films at different temperatures.....	140
Table 5.2. The Gauge Factor values calculated for the irradiated PMDA-ODA films at different temperatures, and their corresponding fluence values.	148

LIST OF EQUATIONS

Equation 1.1: $\sigma = \sigma_0 \exp(-T_c/T)^{1/\gamma}$ or $\log(\sigma / \sigma_0) = -(T_c/T)^{1/\gamma}$	13
Equation 1.2: $\log(\sigma) = \log(\sigma_0) - T_c/T$	13
Equation 1.3: $\log(\rho) = \log(\rho_0) + T_c/T$	14
Equation 1.4: $F \propto \delta t$	18
Equation 1.5: $E = \text{stress} / \text{strain} = \sigma / \epsilon$	18
Equation 1.6: $\epsilon \propto \Delta T$ so $\epsilon = \delta V / V = \text{constant} \times \Delta T$	19
Equation 1.7: $\epsilon = \alpha (T - T_0) = \alpha (\Delta T)$	20
Equation 2.1: $\rho = R (A/L)$	52
Equation 2.2: $R = V / I$	52
Equation 2.3: $\sigma = F / A$	54
Equation 2.4: $E = \sigma / \epsilon$	55
Equation 2.5: $\sigma(t) = \sigma_0 \sin \omega t$	57
Equation 2.6: $\epsilon(t) = (\sigma_0/E) \sin(\omega t)$	57
Equation 2.7: $\epsilon(t) = \epsilon_0 \sin(\omega t)$	57
Equation 2.8: $\epsilon(t) = \sigma_0 \cos(t)$ or $\epsilon(t) = \sigma_0 \sin(t + (\pi/2))$	58
Equation 2.9: $\epsilon(t) = \omega \epsilon_0 \cos(\omega t)$ or $\epsilon(t) = \epsilon_0 \sin(\omega t + (\pi/2))$	58
Equation 2.10: $\epsilon(t) = \epsilon_0 \sin(t + \delta)$	60
Equation 2.11: $\epsilon(t) = \epsilon_0 [\sin(t) \cdot \cos \delta + \cos(t) \cdot \sin \delta]$	60
Equation 2.12: $\epsilon' = \epsilon_0 \sin(\delta)$ in-phase component.....	60
Equation 2.13: $\epsilon'' = \epsilon_0 \cos(\delta)$ out-of-phase component.....	60
Equation 2.14: $\epsilon^* = \epsilon' + i\epsilon''$	60
Equation 4.1: $I = V/R$	115
Equation 4.2: $\rho = (RA)/L$	115
Equation 4.3: $\rho = \rho_0 \exp[-(E_a / kT)^{\gamma}]$	119

Equation 4.4: $\ln(\rho/\rho_0) = - (Ea/kT)^Y$	119
Equation 4.5: $\ln(\rho) = \ln(\rho_0) - (Ea/kT)^Y$	119
Equation 5.1: $GF = ((\Delta R/R_0)/\epsilon)$	145
Equation 5.2: $R_e = R_0 e^{\alpha\epsilon}$	146
Equation 5.3: $\ln(R_e) = \ln(R_0) + \alpha \cdot \epsilon$	146

1

INTRODUCTION AND LITERATURE REVIEW

1.1 Introduction

Polymers have emerged as an important class of advanced material due to their increasingly versatile applications in various fields of modern technology [1]. The five major areas of application are (i) plastics, (ii) rubbers or elastomers, (iii) fibres, (iv) surface finishes and protective coatings and (v) adhesives. Polymeric solids have been used for a number of applications which utilise their exceptional properties, such as low density, the ability to form elaborate shapes, their versatile electronic properties, and low cost of manufacture. However, they have inherent disadvantages, such as low thermal stability and unpredictable dielectric properties which limit their use in many applications. As a result of these disadvantages, polymers such as polyimides (PI), which possess enhanced thermal stability, were developed. Due to current interest in the use of polymeric layers as insulators or conductors in electronic systems [2], the surface properties of polymers such as PI have been modified to incorporate conductive layers within the polymer matrix.

Polyimides constitute an important class of polymers due to their excellent thermal stability, wear resistance, outstanding electrical properties, radiation resistance, solvent resistance, good adhesion properties, long term stability and superior mechanical properties [3]. In particular, their thermal robustness makes them useful in microelectronic systems where the temperature often reaches 400°C [3]. The two

polyimides investigated here were 3,4,3',4'-benzophenonetetracarboxylic dianhydride 4,4'-oxybisbenzenamine (BTDA-ODA), and pyromellitic dianhydride – 4,4'-oxidianiline (PMDA-ODA) also known as Kapton®. These two particular polyimides were formulated to provide high temperature resistance and are illustrated in Figure 1.1.

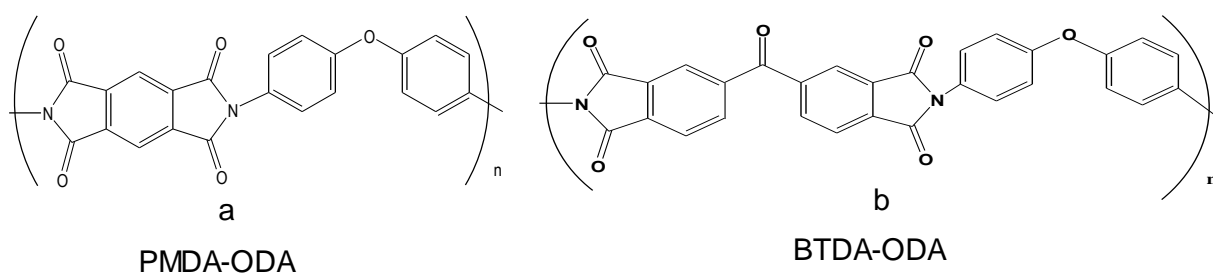


Figure 1.1: The chemical structures of the polyimides, PMDA-ODA and BTDA-ODA

It should be noted that both PI's contain aromatic bifunctional imides linked by a bis-aromatic ether which together create the essential PI backbone. In addition, BTDA-ODA contains a carbonyl link ($>C=O$) in each monomeric unit in the PI chain.

Various chemical and physical processes have been used to modify the behaviour of polymers. In this thesis, the emphasis is on ion-beam irradiation, which is a flexible technique that may be used for the selective modification of the chemical structure, as well as the electrical and mechanical properties of polymers [3-13].

1.1.1 Rationale of Research Project

Significant research studies have been performed on the UV-laser, electron- and ion-beam irradiation of polymers, especially polyimides (PI's) [12, 13], because they have excellent resistance to higher temperatures. Studies by Davenas et al. [25] deduced features of the pristine and irradiated polyimide structure using infrared spectroscopy and showed changes in the functional group bands. Although many studies [3,12, 26] have reported on the pristine structures of polyimides such as PMDA-ODA, very few have

examined BTDA-ODA [97]. In addition, the change in the molecular structure of PI's is of great importance, where much of the characterisation has been performed before, and just after, irradiation [62]. The subsequent effect of the atmosphere on the PI's after irradiation has largely been neglected. In addition, the FTIR analysis of irradiated PI's after heat treatment, in particular, annealing, is an important aspect of molecular structure characterisation, as it provides details of the changes likely to occur within the environment that they operate in. Such thermal treatment studies on polymers, in particular polyimide, have been overlooked, and there are very few studies on the effects of annealing before, or after, irradiation, other than the research reported by Watamori et al. [27].

The structural effects induced by UV-laser and heavy ion irradiation, and the electrical conductivity properties of PI's have been widely studied [31]. However, a detailed description of the electrical transport mechanisms for polyimide films irradiated with a Cu^{3+} ion-beam, in the fluence range of 9×10^{13} to 5×10^{14} ions cm^{-2} , is yet to be established. Thus, there is a need for a systematic study of the possible conduction mechanisms of the irradiated PI films. Also, in the literature, irradiation is discussed in terms of irradiating throughout the polymer film, and the electrical conductivity is discussed as the conduction through, and across, the irradiated film. In the work described here, the polyimide films have only been irradiated to the depth of about 10%, leaving 90% of the film thickness to act as an insulating substrate for the conducting layers of the film; this is advantageous as it eliminates the need to use an external substrate for film support.

The changes in the micromechanical and electromechanical properties of irradiated PI films are examined here. Literature searches have indicated that there are only limited studies [32] on the mechanical properties of irradiated polymers in general, and very few on the mechanical properties of irradiated PI films. Similarly, there have only been a

limited number of studies on the electromechanical properties of composite thin films [65], and a paucity of literature on the electromechanical properties of irradiated PI films [65].

1.1.2 Objectives

The first objective of this study was to identify the chemical and microstructural changes that occur when the PI film surfaces of PMDA-ODA and BTDA-ODA were irradiated with a 5.5 MeV Cu^{3+} ion-beam. In this work, the structural changes were investigated via temperature-dependent FTIR analysis.

The second objective was to characterise the semiconducting behaviour of the irradiated layer of the PI films, and to determine the electrical transport mechanisms that occur in this top 10% of the PI film. The changes in electrical properties were studied and related to alterations in the chemical structure after irradiation.

The third objective was to determine the tensile properties of the irradiated PI films. This included evaluating the temperature dependent static and dynamic mechanical behaviour of the irradiated PI films. The electromechanical properties of the irradiated PI films were also evaluated, and the strain sensitivity of the PI films (gauge factors) were calculated and compared to those reported for nanocomposite films and conventional composite films.

Background and Theory

1.1.3 Polyimides

In the early 1960's a number of aromatic polyimides were reported, some of which were commercialised and their structure and properties were investigated by many research groups [33-36]. In addition to the chemical backbone structure, the molecular packing coefficient and the orientation of the polymer chains have been reported to significantly influence the film's properties, such as water permeability [33-36]. Optical studies of PMDA-ODA polyimide films [33-36] prepared by casting the precursor polymer solutions onto substrates such as glass slides and silicon wafers, followed by imidization, have shown relatively large out-of-plane birefringence and negligible in-plane birefringence.

1.1.4 Polyimide Composites

Composites are heterogeneous materials consisting of a mixture of two or more components present as separate phases, and combined to improve a given property of the composite beyond each individual component [37]. A nanocomposite consists of nano-size particles embedded in a matrix. An electrically conductive composite consists of conductive carbon or metal based particles (fillers) embedded in an insulating matrix (which can be inorganic or an organic polymer). In this manner, an electrically conductive, lightweight and flexible, polymeric material is generated as a result of the formation of electrically conductive channels or pathways.

A considerable literature exists on the preparation and characterisation of nanocomposite conductive films, composed of metal particles or metal oxides dispersed into polymers, for use in gas or vapour sensing applications [19]. The conducting particles used in electro-conductive polymer composites include various forms of carbon such as carbon black, glassy carbon, graphite and carbon nano-tubes (CNT's). Carbon black occurs in the form

of near spherical particles of colloidal size, coalesced into particle aggregates and agglomerates. In a polymer matrix composite, knowledge of the particle size, distribution and concentration is essential, as these parameters affect the chemical and physical properties of the material. It is reported [38-40] that the *in-situ* formation of nanoparticles within nanocomposite films results in well-distributed nanoparticles within the polymer matrix.

During ion beam irradiation of a polymer, the degradation of chemical bonds leads to modification of the physical and chemical properties of the polymer film. The changes induced in the polymer are localized along the ion path in the irradiated material. The formation of carbonaceous material from organic components in the film results in electrical conductivity, and an increase in surface hardness. Marletta et al. [41] reported that the electrical conductivity of an ion-beam irradiated film was comparable to the conductivity obtained in doped poly-acetylene, but, in contrast to polyacetylene, these composite films were reported to exhibit excellent stability.

Since 1991, carbon nanotubes (CNT's) have been widely used for many applications due to their high strength and excellent conductivity. As carbon nanotubes have high aspect ratios, they readily form a conductive network. As a result of these conductive network properties, CNT's possess useful electromechanical properties [42]. For example, when a CNT-polymer composite was investigated for strain sensing [37,43,44], it was found that the change in electrical resistance was linear with respect to the strain. Also, the strain gauge sensitivity (the so-called gauge factor, GF) of a CNT nanoparticle composite was much higher than the gauge factor of other polymer composites [GF≈50]. Since the irradiation of PI films forms cylindrical-like graphitic tracks along the ion path, the electrical conduction mechanism in the irradiated PI's may be similar to that in the CNT particles, and hence they may possess useful electromechanical behaviour [125].

1.2 The Effects of Ion Beam Irradiation

1.2.1 Surface Morphology of Irradiated Polymeric Materials

Ion beam irradiation texturing of thin films has been studied for more than four decades. The earliest studies were performed primarily on face centred cubic metal films *ex-situ*, with the ion-beam incidence angle normal to the films. X-ray diffraction was used to determine beam induced changes in the crystallinity and molecular structure of the films. Simultaneous ion beam bombardment during deposition of the films has also been studied for the past fifteen years.

Irradiation of a polymeric material may induce irreversible changes in their macroscopic mechanical properties such as electrical and optical behaviour [45]. Electron excitations, ionisation, chain scission, cross-link formation and mass losses are some of the fundamental mechanisms that give rise to the observed macroscopic changes [46,47]. Heavy ion irradiation of solid organic polymeric material has been reported to form minute cylindrical-like carbon-rich regions along the ion path due to energy deposition and bond breaking and making processes [48]. The surface properties of the irradiated polymer were found to be affected predominantly by the ion species used in the irradiation process and by the irradiation dosage (fluence). The ions used for irradiation were also reported to be lodged in the polymer layer after penetrating the surface. The ion species in this layer were found to increase the number of conjugated double bonds, resulting in an increase in electrical conductivity of the polymer. During irradiation, Davenas et al. [11] observed the appearance of conductive properties as the polymer darkened in colour. These changes in properties were interpreted as the formation of a carbon layer (i.e. carbonisation of the polymer layer). Similar observations were reported by Furere et al. [23].

As noted earlier, ion beam irradiation-induced changes result in a modification of the chemical structure from a pristine polymer surface to a graphite-like surface, with nanotubes dispersed at a nanoscale. Modification of the chemical structure of polyimides via ion-beam bombardment has been investigated by, for example, Davenas et al. [12], Xu et al. [13] and Constantini et al. [14]. Hirata et al. [18] used ATR-FTIR spectroscopy to study the effect of cluster ion irradiation on the chemical structure of polycarbonates, and Mohammad et al. [19] analysed the microstructural properties of PI and poly(vinylsilsesquioxane) hybrid composite films by FTIR analysis.

1.2.2 Attenuated Total Reflectance Fourier Transform Infrared Spectroscopy (ATR-FTIR)

The infrared spectra of compounds containing structural moieties such as carbonyl, amino, phenyl and nitro groups have certain features that appear at the same general frequency for every compound containing these functional groups. Thus, FTIR spectral data reveal the significant degradation that materials can suffer as a result of bond breaking processes. Previous studies have utilized Attenuated Total Reflectance Fourier Transform Infrared Spectroscopy (ATR-FTIR) to identify the bond types and chemical functional groups in the polymer which are most sensitive to high energy radiation damage [100-105]. ATR-FTIR data were found to be particularly useful to identify the chemical changes that occurred in the evolution of carbon clusters, via the formation of conjugated double bonds and ring fusion processes [23, 56-60].

A simple FTIR spectrum of a polymeric material can be divided into two regions: (i) The high frequency region, approximately $4000\text{-}2000\text{ cm}^{-1}$, and (ii) The low frequency region, approximately $1999\text{-}650\text{ cm}^{-1}$. Characteristic bands due to hydroxyl groups in alcohols or carboxylic acids are observed in the high frequency region, whereas the carbonyl groups

in amides and amino acid have very broad and asymmetric bands extending over a range of several hundred wave numbers (from approximately 1700 to 1400 cm^{-1}) [61-63].

After irradiation of the sample material, the FTIR spectra would show an overall reduction in intensity of the characteristic bands, indicating degradation, and possibly transformation of the material. For example, in an irradiation study of polystyrene (PS) the intensity of the band at 2853 cm^{-1} , assigned to the C-H symmetric stretching band, was reduced [89], and for polyethylene terephthalate (PET) the bands corresponding to the ethylene glycol residue of the trans-configuration at 1472, 1387, 973 and 850 cm^{-1} were reduced in intensity [64].

Kapton[®] polyimide is one of the best known and most extensively studied commercial polyimides, and its FTIR spectrum has been reported to change following exposure to intense electron beam irradiation [65]. After irradiation it was found that there was an increase in the intensity of the general phenyl band centred at 3060 cm^{-1} relative to the C-H band at 2400 cm^{-1} , and a decrease in the intensities of the di- and tri-substituted phenyl bands at 920-775 cm^{-1} was accompanied by an increase in the mono-substituted phenyl band at 690 cm^{-1} , indicating a process of chain scission occurring adjacent to the aromatic groups [65].

The high temperature (250 - 350 $^{\circ}\text{C}$) annealing of carbon polymer composite films has been intensively studied in the literature [30], and recent studies of the annealing effect on the electrical transport properties of Ag nanoclusters embedded in glass matrix was reported by Megudapathy et al. [63]. This study found that there was a significant depletion of hydrogen after annealing for five minute intervals over the temperature range 100 $^{\circ}\text{C}$ to 300 $^{\circ}\text{C}$. Annealing over 300 $^{\circ}\text{C}$ led to the recovery of hydrogen, although other elements such as oxygen, nitrogen and carbon were found to be unaffected. Thus,

although the irradiated polyimide is stable at high temperatures, the annealing process reduces its stability.

1.3 Electrical Properties

Electrical conductivity is not usually observed in organic polymeric materials because they are covalently bonded networks, and any residual conductivity usually depends on the movement of adventitious ions. Where there is charge transfer, it can occur by the movement of an electron from a donor molecule of low ionization potential to an acceptor molecule of high electron affinity.

Polymers with metallic conductivity and other conductive properties are in high demand since they open a gateway for the production of flexible, light weight, enduring and low cost devices [23, 67]. Conductive polymer composites consist of conducting particles and a polymer combined in a solid matrix. The conductive properties of the polymer composites are also affected by the concentration of the conducting particles that form percolation pathways within the transport network of the insulating material [68]. Currently, nanocomposites are used in electromagnetic interference shields as embedded passive (inert) components, since they are unaffected by electrostatic fields and possess a positive temperature coefficient, which are desirable properties for applications in heat regulators and switching devices [68-70].

Enhanced optical and electrical properties and/or enhanced or maintained mechanical properties can be produced in a composite material [119, 71-80]. The electrical conductivity of a composite is dependent on the temperature and the filler content. Another method of achieving enhancement in the electrical conductivity of a polymer is via irradiation. The conductivity of the irradiated polymer is dependent on three factors : (i) the structural changes induced by irradiation; (ii) the temperature of the polymer, and (iii) the relaxation processes in the polymer. The electrical behaviour of composites is

dependent on the type of charge carriers and the charge transport mechanism. The mechanism may involve *hopping* (where the electrons hop between conducting sites) or *tunnelling* (where the electrons "tunnel" through activation barriers between the conducting sites). If charge carriers are lacking in a composite, there is little or no current flow. The term "carriers" refers to the presence of free electrons and positive holes in the material. A *hole* is a vacant electron energy state that is manifested as a charge defect in a crystalline solid, the defect behaving as a positive charge carrier with a charge magnitude equal to that of the electron. Carriers arise from broken bonds which allow an electron to be placed in the conduction band and/or a hole to be created in the valence band.

1.3.1 Hopping and Tunnelling Conduction Processes

Hopping conduction occurs when there is a significant decrease in separation between overlapping orbitals, which limits the mobility of the electronic states, allowing them to become localised. Thus, the gap between the valence and conduction bands becomes a mobility gap rather than an energy gap, therefore the charge transfer can only occur by thermally activated hopping across the energy barriers between the localised states [101]. However, tunnelling occurs when the domains are separated by an orientation boundary or an amorphous region, where the mobility is due to quantum mechanical tunnelling [68].

The movement of electrons in a material requires them to pass over, or tunnel through, an energy barrier depending on the 'shape' of the barrier and the availability of thermal energy. In the case of semiconducting materials, this mobility will increase with an increase in temperature.

In conventional semiconducting materials, the electrical transport mechanism can exhibit two major types of semiconductor behaviour, termed "intrinsic" or "extrinsic".

Intrinsic semiconductors, typified by silicon, have small energy gaps ($\approx 1 \text{ eV}$) between the filled and empty conduction bands, which allows a small number of electrons to be excited into the conduction band at ambient temperatures, and so provide a route for charge conduction.

Extrinsic semiconductors require the addition of a “dopant” which alters the electron population of either the valence or conduction bands to induce conductivity. A *dopant* is a small quantity of a substance such as phosphorus (usually added at the level of parts per million), added to another substance, such as a semiconductor, to alter the latter's properties. For example, phosphorus (Group V, 5 valence electrons) doped silicon (Group IV, 4 valence electrons) leads to a small population of electrons permanently in the conduction band of the silicon due to the extra electrons from the Group V element, which gives rise to n-type ($n = \text{negative charge}$) semiconduction, with electrons as the principal charge carriers. In the case of boron (Group III, 3 valence electrons) doped silicon, there are electron vacancies in the valence band which gives rise to positive holes, and hence they are termed p-type ($p = \text{positive charge}$) semiconductors. In the n-type materials, the Fermi energy level is closer to the conduction band than the valence band, whereas with the p-type, the Fermi energy level is closer to the valence band than the conduction band. The different forms of conduction mechanism discussed above involve the excitation of charge carriers from the valence band into the conduction band across a band gap [170].

In pristine PI materials, the number of electrons in the conduction band are equal to the number of holes in the valence band, but once they are irradiated they exhibit intrinsic semiconduction as a result of bond breaking and making processes which redistribute the electron density.

1.3.2 Temperature Dependent Electrical Conductivity

The temperature dependent conductivity behaviour of a material contains important information about the charge transport mechanism that occurs in the material. It also allows prediction of the electrical conduction properties [15]. Huertas et al. [68] and Migahed et al. [111] report that conduction in a metal can be expressed as the logarithm of the conductivity (symbol σ) ie. $\log(\sigma)$, and it is inversely proportional to temperature, due to an increase in electron scattering at higher temperatures.

ie., $\log(\sigma) \propto 1/T$ for a metal

However, conduction in semiconductors is directly proportional to the temperature, because the carriers are thermally excited across the band gap to enhance the band conduction transport mechanism.

ie., $\log(\sigma) \propto T$ for a semiconductor

The one-dimensional “Nearest Neighbour Hopping” model was found to give rise to a conduction directly proportional to temperature, which is consistent with semiconductor behaviour. The “Variable Range Hopping model” [112] and “Tunnelling Transport” mechanisms give rise to simple fractional temperature exponents, originally proposed for amorphous semiconductors, as expressed in the following relationships [113] :

$$\text{ie., } \sigma = \sigma_0 \exp (-T_0/T)^{1/\gamma} \quad \text{or} \quad \log(\sigma / \sigma_0) = -(T_0/T)^{1/\gamma} \quad (1.1)$$

Where σ is the conductivity, σ_0 and T_0 are constants and T is the absolute temperature.

The value of γ defines the hopping dimension, and is between 4 and 1 for one-, two- or three-dimensional hopping respectively [111].

For example, if $\gamma = 1$, then Equation 1.1 reduces to :

$$\log(\sigma) = \log(\sigma_0) - T_0/T \quad (1.2)$$

and since resistivity (ρ) is related to conductivity via, $\rho = 1 / \sigma$, then it can be shown :

$$\log(\rho) = \log(\rho_0) + T_c/T \quad (1.3)$$

so a plot of log(resistivity) [or log(resistance)] versus reciprocal temperature should be linear for a 3-dimensional charge hopping mechanism.

1.3.3 Electrical Conductivity of Polyimides

The electrical resistivity (ρ) of pristine polyimide films has been reported to be in the range of 10^{12} to 10^{14} ohm cm [83-85] which is typical of an insulating material such as Teflon, as presented in Table 1.1.

Table 1.1: Representative Resistivity and Conductivity data

Material	Resistivity = ρ ρ ohm cm	Conductivity = σ σ S cm ⁻¹ or mho cm ⁻¹	Reference
Copper	1.7×10^{-6}	6×10^5	124
Silver	1.5×10^{-6}	7×10^5	
Carbon	3500×10^{-6}	0.003×10^5	
Glass	$10^{12} - 10^{16}$	$10^{-16} - 10^{-12}$	
Teflon	$> 10^{15}$	$< 10^{-13}$	
Fused silica	75×10^{18}	1.3×10^{-20}	
Polyimide	$10^{12} - 10^{14}$	$(10^{-14} - 10^{-12})\#$	83 - 85
HD Micro- systems PI	$(10^{14})\#$	10^{-14}	106

calculated from the relationship, $\rho = 1/\sigma$

The charge transfer mechanism in polyimides has been discussed in many literature reports, including those of Huertas et al. [68], Brown et al. [86], Suzuki et al. [89] and Loh et al.[88]. Brown et al. [86] have studied the intermolecular interactions in a polyimide in order to understand the influence of the polymer's molecular chains on its electrical properties. Charge transfer was found to be due to interactions between the amine phenyl acting as an electron donor and the diimine moiety acting as an electron acceptor [87].

1.3.4 Electrical Conductivity of Irradiated Polyimides

Ion-beam irradiation of an organic polymer increases its polarity and electrical conductivity, and modifies its surface properties by alteration of its chemical structure [49,90,94]. The chemical effect on a single-ion-irradiated polymer was found to be dependent on two factors: (i) the primary polymer's molecular structure, and, (ii) the deposition of the implanted ion's energy [95,96]. Solid polymer surface irradiation has been discussed by Bertrand et.al [91]. Bertrand et al., Benninghoven et.al, Demirev et al., and Leggett et al. [91-94] reported that the primary ions used in irradiation at various energy levels lead to the sputtering of molecular fragment ions or clusters, and these species were found to receive kinetic and internal energies shared between their different vibrational and rotational modes [100,101]. Schumann et al. [97], Marletta et al. [102] and others [103-105], that found that laser irradiation induced a permanent increase in the electrical conductivity of the polymer which relied on the excitation of particles by visible–laser irradiation or pyrolysis of the polymer. Srinivasan et al [23] observed that the laser-induced conductivity was dependent on the nature of the ambient atmosphere during the irradiation process.

Polyimides are reported to have high chemical and thermal stability [103] and the intrinsic electrical conductivity of a HD Microsystems polyimide was reported to be 10^{-14} S cm⁻¹

[82]. However, the electrical conductivity can be enhanced by irradiation, and this has drawn much attention recently due to the possible application of kapton polyimide as a conducting polymer [97-101]. Although many groups have reported an increase in the polyimide conductivity by several orders of magnitude due to irradiation, an exact mechanism of conduction is yet to be established [102, 103]. Van der Putten et al [113] noted that upon irradiation, free radicals form and may interact with other molecular groups, resulting in an increase in conductivity. Conductive behaviour after pyrolysis was found by Mittal et al. [105] and Phillips et al. [106] and Garnier [112] attributed the induced conducting properties to the formation of dense heterocyclic networks dispersed in an amorphous carbon matrix. Wang et al. [103] and Phillips et al. [107] found a comparable conductivity increase as a result of ion beam irradiation. Hioki et al. [104] and Fureur et al. [23] demonstrated that a laser beam could also cause a pristine polyimide layer to become conductive. Egusa et al. [29] and Singh et al.[31] suggest that the following sequence of events occurs after irradiation and leads to electrical conductivity of the polymer: (i) formation of radiation defects (fine carbon clusters, unsaturated compounds, macroradicals) accompanied by cross-linking of polymer chains, liberation of volatiles and transformation of heteroatom containing functional groups, (ii) π -bonded carbon-rich cluster growth, and, (iii) creation of links between clusters leading to aggregation. This results in electron hopping between the carbon-rich clusters, and overlapping at high fluence creates percolation charge carriers along the irradiation layer, giving rise to electrical conductivity. Popok et al.[15] observed that at high fluence, channel overlapping in the irradiated polymer resulted in an increase of π -conjugation forming a conductive polymer matrix. The transport carriers arise by electron gas formation in extended conglomerates and 3-dimensional hopping from conglomerate to conglomerate in the irradiated layer. Two mechanisms that are possibly responsible for conduction in an irradiated polymer are variable range hopping and band conduction [108].

The conductive behaviour of Kapton-H polyimide in both transient and steady state modes was examined at different temperatures [118], and the current was found to be transient free at temperatures above 423K. The transient current was attributed to the formation of free radicals in the irradiated Kapton-H, with a decay rate consistent with increasing fluence, while the ionic jump distance doesn't support an ion hopping conduction mechanism. In a study of organic semiconducting materials used as thin film transistors, the conductivity of amorphous molecular polymers, and most conjugated polymers, was found to be governed by thermally activated hopping mechanisms with limited charge mobility [119].

1.4 Mechanical and Electromechanical Properties

The mechanical behaviour of materials is the study of their deformation and breakdown when placed under load. Common types of deformation that occur in materials are elastic, plastic and creep deformations. Elastic deformation is the stretching of the material without the breaking of chemical bonds. The elastic modulus is found to be high for strongly bound covalent solids, while for metals it has an intermediate value, and for a polymer the modulus is low. Plastic and creep deformations are inelastic deformations, which involve change in the relative positions of atoms. Plastic deformation is time dependent and shape is not recovered after unloading, and creep deformation is time dependent at an elevated temperature [29]. The stress-strain behaviour is described by the constitutive equations which are developed below.

The elastic behaviour of a material is described by Hooke's Law, which states that, within the elastic limit, the deformation produced is proportional to the stress. Thus, by reference to Figure 1.3 :

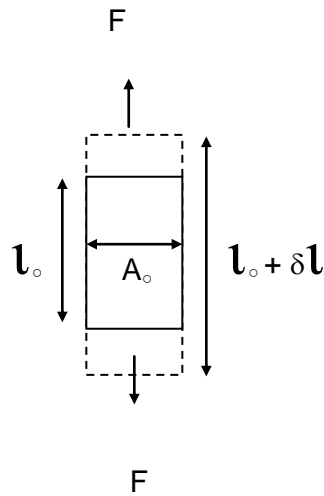


Figure 1.2: Illustration of film extension during application of mechanical stress-strain.

Where the applied force is F , the original length is l_0 , the final length after the force is applied is l ($= l_0 + \delta l$) and the cross-sectional area is A_0 . we can state Hooke's Law as:

$$F \propto \delta l \quad \text{ie., } F = \text{constant} \cdot \delta l = \text{constant} \cdot (l_0 + \delta l) \quad 1.4$$

If the initial length of the material to be analysed was doubled, then a doubling of the extension is observed. On the other hand, doubling of the cross-sectional area halves the extension. Hence, the extension varies linearly with initial length and inversely with cross-sectional area [35].

$$\delta l \propto l_0 / A_0 \quad \text{so, } \delta l = \text{constant} (l_0 / A_0)$$

The stress (symbol σ , units Nm^{-2}) is the force per unit area applied to the sample (F/A_0), and the strain (symbol ϵ) is the relative change in dimension ($\delta l/l_0$) of the sample, and so is unitless. The modulus of elasticity is the ratio of the increment of unit stress to the increment of unit deformation within the elastic limit, and for a sample in tension is also called Young's Modulus, designated E , and defined in equation (1.5):

$$\text{Young's Modulus, } E = \text{stress / strain} = \sigma / \epsilon \quad (1.5)$$

$$E = (F/A_0) / (\delta l / l_0) = F \cdot l_0 / A_0 \cdot \delta l$$

Thus, $\delta l = F \cdot l_0 / E \cdot A_0$

$$= F \cdot [l_0 / E \cdot A_0]$$

$$= F \cdot \text{constant}$$

which is a re-statement of Hooke's law.

On the basis of the expression for Young's modulus, the elastic behaviour of a material with a linear stress-strain relationship can be determined by the calculation of stresses and deflections in simple components. In the stress-strain curve, an initial linear elastic region is observed, so that the slope of that region is used to determine Young's modulus. The elastic limit is the point where the curve starts to deviate from linearity prior to material breakdown.

In plastic deformation, the volume of the material remains constant [114] and if the deformation is uniform along the length of the material, then the shape of the material is changed. The resistance to plastic deformation is indicated by a positive slope of the stress-strain curve. Plastic deformation in metals and ceramics is due to slippage between planes of atoms in the crystal grains of the material. The material's resistance to plastic deformation is roughly analogous to the friction of a block on a plane.

Thermal strain is the elastic strain that occurs due to changes in temperature, and this arises because an increase in temperature causes expansion, while a decrease in temperature leads to contraction. An isotropic material has mechanical properties that are the same in all directions, so temperature affects the material equally in all directions. The thermal strain ϵ (which can be expressed as $\delta V / V$, upon analogy with tensile strain) at a given temperature (T), is proportional to the temperature change (ΔT):

$$\text{ie., } \epsilon \propto \Delta T \quad \text{so} \quad \epsilon = \delta V / V = \text{constant} \times \Delta T \quad 1.6$$

From this we find, $\delta V = \text{constant} \cdot V \cdot \Delta T$, and the proportionality constant is the coefficient of thermal expansion (α).

If T_0 is the reference temperature where the strain is taken to be zero, we can write [124] :

$$\varepsilon = \alpha (T - T_0) = \alpha (\Delta T) \quad (1.7)$$

1.4.1 Mechanical Properties of Irradiated Polymers

Ion irradiation is known to affect the mechanical properties of polymeric materials and the effects have been intensively studied since the 1960's. Changes in the mechanical properties of irradiated materials are mostly dependent on whether or not crosslinking or degradation of the polymer occurs during the irradiation of the material [39,44]. In the study by Roy et al. [115] on the mechanical properties of electron beam irradiated polymer films, using low-density polyethylene (LDPE), biaxially oriented polypropylene (BOPP) and polyethylene terephthalate (PET), the LDPE maintained a high resistance, whereas PET and BOPP developed a low resistance to mechanical forces.

Other studies reported that phenols, amines and secondary aromatic amines are effective in protecting the polymer against loss of performance due to irradiation. It was also noted that irradiation exposes the stabiliser in the polymer to oxidative transformation [116, 121]. Courtney et al. [117] and Klemchuk et al. [120] reported that syringe materials exposed to gamma radiation underwent oxidative degradation with discoloration and a potential loss of mechanical properties, depending on the stabiliser used [118]. This degradation was reported to increase with gamma radiation dose unless a stabiliser was added to the material. In another study of the mechanical properties of electron beam irradiated henequen fibre, the tensile strength and thermal stability were both found to decrease with an increasing dose of radiation.

The bonded electrical resistance strain gauge has been the most powerful tool used in experimental stress analysis since the 1940's, as it is one of the most accurate, sensitive, versatile and easy-to-use sensors. Bulk silicon strain gauges were reported by Khahifirooz et al. [119] to have some disadvantages such as poor flexibility, high fabrication costs and leakage of current. These "semiconducting strain gauges" have sensitivity (gauge factor) at least in an order of magnitude greater than their metallic counterparts. Thus, the development of improved thin film semiconductor strain gauges is of interest for their high sensitivity and good flexibility while having low fabrication costs, and this is one focus of the work reported in this thesis.

1.5 Summary of Chapter Topics

In summary, the modification of the chemical structures of polymers induced by ion-beam irradiation has been investigated by several groups [20, 26-29]. Although numerous studies of chemical structure modification induced by ion-beam irradiation have been reported in the literature, there are few FTIR studies which provide quantitative analysis or an examination of the effect of heat treatment (annealing) on the chemical structural evolution. The impact of chemical structure change on the electrical transport properties of the irradiated polymer assist in establishing the relationship between the chemical structures of the precursor polymer and favourable irradiation conditions. Chapter 3 seeks to provide an insight into the evolution of the microstructure of PMDA-ODA and BTDA-ODA polyimides following Cu^{3+} ion-beam irradiation. PMDA-ODA and BTDA-ODA were chosen because their physico-chemical properties are well characterised. In Chapter 3 the structure evolution after ion-beam irradiation has been analysed by both Attenuated Total Reflectance Fourier Transform Infrared spectroscopy (ATR-FTIR) and X-ray Photoelectron Spectroscopy (XPS), along with a study of the effect of annealing when the irradiated films were heat treated at different temperatures.

The energy transfer from the incident Cu^{3+} ion-beam to the polymer contributes to modification of the microstructure of the irradiated polyimide. This is manifested as a change in the mechanical and thermal stability of the polyimide film which has been characterised over a wide temperature range. In addition, the glass relaxation process in the polymer has also been examined.

Chapter 4 focuses on a study of the change in polyimide (PMDA-ODA) electrical transport properties under different conditions after ion beam irradiation.

Chapter 5 focuses on exploring the impact of ion beam irradiation on the electro-mechanical properties of the PMDA-ODA polyimide by investigating how the energy loss mechanism involved in modification of chemical structure, and electrical transport properties, impacts on the micromechanical properties, particularly with regard to applications in strain gauges.

1.6 References

1. Zheng, L., *X-ray Characterizations of Polyethylene Polyhedral Oligomeric Silsesquioxane Copolymers*. *Macromolecules*. 2002. 35:p. 2375.
2. Haddad, T., Lichtenhan, J., *Hybrid Organic–Inorganic Thermoplastics: Styryl-Based Polyhedral Oligomeric Silsesquioxane Polymers*. *Macromolecules*. 1996. 29:p. 7302.
3. Davenas, J., Boiteux, G., *Ion Beam Modified Polyimide*. *Advanced Materials*. 1990. 2:p. 521.
4. Loh, I., Oliver, R., Sioshansi, P., *Conducting Polymers by Ion Implantation*. *Nuclear Instruments and Methods in Physics Research Section B: Beam Interactions with Materials and Atoms*. 1988. 34:p. 337.
5. Brown, W., ed. *Radiation Effects in Insulators*. Wilson, I.H., Webb, R.B., ed. Gordon-Breach: New York. 1986.
6. Svorcik, A., *Influence of Iodine Implantation on the Properties of Polypropylene*. *Applied Physics Letters*. 1992. 61:p. 1168.
7. Lee, E.H., *Ion Implantation Effects*. *Journal of Materials Research*, 1994. 9:p. 1043.
8. Suzuki, Y., Kusakabe, M., Iwaki, M., *Surface Modification of Polystyrene for Improving Wettability by Ion Implantation*. *Nuclear Instruments and Methods in Physics Research Section B: Beam Interaction with Materials and Atoms*. 1993. 80-81:p. 1067.
9. Sun, Y., Zhu, Z., Li, C., *Correlation Between the Structure Modification and Conductivity of 3 MeV Si Ion Irradiated Polyimide*. *Nuclear Instruments and Methods in Physics Research Section B: Beam Interaction with Materials and Atoms*. 2002. 191:p. 805.
10. Venkatesan, T., *Ion Beam-Induced Conductivity in Polymer Films*. *Journal of Applied Physics* 1983. 54:p. 3150.
11. Davenas, J., *Relation Between Structure and Electronic Properties of Ion Irradiated Polymers*. *Nuclear Instruments and Methods in Physics Research Section B: Beam Interaction with Materials and Atoms*. 1989. 39:p. 754.
12. Davenas, J., *Laser and Ion Beam Processing of Conductive Polyimide*. *Applied Surface Science*, 1989. 36:p.539.
13. Xu, X.L., Myler, U., Simpson, D.J., *Photosynthesis Method for Development of Membranes Using Ion Beam Irradiation of Polyimide Thin Films*, in *Membrane Formation and Modification*. 2000. 10:p. 205.
14. Salvetat, J.P., Costantini, J.M., Brisard, F., *Onset and Growth of Conduction in Polyimide Kapton Induced by Swift Heavy-Ion Irradiation*. *Journals of Physical Review B*, 1996. 55:p. 6238.

15. 'Popok, V.N., *Structure Evolution of Implanted Polymers: Buried Conductive Layer Formation* Nuclear Instruments and Methods in Physics Research Section B: Beam Interactions with Materials and Atoms. 1999. 148:p. 1106.
16. Toulemonde, M., Dufour, C., Paumier, E., *Transient Thermal Process After a High-Energy Heavy-Ion Irradiation of Amorphous Metals and Semiconductors*. Journals of Physics Review B. 1992. 46:p. 14362.
17. Xu. D, Xu, X.L., Du., G.D., Wang, R., Zou, S.C., *Infrared Analysis of the Irradiation Effect in Aromatic Polyimide Films*. Nuclear Instruments and Methods in Physics Research Section B. 1993. 80-81:p. 1063.
18. Hirata, K.Y.S., Narumi, K., Nakajima, Y., Kobayashi, Y., *Non-Linear Effect of Cluster Irradiation on Chemical Modification of Polycarbonate*. Nuclear Instruments and Methods in Physics Research Section B. 2002. 193:p. 816.
19. Mohammad, A., Wahab, I.K., Chang-Sik, H., *Microstructure and Properties of Polyimide/Poly(vinylsiloxane Hybrid Composite Films*. Polymer. 2003. 44:p. 4705.
20. Feurer, T., *Ultraviolet Laser Induced Permanent Electrical Conductivity in Polyimide*. Applied Physics A. 1992. 56:p. 105.
21. Brannon, J.H., Bosise, A.E., Burns, F., and Kaufmann, J., *Chemical transformations of the polyimide Kapton Brought About by Ultraviolet Laser Radiation*. Journal of Applied Physics. 1985. 58:p.2036.
22. Srinivasan, K., *Characterization of Damage Modes in Impacted Thermoset and Thermoplastic Composites*. Journal of Reinforced Plastics and Composites. 1992. 11:p. 141.
23. Davenas, J., *Photon, Beam and Plasma Enhanced Processing*. Golanski, A., ed. Paris. 1987.
24. Davenas. J., Boiteux, G., and Xu, X.L., *Role of the Modifications Induced by Ion Beam Irradiation in the Optical and Conducting Properties of Polyimide*. Nuclear Instruments and Methods in Physics Research Section B. 1988. 32:p. 136.
25. Cella, J., *Degradation and Stability of Polyimides, in Polyimides; Fundamentals and Applications*. Mittal. ed. Marcel Dekker Inc: New York. 1996.
26. Watamori. M., *Change of Hydrogen Concentration after Ion Beam Irradiation on Polyimide Films with 100-400°C Annealing*. Nuclear Instruments and Methods in Physics Research Section B: Beam Interaction with Materials and Atoms, 2006. 249:p. 4.
27. Oshima, A., *Manufacture of UV-Resistant Fibre-Reinforced Composites for Conveying Parts*. (Nisseki Mitsubishi Oil Corporation, Japan). Japan. 2001. p. 7.
28. Egusa. S, Kirk, M.A., Birtcher, R.C., *Neutron Irradiation Effects on the Mechanical Properties of Organic Composite Materials*. Journal of Nuclear Materials. 1984. 126:p. 7.

29. Seguchi, T., *New Material Synthesis by Radiation Processing at High Temperature—Polymer Modification with Improved Irradiation Technology*. Radiation Physics and Chemistry. 2002. 63:p. 35.
30. Singh, A., Silverman. J. *Radiation Processing of Polymers.*, Billingham, N.C. eds Polymer International Vol. 34. 236. Hanser, Munich. 1992.
31. Sun, Y., Zhu, Z., Jin, Y., Liu, C., Wang, Z., Liu, J., Hou, M., Zhang, Q., *The Effect of High Energy Electronic Energy Loss on the Chemical Modification of Polyimide*. Nuclear Instrument and Methods in Physics Research Section B: Beam Interaction with Materials and Atoms. 2002. 193:p. 214.
32. Thalacker, V.P., *Radiation Processing of Coatings and Adhesives - An Overview*, International Journal of Radiation Applications and Instrumentation. Part C. Radiation Physics and Chemistry. 1990. 35:p. 18.
33. Lee, S-G., *Fabrication of Carbon/Polyimide Composite by 2-step Compression Molding Process*. Journal of the Korean Fibre Society. 1999. 7:p.364.
34. Zhou, G., Duan, W., Gu, B.L., *First-Principle Study on Morphology and Mechanical Properties of Single Walled Carbon Nanotube*. Chemical Physics Letter. 2001. 333:p. 344.
35. Woods, R. J., Pikaev, A.K., ed., *Applied Radiation Chemistry: Radiation Processing*. New York; Wiley. p 552. 1993.
36. Zhang, W., Suhr, J., Koratkar, N., *Carbon Nanotube/Polycarbonate Composite as multifunctional strain sensors*. Journal of Nanoscience and Nanotechnology. 2006. 6:p. 960.
37. Wypych, G., *Handbook of Fillers*. Vol.2. Chemical Technology. New York. 2000.
38. Wang. S, Ahmad, Z., Mark, J.E., *Polyimide-Silica Hybrid Materials Having Interfacial Bonding Through Use of a Sol-gel Technique*. Macromolecular Reports. 1994. A31:p. 411.
39. kim, K.J., White, J.L., *Particle Orientation in Talc-Filled Thermoplastics Extruded Through Cylindrical, Rectangular and Annular Dies*. Journal of Nano-Newtonian Fluid Mechanics. 1996. 66:p. 257.
40. Pauleau, Y., *Materials and Processes for Surface and Interface Engineering*. Kluwer Academic Publishers. 1995.
41. Yu. X., Kwon, E., *A Carbon Nanotube/Cement Composite with Piezoresistive Properties*. Smart Materials and Structures. 2009. 18:p. 055010 ([doi:10.1088/0964-1726/18/5/055010](https://doi.org/10.1088/0964-1726/18/5/055010)).
42. Kang, I., Schulz, M.J., Kim, J.H., Shanov V., Shi, D., *A Carbon Nanotube Strain Sensor for Structural Health Monitoring*. Smart Materials and Structures. 2006. 15:p. 737 ([doi:10.1088/0964-1726/15/3/009](https://doi.org/10.1088/0964-1726/15/3/009)).
43. Thastenson, E., Chou, T.-W., *Carbon Nanotube Networks: Sensing of Distributed Strain and Damage for Life Prediction and Self/Healing*. Advance Materials. 2006. 18:p. 2837.

44. Tammula, R.R., Rymaszewski, E.J., eds. *Microelectronics' Packaging Handbook*. Van Nostrand Reinhold: New York. 1989.
45. Hoffman, W., in *Physics of Thin Film*, ed. G. Hass, Thun. R.E., Vol. 3. 1966, New York: Academic.
46. Ree, M., Chen, K-J., Kirby, D.P., Katzenellenbogen, N., Grischkowsky, D., *Anisotropic Properties of High - Temperature Polyimide Thin Films: Dielectric and Thermal Expansion Behaviours*. Journal of Applied Physics. 1992. 72:p. 2014.
47. Bouffard, S., Gervais, B., Leroy, C., *Basic Phenomena Induced by Swift Heavy Ions in Polymers*. Nuclear Instruments and Methods in Physics Research, B. 1995. 11:p. 1 ([doi: 10.1016/0168-583X\(95\)00525-0](https://doi.org/10.1016/0168-583X(95)00525-0)).
48. Long, E.R., Long, J., *Spectroscopic Analysis of Radiation-Generated Changes in tensile Properties of Polyetherimide film*. NASA Technical Paper 2429. 1985.
49. Inoue, H., Okamoto H., Hiraoka, Y., *Effect of the Chemical Structure of Acid Dianhydride in the Skeleton on the Thermal Property and Radiation Resistance of Polyimide*. Radiation Physical Chemistry. 1987. 29:p. 283.
50. Brereton, I., Devasahayam, S., Hill, D.J.T., *Towards Identifying the New Structures Formed on the γ -Radiolysis of Ultem*. Radiation Physical Chemistry. 2004. 28:p. 65.
51. Devasahayam, S., Hill, D.J.T., Pomery, P.J., Whittaker, A. K., *The Radiation Chemistry of Ultem at 77 K as Revealed by ESR Spectroscopy*. Radiation Physical Chemistry. 2002. 64:p. 299
52. O'Donnell, J. H., and Sangster D.F., *Principles of Radiation Chemistry*, Arnold. E. London. 1970.
53. Holmes, J.J., Bobbins, R.E., Brimhall, J.L., *Effect of Fast Reactor Irradiation on the Tensile Properties of 304 Stainless Steel*. Journal of Nuclear Material. 1969. 32:p. 330
54. Mittal, K.L., ed., *Polyimides: Synthesis, Characterization, and Applications*. New York, 1984. 2:p. 537. Ghosh, M.K., and Mittal, K.L., ed. *Polyimides Fundamentals and Applications*. Marcel Dekker (1996).
55. Venkatesan,T., Calcagno, L., Elman, B.S., Foti, G., *Ion Beam Modification of Materials*. Arnold, G.W., and Mazzoldi, P., ed. Elsevier: Amsterdam. 1987.
56. Bodo, P., Sundgren, J. E, *Handbook of Deposition Technologies for Films and Coatings*. Journal of Vacuum Science Technology A6. 1988: p. 2396.
57. Bachman, B. J., *Polyimides in Proceedings*, 1st Europe Technical Symposium 1989. Paris, Montpellier.
58. Svorcik,V., *Polyimide Modified by Irradiation with C⁺ and N⁺ Ion Beams*. Polymer Degradation and Stability. 1999. 65:p. 131.
59. Joseph, B. Lambert, H.F.S., Lighter D.A., and R. Graham Cooks, *Organic Structural Spectroscopy*. New Jersey United States of America: Prentice-Hall, Inc. 1998.

60. Feurer, T., Sauerbrey, R., Smayling, M.C., Story, B.J., *Ultraviolet Laser Induced Permanent Electrical Conductivity in Polyimide*. Applied Physics A. 1993. 56:p. 275.
61. Zhu, Z, Sun, Y., Liu, C., Liu, J., Jin, Y., *Chemical Modification of Polymer Films Induced by High Energy Heavy Ions*. Nuclear Instruments and Methods in Physics Research Section B: Beam Interaction with Materials and Atoms. 2002. 193:p. 271.
62. Devasahayam,S. Hill, D.J.T., Connell, J.W., *FT-Raman Studies of a Range of Polyimides Subjected to High Energy Radiation at Room and Elevated Temperatures*. Journal of Applied Polymer Sciences. 2006. 101:p.1575.
63. Magudapathy, P., Gangopadhyay, P., Panigrahi, B.K., Nair, K.G.M., Dhara, S., *Electrical Transport Studies of Ag Nanoclusters Embedded in Glass Matrix*. Physica B 2001. 299:p142.
64. Todoroki, A., Tanaka, M., Shimanura, Y., High Performance Estimation of Delamination of Graphite/Epoxy Laminate with Electrical Resistance Change Method. Composites Science and Technology. 2003. 63:p.1911.
65. Ezquerro, T.A, Roy, S., Kulescza, M., Fernandes-Nascimento, J., Balta-Calleja, F.J., *Alternating-Current Electrical Properties of Graphite, Carbon-Black and Carbon-Fibre Polymer Composites*. Composites Science and Technology. 2001. 61:p. 903.
66. Mora-Huertas, N., *Functional Thin Film Polyimide Nanocomposites*, in School of Applied Sciences. RMIT University: Melbourne. 2005:p. 209.
67. Jagur-Grodzinski, J., *Electronically Conductive Polymers for Advanced Technologies*. 2002. 13:p. 615.
68. Nakamura, S., Tomimura, T., *Temperature Dependence of Resistivity of Carbon Black-Polyethylene Composites Below and Above the Percolation Threshold in Dielectric Materials, Measurements and Application*. IEEE Conference Publication. 2000. p. 265.
69. Ahmed, S., Jones, F. R., *A Review of Particulate Reinforcement Theories for Polymer Composites*. Journal of Material Science. 1990. 25:p. 4933.
70. Strumpler, R., Glatz-Reichenbach, J., *Conducting Polymer Composites*. Journal of Electro Ceramics. 1999. 3:p. 329.
71. Rao, Y., Ogitani, S., Kohl, P., Wong, C.P., *Novel Polymer-Ceramic Nanocomposite Based on High Dielectric Constant Epoxy Formula for Embedded Capacitor Application*. Journal of Applied Polymer Science. 2001. 83:p. 1084.
72. Wong, C. P., Luo, S., *Study on the Effect of Carbon Black on the Behaviour of Conductive Polymer Composite with Positive Temperature Effect*. IEEE Transactions on Component and Packing Technology 2000. 23:p. 151.
73. Glatz-Reichenbach, J., Strumpler, R., *Conducting Polymer Composites*. Journal of Electroceramics. 1999. 3:p. 329.
74. Yung, W.K.C., Jillek, W., *Embedded Components in Printed circuit Board: A Processing Technology Review*. International Journal of Manufacturing Technology, 2005. 25:p. 350.

75. Maier, G., *Low Dielectric Constant Polymers for Microelectronics*. Progress in Polymer Science. 2001. 26: p. 3.
76. Wong, C. P., Luo, S., *High-Dielectric Polymer Composites Containing Conductive Materials and Their Preparation*, in Georgia Tech Research Corporation. Georgia USA. 2002.
77. Wong, C. P., Luo, S., *Novel Polymer Ultra-High Dielectric Constant Polymer Based Composite Development for Embedded Capacitor Application*. in 4th Proceedings of Electronics Packing Technology Conference. Singapore. 2002.
78. Satoo, J., Suzuki, H., Makino, D., *Polyimide for Semiconductor Application*, in Polyimide, ed. Stenzenberger, H.D., Wilson, D., and Hergenrother. P.M., 1990. London: Blackie.
79. HD-Microsystems, product information, Pyralin PI2525, PI2555, PI2572, and PI2556. 2001.
80. Feger, C., Franke, H., *Polyimides in High Performance Electrical Packing and Optoelectronic Application, in Polyimides; Fundamentals and Application*. Mittal, K.L. ed. 1996, Marcel Dekker Inc: New York. p. 769.
81. Dine-Hart, R. A., Wright, W. W., *Thermal Stability of Aromatic Polyimide. Factors Affecting the Oxidative Stability of Poly-N,N'-(4,4'-diphenyl ether) Pyromellitimide*. British Polymer Journal. 1971. 3:p. 163.
82. Neuhaus, H.J., *Electronic Conduction in Polyimides*. Massachusetts Institute of Technology Department of Physics. 1989.
83. Hughes, A.E., Wilson, I.H., *Radiation Effect in Insulators 3*, ed. Webb. R.B., Goron-Breach. New York. 1986
84. Lee, E.H., Rao, G.R., Lewis, M.B., Mansur, L.K., *Ion Implantation Effects*. Journal of Material Resistance. 1994. 9:p. 1043.
85. Loh, I.H., Oliver, R.W., Sioshansi, P., *Conducting Polymers by Ion Implantation*. Nuclear Instruments and Methods in Physics Research Section B: Beam Interactions with Materials and Atoms. 1988. 34:p. 295.
86. Suzuki, Y., *Surface Modification of Polystyrene for Improving Wettability by Ion Implantation*. Nuclear Instruments and Methods in Physics Research Section B: Beam Interactions with Materials and Atoms. 1993. 80-81:p. 729.
87. Marletta, G., *Chemical Reactions and Physical Property Modifications Induced by keV Ion Beams in Polymers*. Nuclear Instruments and Methods in Physics Research Section B: Beam Interactions with Materials and Atoms. 1990. 46:p. 295.
88. Bertrand, P., *Metastable Decay of Molecular Fragment Ions Sputtered From Hydrocarbon Polymers under keV Ion Bombardment*. International Journal of Mass Spectrometry. 1999. 18:p. 217.
89. Benninghoven, A., Nihei, Y., Shimizu, R., Werner, H. W., *Secondary Ion Mass Spectrometry*. Wiley. 1987.
90. Demirev, P.A., *Mass Spectrometry Review*, 1995. 14:p. 279.

91. Leggett, G.J., Vickerman, J.C., *Sample Charging During Static SIMS Studies of Polymers*. Applied Surface Science. 1995.84:p. 253
92. Hoogerbrugge, R., Kistemaker, P.G., *Analytical Expressions for the Internal and Kinetic Energy Distributions of Sputtered Clusters and Molecules*. Nuclear Instruments and Methods in Physics Research Section B: Beam Interactions with Materials and Atoms. 1987. 21:p. 37.
93. Urbassek, H.M., *Sputtering of Molecules*. Nuclear Instruments and Methods in Physics Research Section B: Beam Interactions with Materials and Atoms. 1987. 18:p. 587.
94. Schumann, M. Sauerbrey, R., Smayling, M. C., *Permanent Increase of the Electrical Conductivity of Polymers Induced by Ultraviolet Laser Radiation*. Applied Physics letter. 1991. 58:p. 502.
95. Davenas, J., *Laser and Ion Beam Processing of Conductive Polyimide*. Applied surface science. 1989. 36:p. 539.
96. Raffel, J. I., Freidin, J. F., Chapman, G. H., *Laser-Formed Connections Using Polyimide*. Applied Physics letter. 1983. 42:p. 705
97. Feurer, T., Sauerbrey, R., Smayling, M.C., Story, B.J., *Ultraviolet-Laser-Induced Permanent Electrical Conductivity in Polyimide*. Journal of Applied Physics A: Materials Science & Processing. 1993. 56: p. 275.
98. Huertas, N.E.M., *Functional Thin Film Polyimide Nanocomposites*. School of Applied Sciences, Engineering and Technology Portfolio, RMIT University Melbourne. 2005.
99. Chang, G.S., Jung. S.M., Lee, Y.S., Choi, I.S., Whang, C.N., Woo, J.J., Lee, Y.P., Marletta, G., Fera, G., Pignataro, S., *Adhesion Enhancement of Ion Beam Mixed Cu/Al/Polyimide*, Journal of Applied Physics. 1997. 81:p. 135.
100. Wang, Y., Mohite, S.S., Bridwell, L.B., Giedd, R.E., Sofield, C.J., *Modification of High Temperature and High Performance Polymers by Ion Implantation*. Journal of Material Resistance. 1993. 8:p. 388.
101. Hioki, T., Noda, S., Sugiura, M., Kakeno, M., Yamada, K., and Kawamoto, J., *Electrical and Optical Properties of Ion Irradiated Organic Polymer Kapton H*. Applied Physics letter. 1983. 43:p. 30.
102. Phillips, H.M., D. L. Callahan, D.L., Sauerbrey, R., Szabó, G., Bor, Z., *Sub 100 nm Lines Produced by Direct Laser Ablation in Polyimide*. Applied Physics Letter. 1991. 58:p. 2761.
103. Phillips, H.M., D. L. Callahan, D.L., Sauerbrey, R., Szabó, G., Bor, Z., *Femtosecond excimer-Laser-Induced Structure Formation on Polymers*. Applied Physics A. 1992. 54:p. 158.
104. Chu, A.-S., Zaidi, S. H., Torres, A. B., Brueck, S. R. J., Draper, B. L., *Submicron Electrically Conducting Wires Produced in Polyimide by Ultraviolet Laser Irradiation*. in OSA Annual Meeting Technical Digest. 1992

105. Schumann, M., Sauerbrey, R., Smayling, M.C., *Lasers in Surface Engineering*. Applied Physics letter. 1991. 5:p. 428.
106. Feurer, T., Sauerbrey, R., Smayling, M.C., Story, B.J., *Lasers in Surface Engineering*. Applied Physics A. 1993. 56:p. 275.
107. Angelié, C., Capitini, R., Girard, P., *Longitudinal Mode Selection by Injection in a High Pressure CO2 Laser*. Applied Optics. 1987. 26:p. 396.
108. Garnier, F., *Thin-Film Transistor Based on Organic Conjugated Semiconductors*. Chemical Physics. 1998. 227:p. 253.
109. Van der Putten, D., Brom, H.B., Brokken-Zijp, J.C.M., Michels, M.A.J., *Evidence for Super Localization on a Fractal Network in Conductive Carbon-Black-Polymer Composite*. Physical Review Letters. 1992. 69:p. 494.
110. Migahed, M.D., M.Ishra, T.F., Barakat, A. *Preparation, Characterisation and Electrical Conductivity Polypyrrole Composite Films*. Polymer Testing, 2003. 5:p. 1.
111. Roy, R., Digar, M., Bhattacharya, S.N., Journal of Applied Physics A: Condensed Matter. 1991. 3:p. 7849.
112. Paul, A., Sarkar, D., Misra, T.N., *Electrical Properties of Organised Assemblies of Pyrrole-N-methylpyrrole Copolymer in Langmuir-Blodgett films*. 1993. 227:p. 105.
113. Courtney, T.H., *Mechanical Behaviour of Materials*. McGraw-Hill Publishing Company. Virginia. 1990.662.
114. Zenkiewicz, M., *Effect of Electron-Beam Irradiation on Some Mechanical Properties of Polymer Films*. Radiation Physics and Chemistry. 2003. 69:p.77
115. Horng, P., Klemchuk, P.P., *Stabilizers in Gamma-Irradiation Polypropylene*. Plastics Engineering. 1984. 4:p.84.
116. Klemchuk, P.P., *Protecting Polymer Against Damage From Radiation*. Radiation Physics and Chemistry. 1993. 41:p.165.
117. Williams, J.L., *Stability of Polypropylene to Gamma Irradiation in: Radiation Effects on Polymers*. ed. R.L. Clough and S.W. Shalaby. 1991. 4:p.554.
118. Khakifirooz, A. Mohajerzadeh, S.S. Shafiiha, R., *A Miniaturized Thin Film Germanium Strain Gauge*. Microelectronics. 1999. ICM '99. The Eleventh International Conference.p: 71.
119. Balanzat, E., Betz, N., Bouffard, N., *Swift heavy ion modification of polymers*. Nuclear Instrumentation and Method in Physics Research Section B: Beam Interaction with Materials and Atoms. 1995. 105:p. 46
120. Rajulu, A.V., *Infrared Spectroscopy Investigation of Polymethyl methacrylate/Polyvinyl Chloride Blends Films Irradiated by a 28Si Ion Beam*. Nuclear Instrumentation and Method in Physics Research Section B: Beam Interaction with Materials and Atoms. 1999. 5:p. 195

- 124 Richards, J. A., Sears, F. W., Wehr, M. R., Zemansky, M., *Modern University Physics: Fields, Waves, and Particles Part 2*. Addison Wesley Publishing company, Inc. London. 1960.
- 125 Murugaraj, P. Mainwaring, D., Siegele, R., *Electron Transport Properties of Irradiated Polyimide Thin Films in Single Track Regime*. Applied Physics Letters. 2009. 94:p. 122101.

2

MATERIALS AND METHODS

2.1 Introduction

Ion beam irradiation is a process by which effective modification of the chemical structure and microstructure of a polymer can be achieved. Ion beam irradiation is of great interest since the beam can be focused to influence a very small region of the polymer. In this work, two polyimides with similar chemical structures (PMDA-ODA and BTDA-ODA) were irradiated with a Cu^{3+} ion-beam over a wide range of ion fluences. Several factors are expected to increase the permeability of the polymer, such as the polymer type, the ion-beam type and energy, and the time of exposure. To reproducibly modify the polymer surface and to alter the electrical and mechanical properties of the irradiated region, a systematic investigation was carried out on the effect of ion-beam irradiation on the chemical structure and microstructure of the polymer. The investigation concentrated on understanding the change in the chemical structure caused by ion-beam irradiation, and the resulting effect on the electrical, mechanical and electromechanical behavior of the polymer. Specifically, the effect of the ion-beam modification on the polymer structure was studied to examine any possible rearrangement of the chemical bonds and the loss of volatiles [1-7].

Polyimides, in particular PMDA-ODA and BTDA-ODA, were selected because they were commercially available and well characterized, and they had excellent potential for applications as sensor materials. The essential experimental approach was to

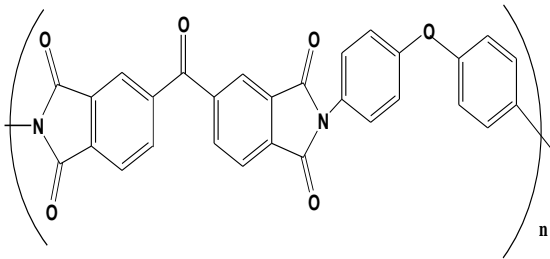
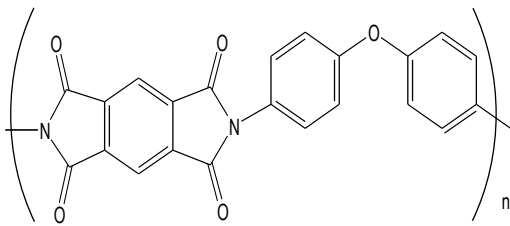
homogeneously irradiate the PI films under an inert atmosphere, and then characterise the ion-beam induced modification of the film via its infrared spectrum, electrical conductivity, mechanical properties and electromechanical properties. For the experimental set-up used in these studies, the thin films consisted of an irradiated layer which penetrated to about 10 % of the film thickness, with the remaining 90 % (the un-irradiated, underlying layer) acting as a substrate. The choice of research method was based on the “particle dispersed *in situ* method” reported for forming polyimide composites, and closely followed the study of carbon-PI composites reported by Huertas et al. [17]. An example of this process has been reported for studying the onset and growth of conduction in a PI film which was subject to high-energy ion-beam irradiation [7]. This project focuses on a study of the effect of Cu^{3+} ion-beam irradiation of PMDA-ODA and BTDA-ODA thin films.

This chapter describes the experimental methods used to characterize the properties of the polymer prior to, and following, ion-beam irradiation. ATR-FTIR and XPS studies were carried out to analyse the change in chemical structure induced by ion-beam irradiation. The change in the microstructure was determined by the depletion of hydrogen and nitrogen atoms, and rearrangements of bonds and atoms of the polyimide films. The fabrication and preparation of the polyimides are discussed in section 2.2.1 and the irradiation conditions are discussed in section 2.2.4. The irradiated films were prepared by an *in situ* method.

2.2 Materials

Two polyimides (PMDA-ODA and BTDA-ODA) were examined in this work, and the results were used to provide a theoretical basis for understanding the mechanism of reaction that occurs between the irradiation ion and polymer. The chemical structure and physical properties of each polyimide are presented in Table 2.1.

Table 2.1: Chemical structure and physical properties of each polyimide.

Repeat Unit Structure	Polymer Properties	
BTDA-ODA	Curing Temperature	295°C
	Tg	325°C
	1% (wt) loss	560°C
	Coefficient of thermal expansion	50 ppm/m°C
	Tensile Strength	130 MPa
	Tensile modulus	2.5 GPa
	PMDA-ODA	Curing Temperature
	Tg	360-4°C
	1% (wt) loss	500°C
	Coefficient of thermal expansion	20 ppm/m°C
	Tensile Strength	231 MPa
	Tensile modulus	2.5 GPa

The polyimide PMDA-ODA was obtained from Dupont, UK. However, the polyimide BTDA-ODA, PI2525 BTDA-ODA was synthesized using the method of Ghosh et.al [8]. The polyamic acid solution (PAA) obtained from HD Microsystems (Parlini, NJ, USA). The monomers (dianhydride and diamines) were purchased from the Aldrich Chemical Company. The solvent, N-methyl pyrrolidine (NMP) reagent grade, was also purchased from the Aldrich Chemical Company. The thin film fabrication process is described in section 2.2.1.

2.2.1 BTDA-ODA PI Thin Film Fabrication Process

The PAA was diluted with NMP (Sigma-Aldrich, St Louis, MO, USA) until the PAA content became 10-12% (w/w). A flowchart of the fabrication process is shown in Figure 2.1. Three types of films were prepared; one type was a freestanding virgin polyimide film and the other two films were formed by slip casting onto a glass surface, with a thickness of about 40 to 100 microns [7]. Table 2.1 (shown previously) summarizes the properties of the fabricated BTDA-ODA films.

Flowchart in Figure 2.1 shows the step by step preparation of the BTDA-ODA thin films, these steps were as follows: I) Mixing of the PAA precursor into the solvent NMP. II) Mixture was placed in a sonic bath. III) In a fume hood the thin films were cast on mercury inside a dry desiccator. IV) The films were removed from the desiccator and placed between two metal rings before placing them into the vacuum oven to be cured at 250 °C. VI) Pristine BTDA-ODA thin films. This set of films was used in this research project.

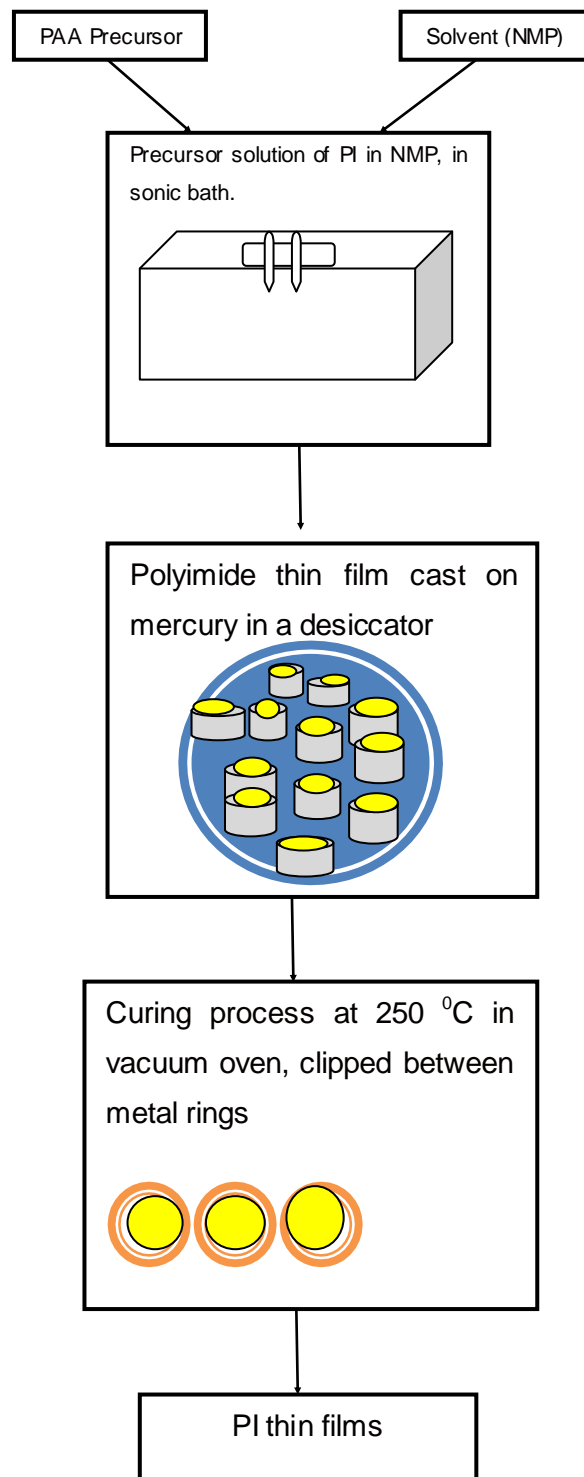


Figure 2.1: The flow chart of BTDA-ODA film fabrication. The PAA viscosity was 3.5 Pa.s and BTDA-ODA concentration was 25% (w/w) in N-methyl pyrrolidinone (NMP) [7].

2.2.2 Film Casting

Free standing and supported BTDA-ODA films were fabricated by slip casting on mercury. The films were cured in a vacuum oven at a temperature of 250°C for 30 minutes. The curing times and temperature are shown in Figure 2.2.

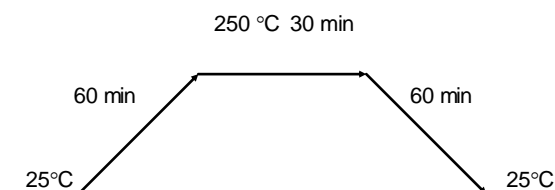


Figure 2.2: Shows a schematic of the time and temperature at which the free standing films were cured in a vacuum oven.

In preparation for irradiation, the polyimide thin film was cast as follows: the polyimide (0.5mL) and NMP (0.5mL) were mixed and the solution placed in a sonic bath for 2 hours at a temperature of 20 °C – 30 °C. The BTDA-ODA PI solution (200 μ L) was then cast over mercury. After formation of the thin films on the surface of the mercury, tweezers were used to remove the films. This was carried out in a fume hood, while appropriate dress code, in gloves, lab coat and safety glasses. Then the films were removed and placed on a doughnut shaped metal ring. Each film was sandwiched between two metal rings were then placed in a desiccators and were moved by the oven. Films were removed from desiccators and placed in the vacuum oven where they were cured at 250 °C.

Accurate measurement of the film thickness is important as it is required for the calculation of electrical conductivity and other electrical properties of the irradiated film. The thickness of the BTDA-ODA films was measured using an ultrasonic thickness gauge

(Alcolmeter, Manchester England). This thickness measurement was not required for the PMDA-ODA as its thickness measurement were sent with it.

The electrical conductivity of the unirradiated BTDA-ODA polyimide has been reported to be 10^{-14} S/cm [7]. Polyimide intermolecular interactions and the ordering of the polymer chain were studied using spectroscopic techniques [21]. Hasegawa *et al.* [9] and Wachsman *et al.* [10] have studied charge transport occurring between donor and acceptor moieties in the PI, where the donor is a segment of the amine phenyl and the acceptor is the diamine [11].

2.2.3 Irradiation

Ion-beam irradiation was performed using the Tandem Accelerator at The Australian Nuclear Science and Technology Organization (**ANSTO**), Lucas Heights, NSW. All irradiation was performed at room temperature within a vacuum chamber at a pressure of 7×10^{-3} mbar.

The accelerator consists of several units as shown in Figure 2.3, the areas labelled 1 to 7 are explained in Table 2.3.

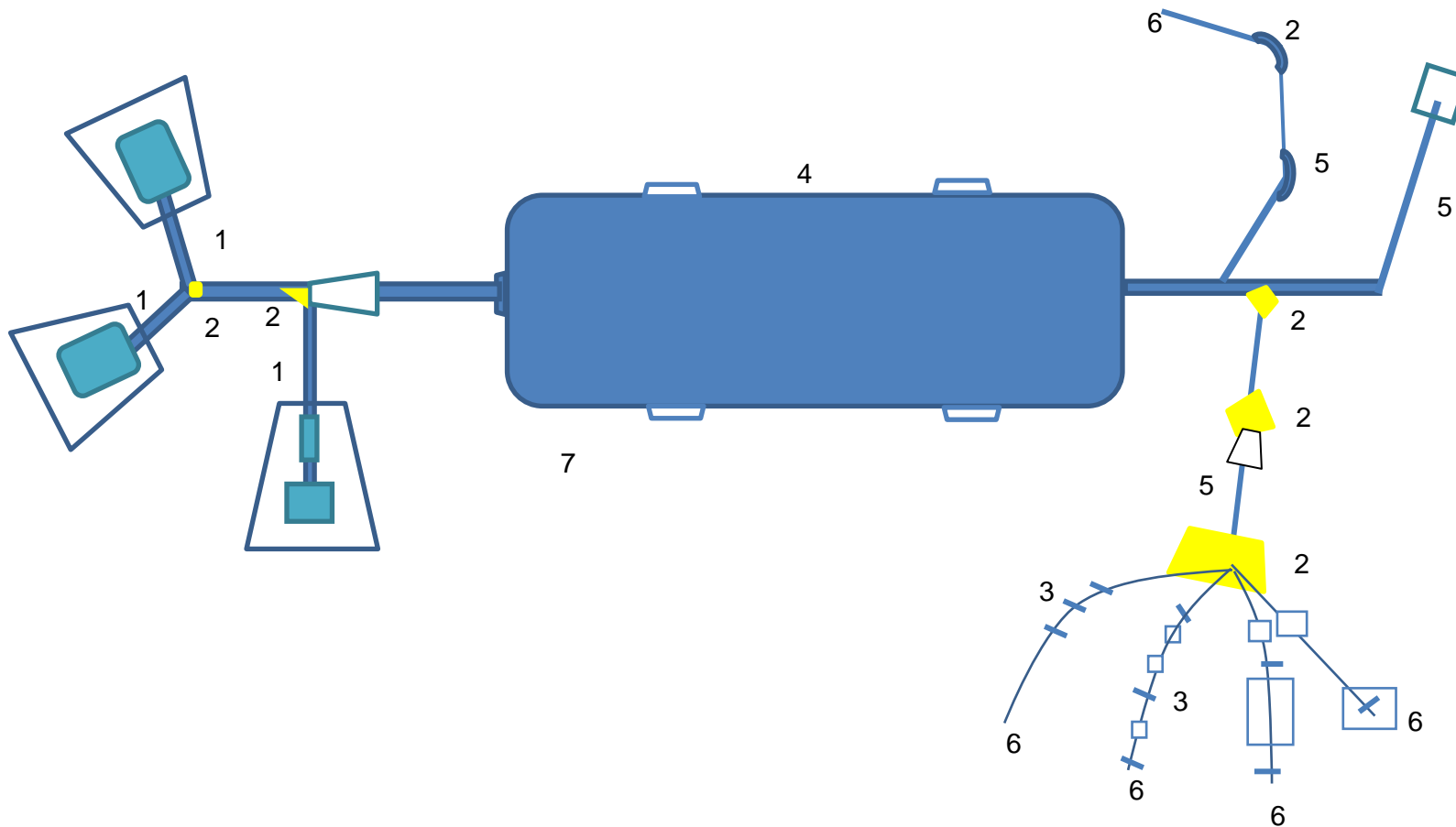


Figure 2.3: shows the tandem accelerator used at ANSTO with its different units.

Table 2.2: shows the various areas and the explanation of their operations.

Area Numbers	Functions /Purpose
1	The ion sources where the ion beam is formed to be accelerated.
2	The magnet
3	The electric analysers, where the ion mass, energy and electrical charge are selected.
4	The voltage accelerator is surrounded by gas insulation in a high pressure vessel,. This high pressure is necessary to stop the high voltage from discharging into the surrounding environment.
5	The beam lines provide a path way along which the ion-beam will travel to its destination whilst being focused directionally.
6	The target is where a high energy beam of the ions are measured and information about the surface targeted is gathered by the beam.
7	The ions used in the accelerator are knocked out of an atom of a sample material in the ion source, and accelerated by an electrostatic field. The ions are deflected by an electromagnet through a precise angle, where ions with specific mass are deflected and the ions with different mass are lost.

To avoid over-heating of the PI samples, an aluminium plate (Figure 2.4) was used to dissipate heat and support the films when irradiating them. The energy of the incident ion-beam was adjusted to ensure that only 10% of the film depth was modified using one type of ion (Cu^{3+}) over a wide range of ion fluences. The variables to achieve each fluence were the current and exposure times. The fluence was calculated, and samples with fluence values ranging from 10^{13} to 10^{14} ions cm^{-2} , were selected for study.

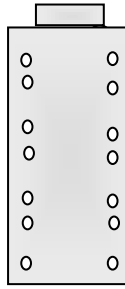


Figure 2.4: Shows the films supported by the aluminium plates for irradiation

The ion beam irradiated polyimide films and their current density and exposure times are summarized in Table 2.4.

Table 2.4: The fluence values achieved and the exposure time and current density.

PMDA-ODA			BTDA-ODA		
Current (nA/cm ²)	Time (sec)	Fluence Ions cm ⁻²	Current (nA/cm ²)	Time (sec)	Fluence Ions cm ⁻²
47.53	1800	1 x10 ¹⁴	52.69	1500	1 x10 ¹⁴
108.09	900	2x10 ¹⁴	54.18	1800	2x10 ¹⁴
114.36	1380	3x10 ¹⁴	63.31	2400	3x10 ¹⁴
120.34	1620	4x10 ¹⁴	51.87	4200	4x10 ¹⁴
102.22	2460	5x10 ¹⁴	53.53	4800	5x10 ¹⁴

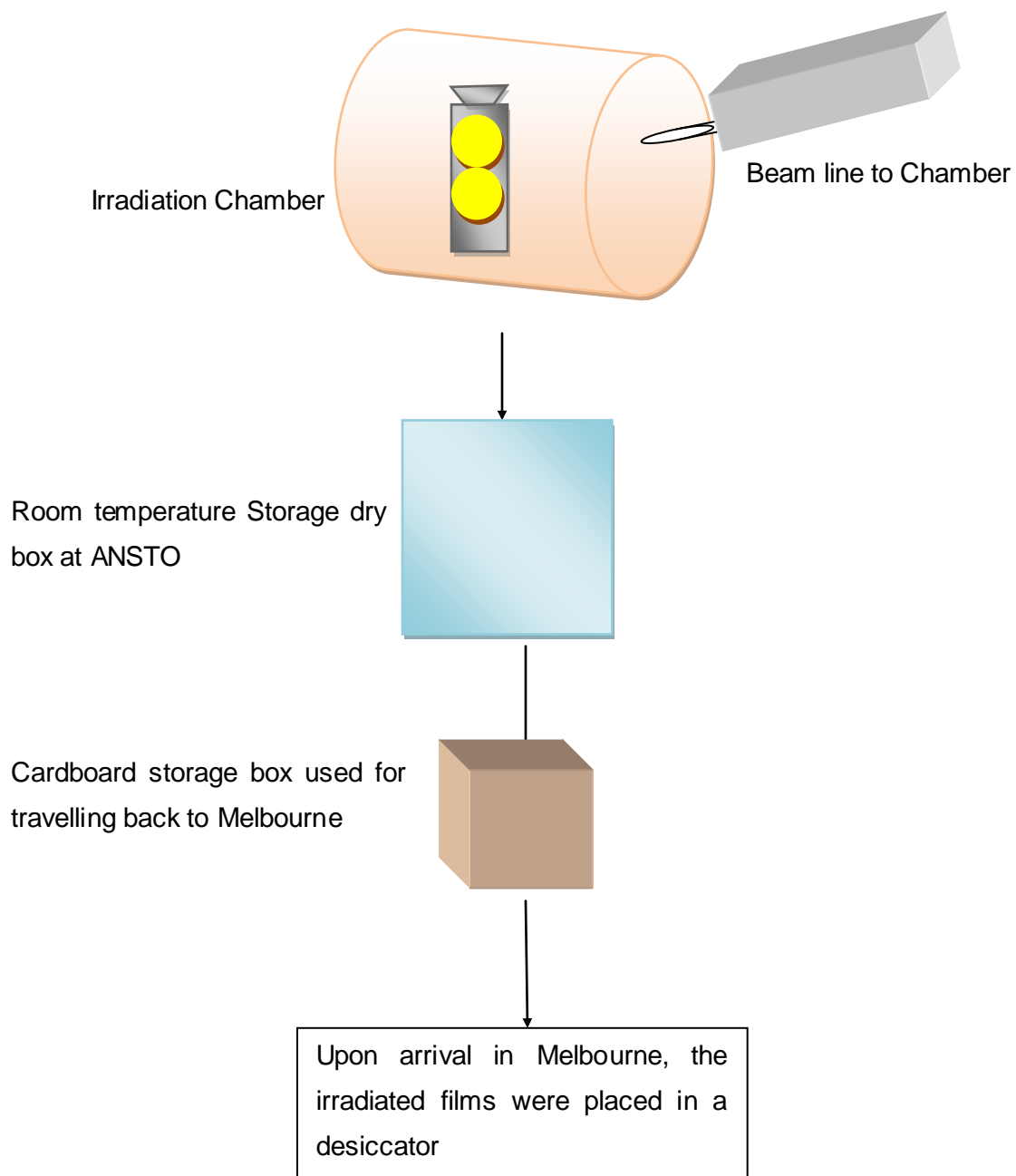


Figure 2.5: presents a schematic diagram of the irradiation process and storage sequence of the films after irradiation.

2.3 Characterisation Techniques

2.3.1 Thermogravimetric Analysis

Thermogravimetric Analysis (TGA) is an analytical technique that is used to determine a material's thermal stability and the fraction of volatiles in the material. These properties are measured by the change in weight that occurs during the heating of the analysed specimens. These analyses can be carried out in air or under an inert atmosphere, such as helium, nitrogen or argon.

There are two different types of TGA, one uses a vertical balance, and the other uses a horizontal balance. The vertical TGA balance, as used at RMIT and shown in Figure 2.6, has a specimen pan hanging from the TGA instrument above the balance on a sample stem. It is important for this type of instrument to be calibrated to compensate for the buoyancy effect due to variation in the density of the purge gas with a change in temperature.



Figure 2.6: Perkin Elmer TGA at RMIT University.

2.3.2 Thermal Stability Properties

The thermal stability behaviour of each sample was measured using a Perkin-Elmer TGA series 7 instrument, shown in Figure 2.6. The samples, with masses ranging from 0.1 to 5mg, were placed in an open platinum pan. The analysis of each sample was performed over the temperature range from 25 °C to 800 °C at a heating rate of 20 °C min⁻¹. To obtain a stable thermal environment at 800 °C the chamber was purged with nitrogen gas. The onset of degradation, at a temperature T_d , and the maximum rate of weight loss under nitrogen, were then determined.

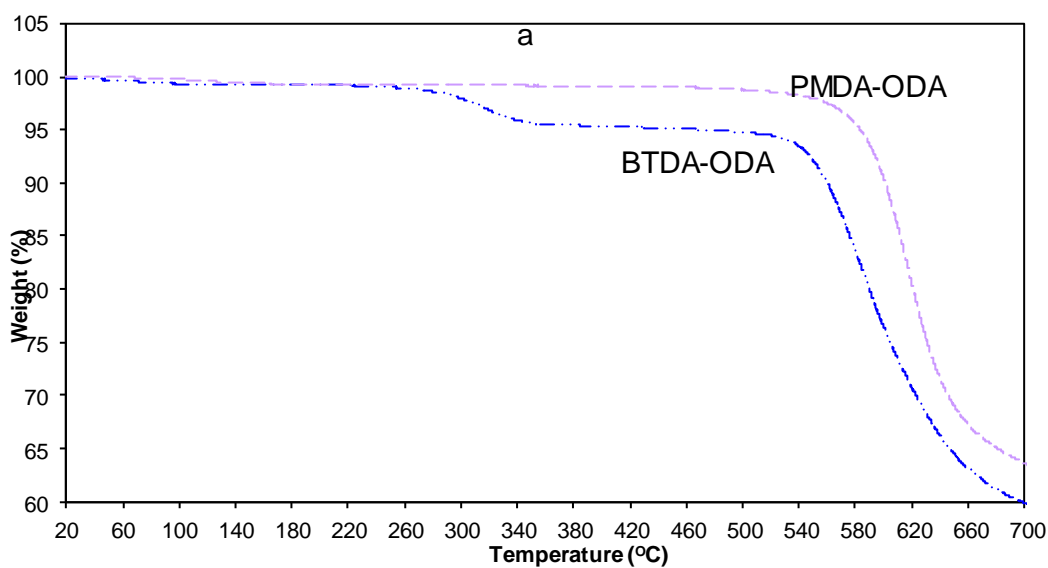
2.3.3 Thermal Stability of Polyimide

The thermal degradation behaviour of the un-irradiated and irradiated polyimide samples were studied using the TGA. The thermal stability of polyimides is generally quite good, as they can withstand temperatures of up to 400 °C, in particular the PMDA-ODA polyimide. The effect of the filler on thermal stability was studied in the composite thin film structure investigation by Cella *et al.* [12], where the thermal stability of the polyimide was found to withstand temperatures between -260 to 600 °C [12]. The un-irradiated and irradiated PI samples were heated from 20 °C to 800 °C under a nitrogen atmosphere at a heating rate of 10 °C/min. The weight loss curves (TGA curves) and the derivative weight loss (%) curves (DTG curve) of PMDA-ODA films changed with varying fluence values.

The TGA curve presented in Figure 2.7 shows that the un-irradiated PMDA-ODA exhibits a small weight loss below 500 °C, in the temperature range of 240 °C to 380 °C, resulting from the evaporation of NMP. The decomposition temperature of the films was obtained from the dw/dt versus temperature plot, where the weight loss was reported to be above 10%. In the un-irradiated PMDA-ODA the weight loss percentage curve showed a steady weight loss of 99.06 wt%, starting at a temperature of 530 °C and ending at 700 °C. The derivative weight loss occurs at a temperature of 620 °C, where a broad and moderate

intensity peak was observed. This one step decomposition between 530 °C to 700 °C is attributed to the break-up of the molecular structure of the polyimide as it is thermally decomposed.

Compared to the pristine BTDA-ODA exhibit a small weight loss below 500 °C where as the PMDA-ODA exhibit no weight loss below 500 °C. The first small weight loss in the BTDA-ODA was observed at 310 °C. This was reported by Cella et.al[12] to be due to small presences NMP in the BTDA-ODA film. The major weight loss was observed to occur at 590 °C. These high weight losses were indicative of the high thermal stability exhibited by these films. The decompositions temperature of the films is obtained from the dw/dt Vs temperature graphs, where the weight loss is above 10%.



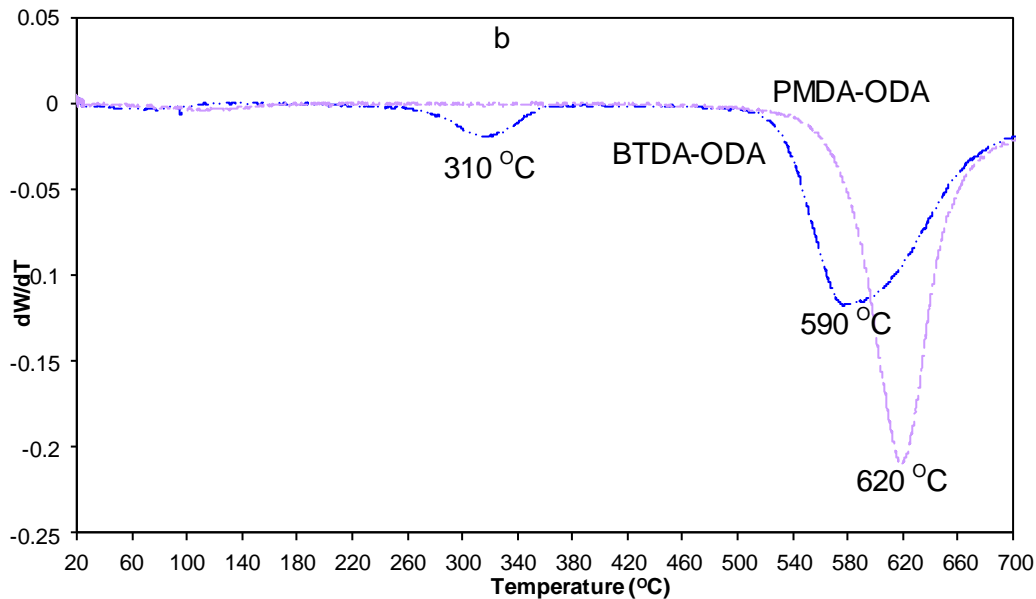


Figure 2.7: (a) and (b) shows the weight loss percentage versus temperature and the derivative weight percentage vs. temperature of PMDA-ODA irradiated thin films.

2.3.4 Drying and Annealing For ATR-FTIR Analysis

The irradiated PI films were heat treated in two stages as shown schematically in Figure 2.8: In stage 1, the *drying* of the polyimide films was performed in three steps, the first step involved the storage of the irradiated films in a dry desiccator, in the second step the irradiated films were heated to 80 °C, at a rate of 20 °C/10min in a vacuum oven, and held at a constant temperature of 80 °C for a period of one hour, then cooled to room temperature at a rate of 1 °C/min. Thirdly, the films were immediately placed in a desiccator and directly taken to the dry oven beside the FTIR. The films were in the dry oven for the duration of the analysis.

In stage 2 of the analysis, the films were placed back in the vacuum oven for *annealing* at a temperature of 100 °C for an hour. Stage 2 was again performed in 3 stages, then the FTIR analysis was promptly performed. The total annealing temperature was 280 °C for each of the films.

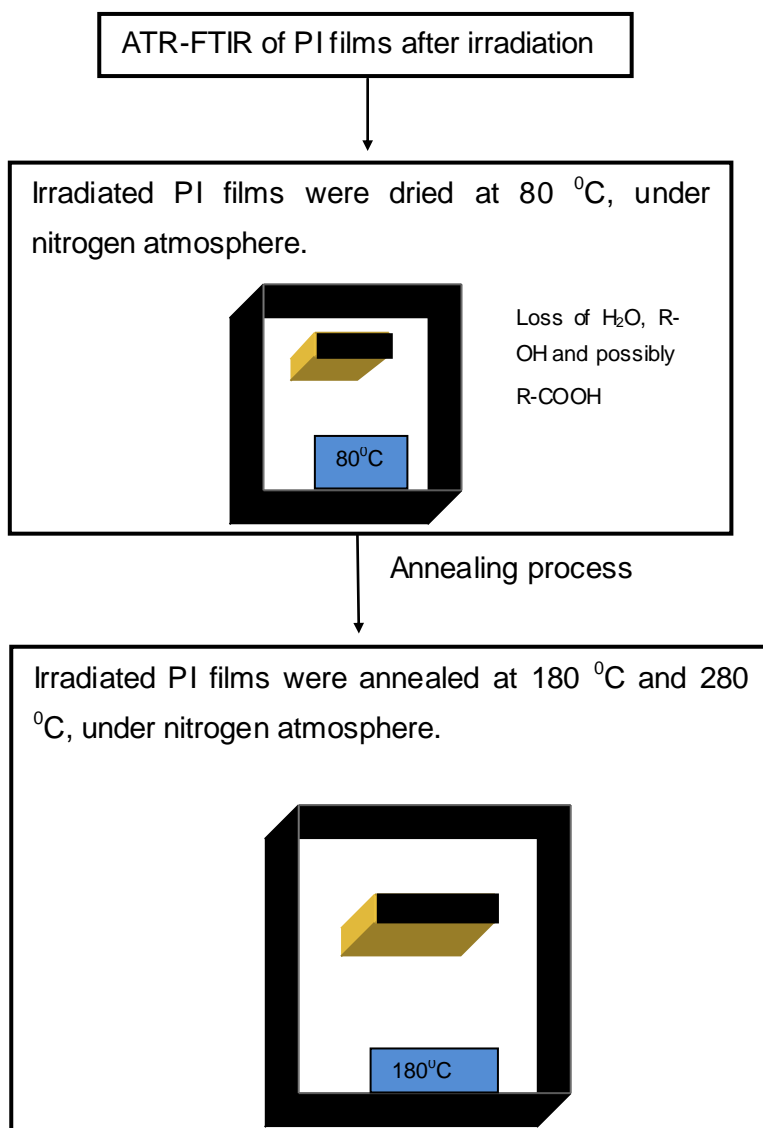


Figure 2.8: Schematic diagram of the drying and annealing process of the films.

2.3.5 Annealing effect on electrical conductivity

The electrical resistance behaviour during the first thermal cycle is higher than in the remainder of the thermal cycles due to possible residual stress formed during preparation processes. Heat treatment of the films removes the possible stress and yields consistent and reproducible behaviour during the following cycles. During the thermal cycling of this semiconductor material, the resistance was found to decrease, thus increasing the electrical conductivity. Therefore, the thermal treatment (or annealing) removes the

stress in the film and provides electrons with sufficient energy to pass through (or hop) from one valence state to another.

2.3.6 Temperature cell (Annealing)

To determine the electrical conductivity, annealing of the irradiated films was carried out at a temperature of 200 °C. A low temperature thermal treatment process of the irradiated film was carried out at temperatures of between 25 °C to 55 °C at a rate of 1 °C/min as demonstrated in Figure 2.9. The time required for each cycle was found to be about 2 hours. This process was essential for the removal of moisture and other volatiles that are adsorbed onto the films. This measurement was carried out in the cell shown in Figure 2.10. [17] under an inert atmosphere.

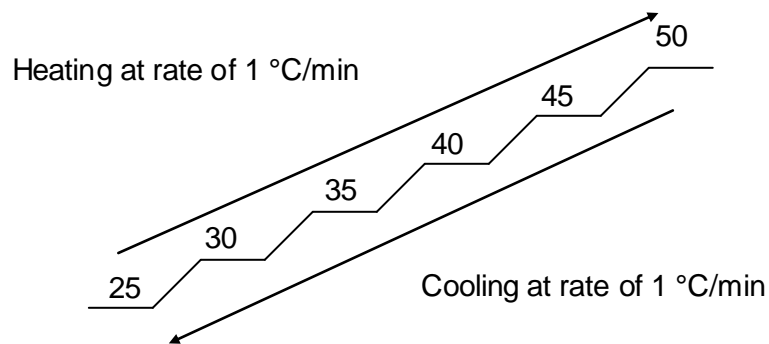


Figure 2.9: The step-by-step heating and cooling cycle of the films.

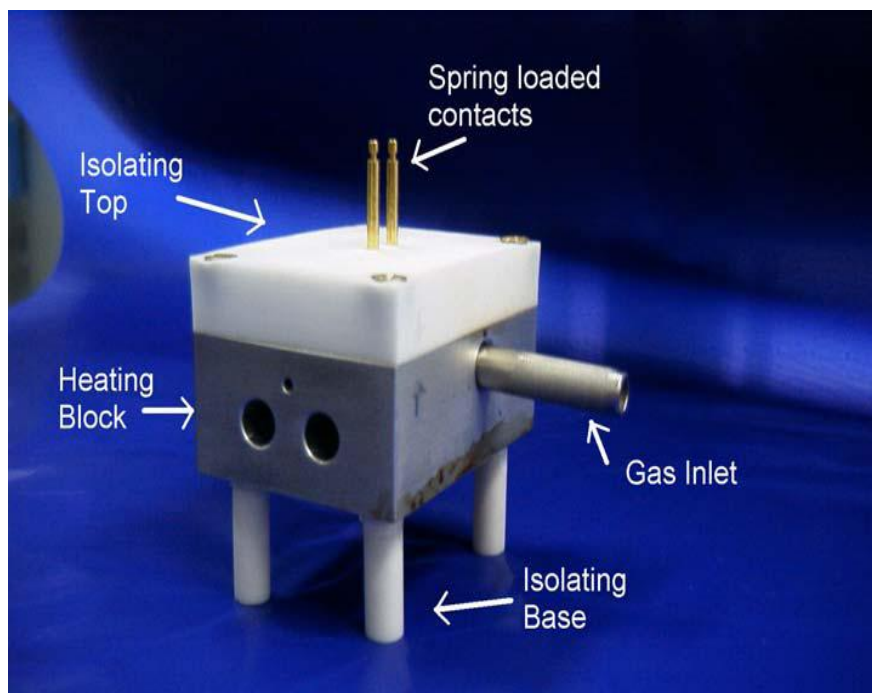


Figure 2.10: Cell [17] used for electrical conductance measurements of irradiated films, under an inert atmosphere, during thermal cycling of the films.

2.4.1 Fourier Transform Infrared and XPS Spectroscopy

Attenuated Total Reflectance Fourier Transform Infrared (ATR-FTIR) spectroscopy was used to study the changes in the chemical structure of the polyimide films following irradiation. All the measurements were performed using a Perkin Elmer FTIR 100 . The use of conventional Fourier Transform Infrared (FTIR) was not possible for two reasons (I) High background (II) Difficulties in compressing the carbonised PMDA-ODA film into a KBr pellet. The ATR-FTIR spectrum is measured by allowing the IR beam to penetrate a few microns into the surface of the irradiated polyimide. In the ATR-FTIR measurement, the evanescent wave produced on total reflection of the incident infrared beam at the prism surface is used to measure the FTIR spectra of the near surface regions of the films. The films were placed in contact with the transparent prism and pressure was applied to the films by the flat surface. The spectra of the films were measured under the same

conditions prior to, and following, ion irradiation to monitor any change of the spectrum induced by ion-beam irradiation. For ATR-FTIR analysis, the change in the amount of each relevant functional group was determined by the area under the peaks in the FTIR spectra. Figure 2.11 show the ATR-FTIR spectrometer setup, the lettering and numbering corresponds to the parts of the ATR-FTIR spectrometer, which are described as follows: Mirrors (M1-M6), Movable Mirrors (MM), Detector (D), Sample Holder (SH), Sample (S) and Prism (P).

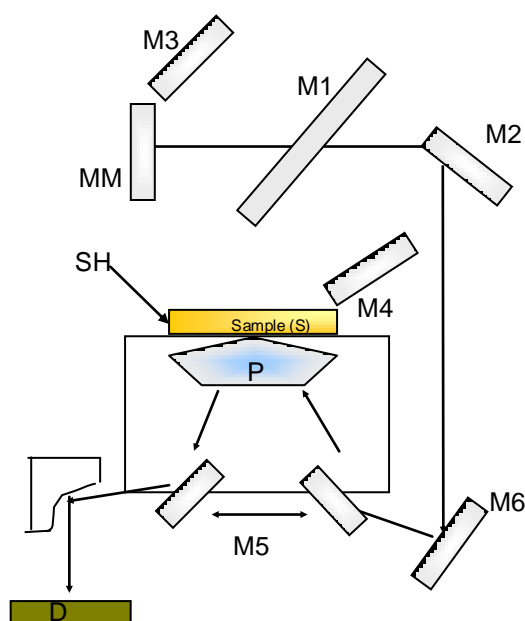


Figure 2.11: ATR-FTIR spectrometer experimental setup. Diagram in this Figure is adapted from Hirata et al. [12] and the Perkin Elmer FT-IR user manual [21].

PMDA-ODA polyimide films of 125 μ m thickness were irradiated with 5.5 MeV Cu^{3+} ions at fluencies of 9×10^{13} , 1×10^{14} , 2×10^{14} , 3×10^{14} , 4×10^{14} and 5×10^{14} ions cm^{-2} . These samples were investigated via ATR-FTIR using an instrument resolution of 32, which was found to give well-defined peaks.

XPS measurements were carried out using a Thermo KAlpha XPS instrument at a pressure better than 1×10^{-9} Torr (1Torr = 1.3336102 Pa) as shown schematically in Figure

3.2. The general scan and C 1s, O 1s, and N 1s core level spectra for the samples were recorded with polychromatic Mg K α radiation (photon energy of 1253.6 eV) at a pass energy of 20 eV, an overall resolution of 0.1 eV, and an electron take off angle of 90 degrees. The core level spectra were background corrected using the Shirley algorithm, and chemically distinct species were resolved using a nonlinear least squares fitting procedure. The core level binding energies (BE) were aligned with a carbon binding energy of 285 eV.

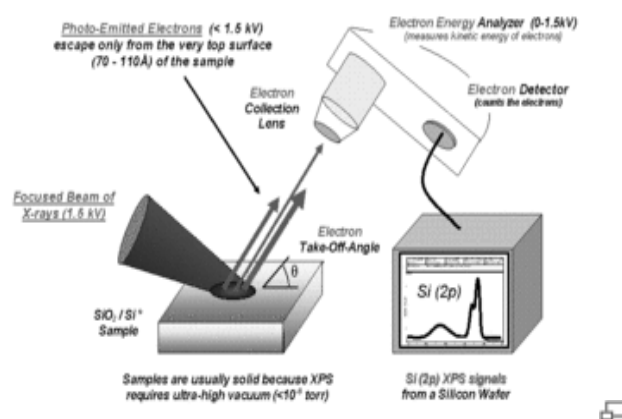


Figure 3.2: Schematic outline of XPS instrumentation.

(http://en.wikipedia.org/wiki/X-ray_photoelectron_spectroscopy)

2.5.1 Measurement of Electrical Resistance of Thin Films

2.5.2 Sample Preparation

All the films were cut into strips with specific dimensions of 2.00 mm in length and 1.56 mm in width, and metallic contacts were applied to eliminate contact resistance. Prior to the application of the contact, the surface of the sample was wiped clean of dust or grease with a soft cloth and ethanol. Silver paint electrodes were then applied and tested for good ohmic contacts in the cell by using the two point method.

2.5.3 Electrodes

Micro Tip™, (SPI Supplies, West Chester, PA, USA) was a commercially available silver epoxy that was used in this study. The silver epoxy was applied to the film surface and allowed to dry at room temperature for a period of 24 hours to achieve good electrical contact.

The electrodes provide two contact points at a distance (L) and of cross sectional area ($A = \text{width} \times \text{thickness}$) on the films, as shown in Figure 2.12

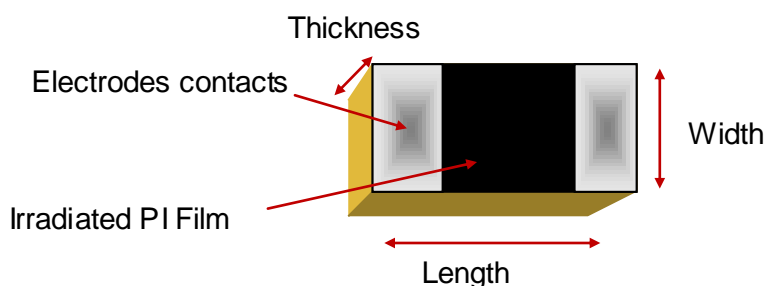


Figure 2.12: The electrodes' contact and shaded area with Thickness, Length and Width.

2.5.4 DC Electrical Resistance Measurement

The electrical resistance of the irradiated polyimide was studied using the two probe method, as suggested in the Handbook of Polymer testing for measurement of polymer resistance [21]. The electrical resistance of carbon-polyimide films was measured across the film and then the resistivity was calculated. The electrical resistivity was obtained using Equation 2.1. [21].

$$\rho = R (A/L) \quad (2.1)$$

Where ρ is the resistivity, R is the resistance of the film, A is the cross-sectional area of the film, and L is the film thickness between the electrodes.

2.5.5 Current-Voltage Measurement

The electrical resistance of each film was measured at different voltages, so as to; (a) evaluate the ohmic behaviour of the metallic contact, and (b) to confirm the sample has a very high resistance. The current (I), voltage (V) and resistance (R) are related via Ohm's law, Equation 2.2 :

$$R = V / I \quad (2.2)$$

Different voltages were applied to different films. Some films required voltages between 1 and 30 V, but because of very high resistance, other samples required voltages of about 170 or 320 V. Figure 2.13 is a schematic diagram of the experimental set up. Similar current-voltage (I - V) experiments were carried out on a carbon nanotube-polyoctylthiophene composite by Valentine et al. [15].

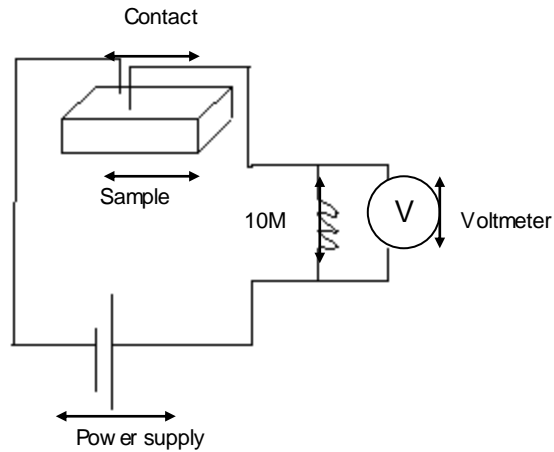


Figure 2.13: Schematic of the current-voltage circuit set-up used for the resistance vs. temperature measurements.

The electrical conductivity conditions were optimised for this research project using a polyimide-glassy carbon composite film. The resultant thermal cycles of electrical conductivity data are shown in Figure 2.14. The Arrhenius plot and the calculated activation energies are shown in Figure 2.15.

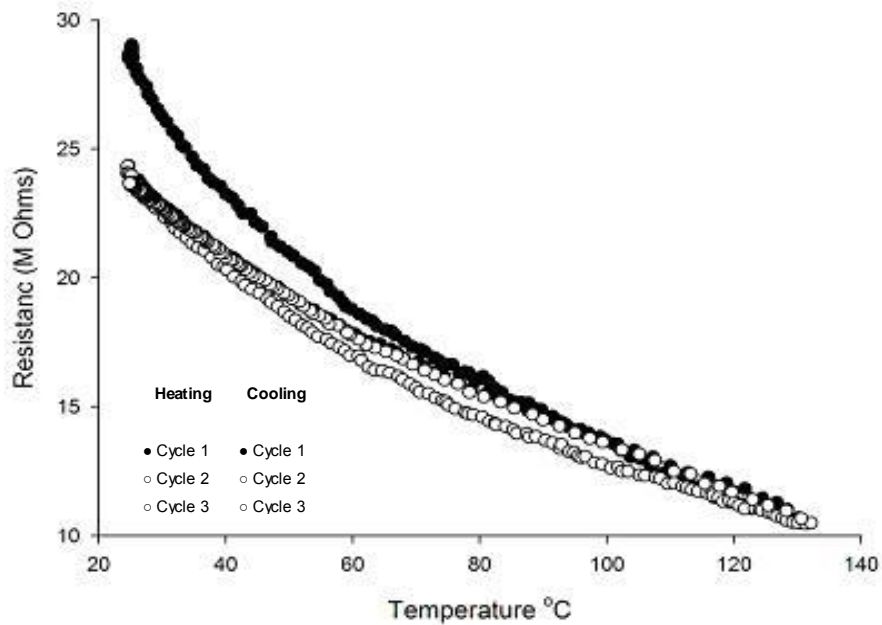


Figure 2.14: Graph of polyimide-glassy carbon thin film composite. The resistance is observed to be decreasing with increasing temperature.

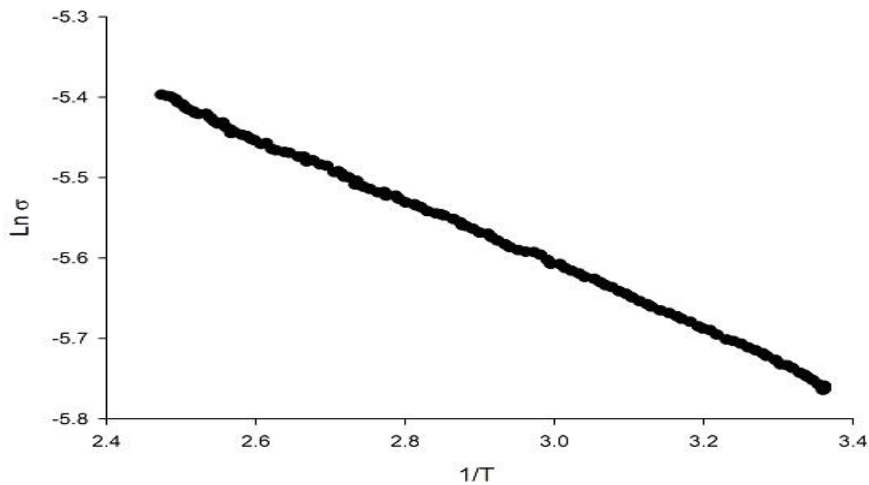


Figure 2.15: An Arrhenius plot which was used to calculate the activation energy (AE) for the polyimide-glassy carbon thin film composite. AE was calculated to be 34.35 meV/K.

The magnitude of the activation energy provides a means of identifying the electron transfer mechanism and it also indicates the energy required for an electron to go from one electron state to another. For example, when an electron is activated it moves from its ground state level to a higher energy empty, or unfilled, level.

2.6.1 Mechanical Measurements

Mechanical analysis is a technique used to measure a material's deformation in response to an applied stress or strain force. A stress-strain curve is obtained by measuring the applied force as a material is continuously elongated at a constant rate of extension until the breaking point of the material is reached. The stress σ is defined in Equation 2.3 :

$$\sigma = F / A \tag{2.3}$$

Where F is the applied force (in Newton) and A is the cross-sectional area of the material (m²).

A typical stress-strain curve is shown in Figure 2.16. The slope of the curve in the elastic linear region is termed the elastic or shear modulus (also called Young's modulus, symbol E), which is a measure of the stiffness of the material analysed, and is defined by

$$E = \sigma / \epsilon \quad (2.4)$$

Where E is the elastic modulus (Pa), σ is the stress (n/m^2) and ϵ is the strain.

The yield stress is the point where the material cross-sectional area begins to decrease, and is a measure of two properties of the material: its strength and its resistance to permanent deformation. The measure of the energy or toughness required to cause failure in the material is given by the total area under the stress-strain curve. The strength required to fracture the material completely is the ultimate strength, which is a measure of the force (stress or strain) required at breaking point.

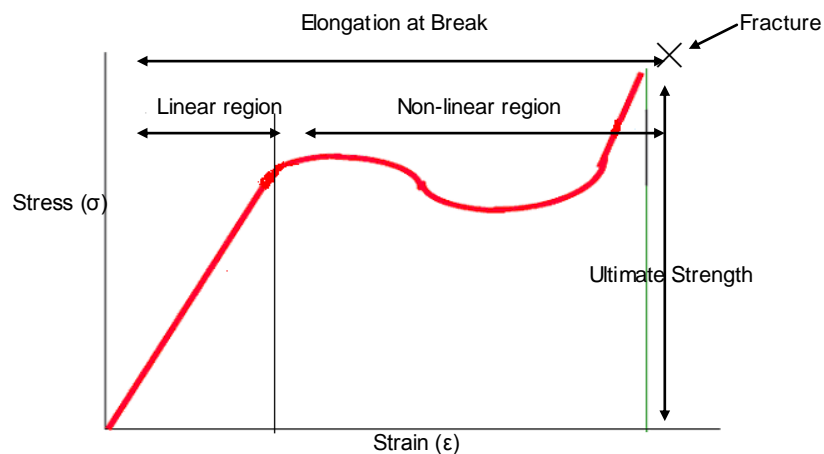


Figure 2.16: General stress-strain curve for polymeric materials adapted from Mernard et al.[16].

2.6.2 Dynamic Mechanical Measurements

A Perkin Elmer-DMA-7e Dynamic Mechanical Analyser (See Figure 2.17) was used to obtain mechanical measurements on the PI films.

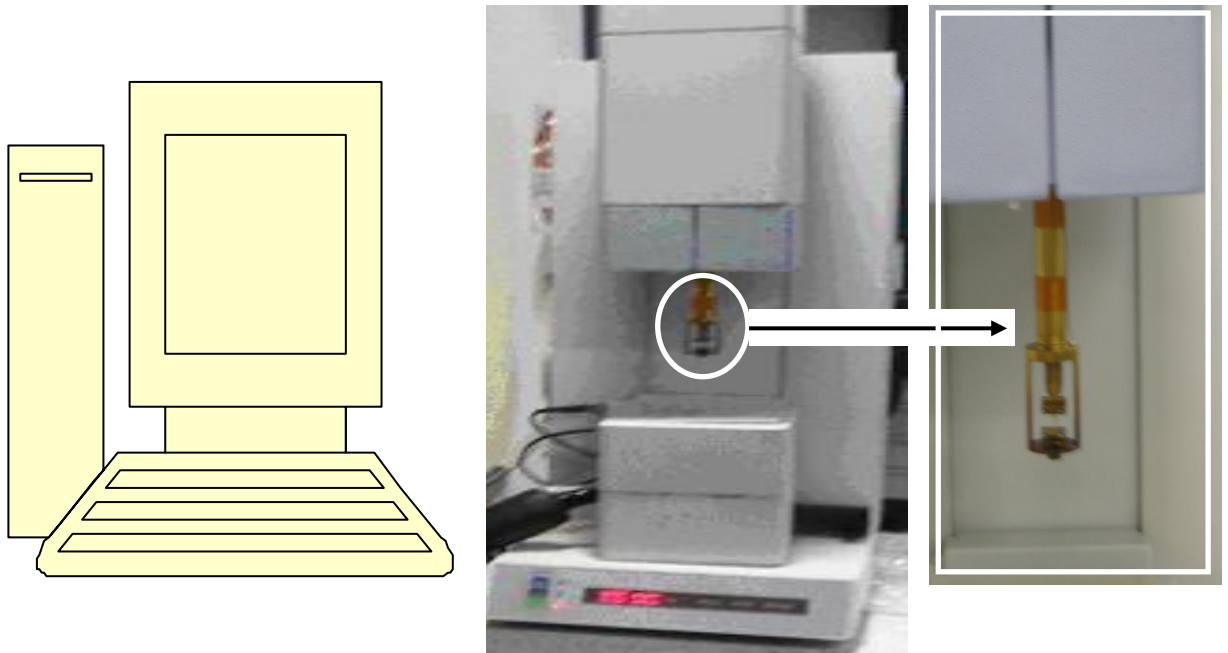


Figure 2.17: The Perkin-Elmer DMA-7e.

Mechanical testing is used to measure the deformation of a material in response to the application of a controlled strain or stress.

Dynamic mechanical analysis (DMA) is a widely used technique for the micromechanical characterization of polymers and polymer composites and gives information about the viscoelastic properties of the polymer. The modulus and damping measurements can be made as a function of temperature, time, frequency and stress or strain. A sinusoidal oscillating stress is applied to a material by a precision motor. A force transducer measures the response stress in the material (flexural, tensile or rotational), which is also in the form of a sinusoidal strain response. The response measured is reproducible if the material analysed is within its linear viscoelastic region, meaning the deformation can be

recovered on the removal of the applied stress force. The applied stress at time t , $\sigma(t)$, is given by Equation 2.5 [16].

$$\sigma(t) = \sigma_0 \sin \omega t \quad (2.5)$$

Where σ_0 is the maximum stress, ω is the frequency of oscillation and t is the time.

The viscoelastic properties of a material determine the shape of the strain wave, thus if the material behaves elastically with applied stress, its response will be in accordance with Hooke's law for an ideal spring, where the elastic component of the strain curve may be described as follows in Equation 2.6 [16]

$$\varepsilon(t) = (\sigma_0/E) \sin(\omega t) \quad (2.6)$$

Where $\varepsilon(t)$ is strain and E is the elastic modulus (Young's modulus). As σ and ε are related to E in the linear region by $E = \sigma / \varepsilon$, Equation 2.6 can be written as Equation 2.7 [16].

$$\varepsilon(t) = \varepsilon_0 \sin(\omega t) \quad (2.7)$$

Where ε_0 is the strain at maximum stress. The sinusoidal in-phase part of the curve for equation 2.7 [16] is illustrated in Figure 2.18 (a). This curve has no lag between the stress and strain curve along the time axis. If the material analysed behaves in a viscoelastic manner with the applied stress, the strain response can be written as follows in Equation 2.8

$$\varepsilon(t) = (\sigma_0 \cos(\omega t)) \quad \text{or} \quad \varepsilon(t) = (\sigma_0 \sin(\omega t + (\pi/2))) \quad (2.8)$$

Where η is the viscosity of the material. Equation 2.8 can also be rewritten as follows in

Equation 2.9 :

$$\varepsilon(t) = \varepsilon_0 \cos(\omega t) \quad \text{or} \quad \varepsilon(t) = \varepsilon_0 \sin(\omega t + (\pi/2)) \quad (2.9)$$

Figure 2.18 (b) shows the strain in the viscoelastic material is out-of-phase with the applied stress. This is due to the materials ability to dissipate part of the deformation through damping, usually as heat, thus delaying the strain response behind the applied stress.

The distance between the peaks of the stress and strain curves is known as the phase lag, which is given as an angle, the so-called phase angle, (due to the trigonometric relationship between the curves).

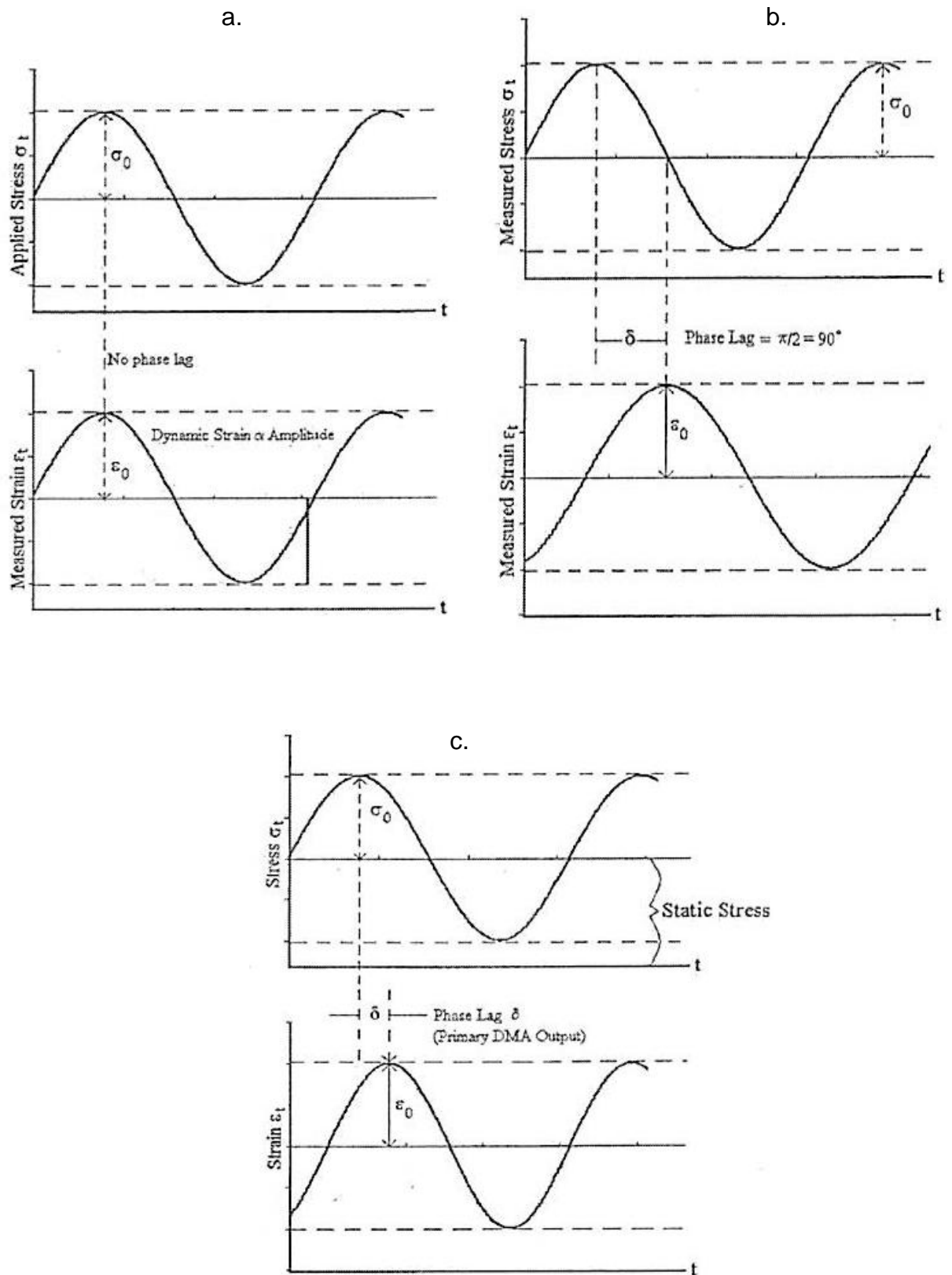


Figure 2.18: (a) shows the in-phase (elastic), (b) Out of phase (viscous) materials strain response to applied stress and (c) material between the viscous and elastic extremes [8].

The strain response of a material whose behaviour lies between the elastic and viscoelastic extremes can be described by Equation 2.10 [16] :

$$\varepsilon(t) = \varepsilon_0 \sin(\omega t + \delta) \quad (2.10)$$

Where ε_0 is the frequency of the oscillation and δ is the phase angle, t is the time. By using the trigonometry model described in Equation 2.10, it can be rewritten as follows.

$$\varepsilon(t) = \varepsilon_0 [\sin(\omega t) \cos(\delta) + \cos(\omega t) \sin(\delta)] \quad (2.11)$$

The strain response described by equation 2.6 [16] is illustrated in Figure 2.18 (c)

The elastic and viscous, in-phase and out-of-phase, strain components of the analysed material are denoted as follows :

$$\varepsilon' = \varepsilon_0 \sin(\delta) \quad \text{in-phase component} \quad (2.12)$$

$$\varepsilon'' = \varepsilon_0 \cos(\delta) \quad \text{out-of-phase component} \quad (2.13)$$

The sum of the vectors ε' and ε'' results in a complex modulus ε^* , which is given by Equation 2.14[2]

$$\varepsilon^* = \varepsilon' + i\varepsilon'' \quad (2.14)$$

Where i is the $\sqrt{-1}$, and the complex number, ε^* , is resolved into two components that describe material behaviour, a real component, ε' , whereby the energy is stored and

recoverable and an imaginary component ϵ'' whereby the energy is non recoverable, and lost as heat. The relationship between the vector components is illustrated in Figure 2.19 :

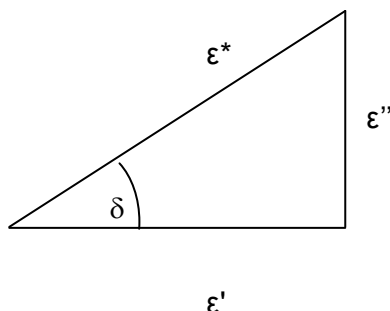


Figure 2.19: ϵ' In-phase, ϵ'' out-of-phase strain vectors, and ϵ^* the vector sum for materials behaving between viscous and elastic extremes [16].

2.6.3 Thermo-Mechanical Measurement

The thermo-mechanical properties of the films were measured using the Perkin-Elmer DMA-7e instrument, using Pyris software, version 3.81. The instrument was calibrated using indium and zinc standards. The film specimens, having a thickness of 0.125 mm (= 125 micron) and 199 mm long x 156 mm wide, were analysed in the extension mode.

The elastic behaviour of the materials studied was assessed by E' , and E'' and $\tan(\delta)$, the peak maxima of their curve can be used to determine the T_g of a material. The extension mode was performed at both room temperature and selected temperatures from 25 °C to 125 °C, with loadings scanned from 110 to 1000 mN at a rate of 100 mN/min. The dynamic measurement was performed by holding the sample at 25°C for 2 min, then heating the sample from 25 °C to 400 °C at a rate of 10°C/min.

2.6.4 Electromechanical Measurement

Measurements of electromechanical properties in extension mode were performed on un-irradiated and irradiated PI nanocomposite films. A photograph of the arrangement used to measure the electrical conductivity of the nanocomposites while the samples were strained is shown in Figure 2.20 .

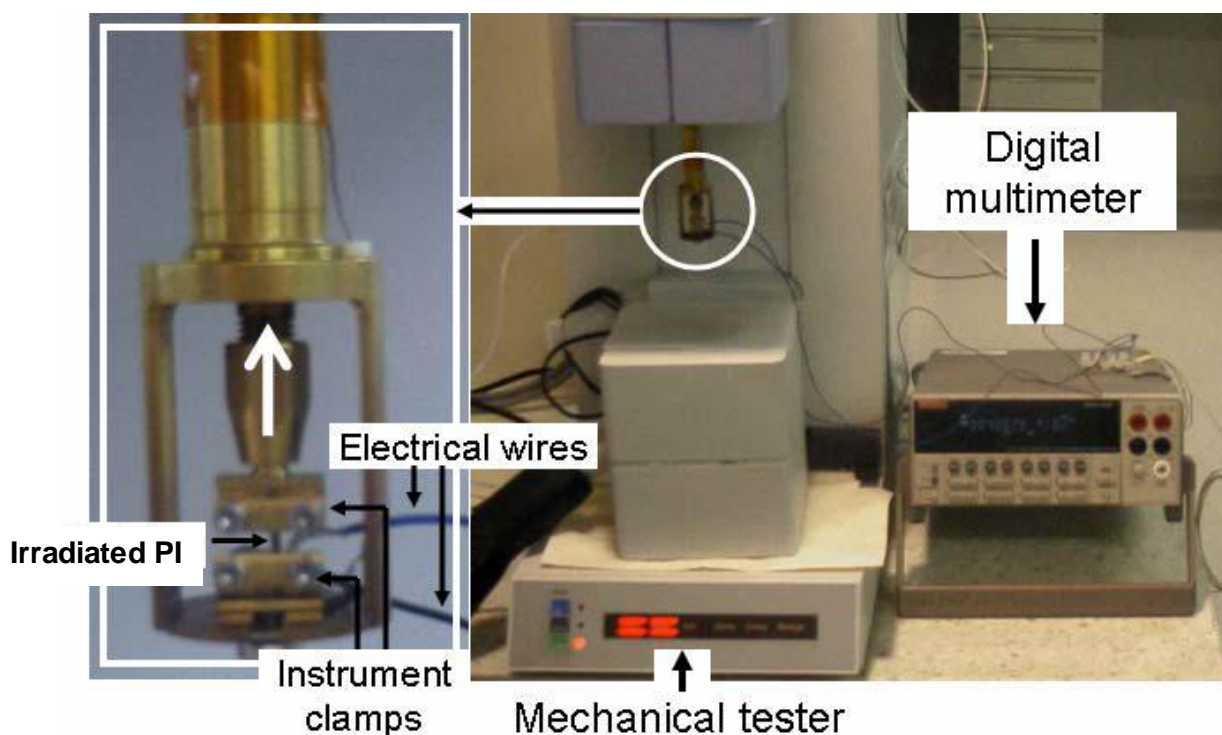


Figure. 2.20: The Perkin-Elmer DMA-7e using the Mora-Huertas *et al.* [17] set up.

The arrangement was the same as that used by Mora-Huertas *et al.* [17] and similar to that used by Knite *et al.* [19] and Flandin *et al.* [18] for the measurement of the electromechanical properties of carbon-black-polyimide nanocomposite films, polyisoprene-carbon-black and styrene-butyl acrylate copolymer containing polypyrrole particles. The set-up consisted of a Perkin Elmer DMA-7e performing the extension of the films, and a computer controlled data acquisition system, which included a Keithley multimeter to measure and collect the electrical resistance data. Sample dimensions (199 mm width x 1.56 mm length) were measured using a calliper. The samples were provided with electrical contacts as described previously.

Once the strip of film was mounted, the electrical connections were verified and the mechanical analyser set to start the extension of the film, then the electrical resistance measurements were commenced. Mechanical extension of the films was carried out by applying an initial force of 110 mN, then increasing at 100 mN/min up to 2000 mN. This analysis was performed at temperatures of 25, 40 and 55 °C. Stress and strain data obtained from the DMA-7e, and electrical resistance data, were synchronised to establish the values of electrical resistance and their corresponding value of strain.

2.7 References

- 1 Loh, I. H., Oliver, R. W., Sioshiansi, P., *Conducting Polymer by Ion Implantations*. Nuclear Instruments and Methods in Physics Research Section B. 1988. 34:p. 337. [doi: 10.1016/0168-583X\(88\)90054-7](https://doi.org/10.1016/0168-583X(88)90054-7)
- 2 Svorcik, V., Rybka, V., Volka, K., Hnatowicz, V., Kvitek, J., Perina, V., *Influence of Iodine Implantation on The Properties of Polypropylene*. Applied Physics Letter. 1992. 61:p. 1168.
- 3 Brown, W.L., *Radiation Effect in Insulators 3*, ed. Webb. R.B., Goron-Breach. New York. 1986.
- 4 Davenas, J., Boiteux, G., *Ion Beam Modified Polyimide*. Advanced Materials. 1990. 2:p. 521.
- 5 Lee, E.H., Rao, G.R., Lewis, M.B., Mansur, L.K., *Ion Implantation Effects*. Journal of Materials Research. 1994. 9:p. 1043.
- 6 Suzuki, Y., Kusakabe, M., Iwaki, M., *Surface Modification of Polystyrene for Improving Wettability by Ion Implantation*. Nuclear Instruments and Methods in Physics Research Section B: Beam Interaction with Materials and Atoms. 1993. 80-81:p. 729.
- 7 HD-Microsystems, *Product Information Pyralin PI2525, PI2555, PI2575 and PI2556*. 2001.
- 8 Ghosh, M.K., Mittal, K.L., *Degradation and Stability of Polyimides Fundamentals and Applications*, Cella. J., ed. Marcel Dekker, Inc. New York. 1996
- 9 Hasegawa, M., *Molecular Aggregation and Fluorescence Spectra of Aromatic Polyimide*. European Polymer Journal. 1989. 25:p. 349.
- 10 Wachsmann, E.D., Frank, C.W., *Effect of Cure History on The Morphology of Polyimide: Fluorescence Spectroscopy as a Method for Determining the Degree of Cure*. Polymer. 1988. 29:p. 1191.
- 11 Dine-Hart, R.A., Wright, W.W., *Thermal Stability of Aromatic Polyimides: Factors Affecting the Oxidative Stability of Poly-N,N'-(4,4'-diphenyl ether) Pyromellitimide*. British Polymer Journal. 1971. 3:p. 163.
- 12 Hirata, K., Saitoh, Y., Narumi, K., Nakajima, Y. and Kobayashi, Y. *Non-linear Effect of Cluster Irradiation on Chemical Modification of Polycarbonate*. Nuclear Instruments and Methods in Physics Research B. 2002. 193:p. 816.
- 13 Brett, Christopher M.A., Alves, V. A. and Fungaro, D.A. *Nafion-Coated Mercury Thin Film and Glassy Carbon Electrodes for Electroanalysis: Characterization by Electrochemical Impedance*. Electroanalysis. 2001. 13:p. 212.
- 14 Valentine, L., Armentano, I., Santillib, P., Kenya, J.M., Lozzic, L., Santuccic, S., *Electrical Transport Properties of Conjugated Polymer onto Self-Assembled Aligned Carbon Nanotube*. Diamond and Related Materials. 2003. 2:p. 1524.

- 15 Menard, K.P., *Dynamic Mechanical Analysis: A Practical Introduction* in CRC Press. Boca Raton. 1999.
- 16 Huertas, N.E.M. *Functional Thin Film Polyimide Nanocomposites*. Ph.D. Thesis, Science Engineering and Technology Portfolio, RMIT University, 2005.
- 17 Flandin, L., Brechet, Y. and Cavaille, J.Y., *Electrically Conductivity Polymer Nanocomposites as Deformation Sensors*. Composites Science and Technology, 2001. 61:p.895.
- 18 Kinte, M., *Polyisoprene-Carbon Black Nanocomposites as Tensile Strain and Pressure Sensor Material*. Sensors and Actuators, A:Physical. 2004. 110:p.142.
- 19 Wang, H.S., Ju, H. X., *Adsorptive Stripping Voltametric Detection of Single-Stranded DNA at Electrochemically Modified Glassy Carbon Electrode*. Electroanalysis. 2002, 14:p.1615.
- 20 Brown, R.P., *Handbook of Polymer Testing: Physical Methods*. CRC Press, 1999.p:845.
- 21 FTIR User guide, Perkin Elmer

3

ATR-FTIR & XPS SPECTROSCOPIC CHARACTERISATION OF Cu^{3+} ION-BEAM IRRADIATED POLYIMIDE FILMS

3.1 Introduction

The extensive studies undertaken by Devasahayam et al. [17] and by Long and Long [2], which examined the property modification of polyimide (PI) films by irradiation processes, found that changes in chemical structural could be identified from the infrared spectrum. These studies indicated the presence of triple ($\text{C}\equiv\text{C}$), double ($\text{C}=\text{O}$) or single ($\text{C}-\text{N}$) bonds that were not evident in the unmodified, pristine PI films, and also noted the growth of new bands attributable to aromatic and functional group developments [1]. The chemical and physical modification processes induced by ion-beam irradiation of polymer films were examined by Davenas et al. [3], Xu et al. [4] and Sun et al. [5], who found a reduction in the infrared absorbance of the original functional groups present in the film, indicating pyrolytic conversion of material in the area exposed to radiation [3-6].

Degradation of polyimide due to irradiation appears as an overall reduction in the intensities of the characteristic bands in the FTIR spectra. The first stage of degradation involves bond scission or cross-linking, and then rearrangement of the damaged macromolecules leading to the emission of some gaseous species [7]. The major gases evolved during irradiation were identified as carbon dioxide and carbon monoxide [8], thereby suggesting that the irradiation-induced damage occurred at the imide ring sites. Other studies have reported that degradation processes occur in multiple stages in radiation exposed polyimide [9]. In the

early stages of degradation, small losses of oxygen and nitrogen occurred. In later stages of degradation, the polymer loses other moieties identified as the imide ring structure and the depletion of hydrogen, which occurred with increased irradiation dose [6, 10-15].

Observations by Terai et al. [16] have shown that ion-beam irradiation causes carbonization and doping of the polymers near the surface region. However, polymers containing benzene rings or aryl-rings with multiple substituents such as polyimides, have considerable resistance to irradiation [17]. Therefore, it requires intense ion bombardment of a PI film to change its properties. This high energy irradiation results in an increase in the thickness of the carbonaceous layer and a reduction in the concentration of implanted ions.

In this chapter, the structural changes induced by Cu^{3+} ion-beam irradiation of two different polyimide films, BTDA-ODA and PMDA-ODA (see Figure 1.1) have been investigated. These polyimide films have been reported to be unaffected by temperatures as low as $-269\text{ }^{\circ}\text{C}$ or as high as $400\text{ }^{\circ}\text{C}$ [18]. This stability has been attributed to the influence of the aromatic rings present in the molecular structure, which gives the films protection against heat damage through an energy dissipation mechanism brought about by the polyimide vibrational states [5, 17-21].

Also in this study, through the use of ATR-FTIR and XPS, additional key molecular structure changes have been identified that were not previously reported in the literature. Further work, examining the effect of heat treatment, 'annealing', found other modifications to the molecular structures of the irradiated PI films, as shown by changes to band positions and intensities in characteristic FTIR bands. These changes in molecular structure provide an opportunity for measuring the unique conductive properties of the PI films, due to the graphite-like fused rings structures, which provide a network of conductive π -electron pathways. This aspect of the modified PI films is explored in depth in Chapter 4. In Chapter 5, studies of the micromechanical properties of the irradiation-modified PI films revealed that

there were fractures in the films due to the formation of the graphitic network. Thus, the ion-beam irradiation that improved the electrical conductance properties generally compromised the mechanical properties of these films. The electromechanical properties of the modified films exhibited very high Gauge Factors (GF = strain sensitivity), in the range of 200 to 1000, in comparison to those reported in standard composites, which ranged from 2 to 50. These extraordinary GF values are indicative of the use of such irradiated films as strain gauge sensors. Further discussion of the GF values in relation to their mode of action is detailed in Chapter 5.

The present chapter addresses the impact of ion-beam modification on the molecular structures of the two PI films, PMDA-ODA and BTDA-ODA, in particular, the effect on their thermal stabilities. These effects were principally examined by ATR-FTIR, supplemented by X-ray Photon Spectroscopy (XPS), and a detailed description of the various IR absorption bands arising from the molecular structures of the pristine PI's is provided. The relationship between the ion-beam intensity (fluence) and the changes in functionality within the PI structure is discussed.

3.2 Sample Preparation and Characterisation

Polyimide surfaces were prepared as described in Section 2.2.1, with particular attention paid to the prevention of contamination and the removal of dust particles that may be attracted to the surface. The Cu^{3+} ion-beam fluence used to modify the films ranged from 9×10^{13} to 5×10^{14} ions cm^{-2} , as listed in Table 2.1. After irradiation, the films were kept in a desiccator.

The films were dried at a temperature of 80°C , and then annealed under vacuum in a temperature-controlled oven, at two pre-selected temperatures (180°C and 280°C) for 5

minutes, as detailed in Section 2.1. Following annealing, the films were stored in a desiccator.

Initial ATR-FTIR analyses were performed on the pristine, as prepared, PI films, with no heat treatment. After irradiation, the PI films were first dried at 80°C to remove residuals and then analysed by ATR-FTIR. Finally, the dry, irradiated PI films were “annealed” and then analysed by ATR-FTIR to investigate their thermal stability. The ATR-FTIR resolution was optimized at room temperature as described in Section 2.2, using the reflectance mode at a resolution of 32 and over the wave number range, 4000 to 650 cm^{-1} .

The following diagram shows the film contact with the prism, and the evanescent wave penetrating the film sample during analysis.

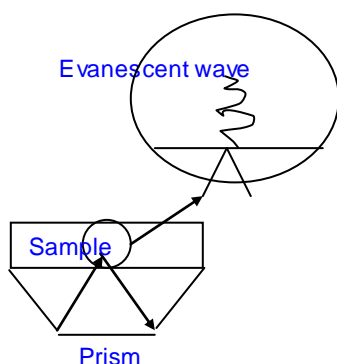


Figure 3.1: Film contact with the single bounce transparent prism during ATR-FTIR analysis.

The ATR-FTIR analysis technique involved placing the PI film in direct contact with the instrument’s transparent prism, and then applying pressure to maintain contact between the film and the prism. The infrared penetration depth in this arrangement was less than 10 microns [22].

The initial XPS analyses were performed on the pristine PI films. After irradiation and before heat treatments, measurements were carried out using a Thermo KAlpha XPS

instrument at a pressure better than 1×10^{-9} Torr (1Torr =1.3336102 Pa) as described in Section 2.4.1

3.3 Irradiation-Induced Molecular Structure Changes of Films

3.3.1 Molecular Characteristics of Pristine Polyimide

Table 3.1 summarizes the infrared assignments of the functional group vibrations associated with the polyimides. The chemical structures of both the PMDA-ODA and BTDA-ODA polymers used in this study are displayed in Figure 3.2 (a) and (b), where the numbering corresponds to the characteristic infrared bands in the spectra, as indicated in Table 3.1, Figure 3.2 and Figure 3.3 (b).

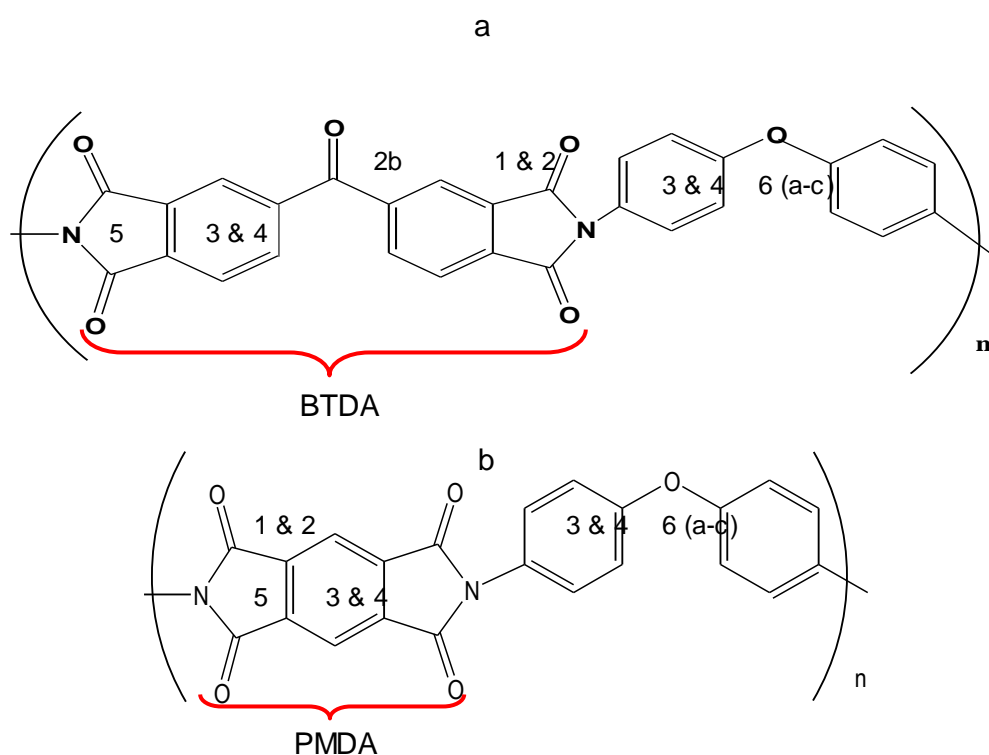
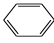


Figure 3.2: (a) Molecular structure of 3',4,4'- benzophenonetetracarboxylic dianhydride; 4,4'-oxidianiline (BTDA-ODA), (b) Molecular structure of pyromellitic dianhydride–4,4'-oxidianiline (PMDA-ODA).

Table 3.1: Band assignments of ATR-FTIR spectra of PMDA-ODA and BTDA-ODA films before ion-beam modification.

Number	Type of vibration	PMDA-ODA Band [cm^{-1}]	BTDA-ODA Band [cm^{-1}]
1&2	Imide carbonyl C=O stretching	1775 and 1709	1778 and 1713
2b	benzophenone carbonyl C=O stretching		1671
3	Aromatic C=C stretching	1599	1598
4	Benzene ring 	1497, 1456	1496, 1426
5	Imide C-N stretching	1373, 1305 and 1089 -1013	1361 and 1288,
6 (a-c)	Ether C-O-C stretching	1239 -1200, 1165 and 1113	1229 1160 and 1090
7 (a-b)	Aromatic C-H bending	937 and 883, 815, 799, 775	981, 922 and 829
8	Imide C-H bending	751-721	755-713

The spectra of the PI films are similar. The PMDA-ODA had aromatic carbon bands at 1497 and 1456 cm^{-1} , attributed to the para-disubstituted phenyl group, whereas in BTDA-ODA, bands indicative of benzene ring vibrations were observed at 1598 and 1426 cm^{-1} . This difference in the frequency may be due to the isolated benzophenone carbonyl in BTDA-ODA causing the vibrational modes of the neighbouring atoms to be affected.

The spectra of both PI films show asymmetric stretching ether (C-O-C) bands at 1239-1200, 1160 and 1090 cm^{-1} and aromatic C-H bending bands between 981 to 775 cm^{-1} [3, 28-30]. The imide C-H bending appeared at 755-713 cm^{-1} . The evaluation of the frequency bands after Cu^{3+} ion-beam irradiation will be discussed in the next section.

The values of the FTIR frequencies of the pristine PI compare favourably with those described in the literature [23-27], As a comparison, for the well characterised [23] PMDA-ODA (kapton), the infrared bands of interest are given in Table 3.2, and their similarity to

the PMDA-ODA and BTDA-ODA bands in Table 3.1 provides confirmation of the band assignments.

Table 3.2: Literature Infrared band assignment for unirradiated kapton film [23].

Type of vibration	Band Frequencies cm^{-1}
(PMDA-ODA)	
Aromatic C-H stretching	3040, 2900
Carbonyl C=O	1775, 1709
Aromatic C-C	1605, 1501
Imides C-N	1369, 1300, 1115, 1088
Ether C-O-C	1239
Aromatic C-H bending	922, 879, 810
Imides C-N or C-H bending	721

Figure 3.3(a) presents typical ATR-FTIR spectra of the pristine PI films of PMDA-ODA and BTDA-ODA obtained at room temperature, and Figure 3.3(b) shows an expanded view of the lower frequency region, along with band identification. Note that in the spectra of the pristine PI films bands in the high frequency region of $3000\text{-}2000\text{ cm}^{-1}$ are very weak compared to the bands appearing at lower frequencies.

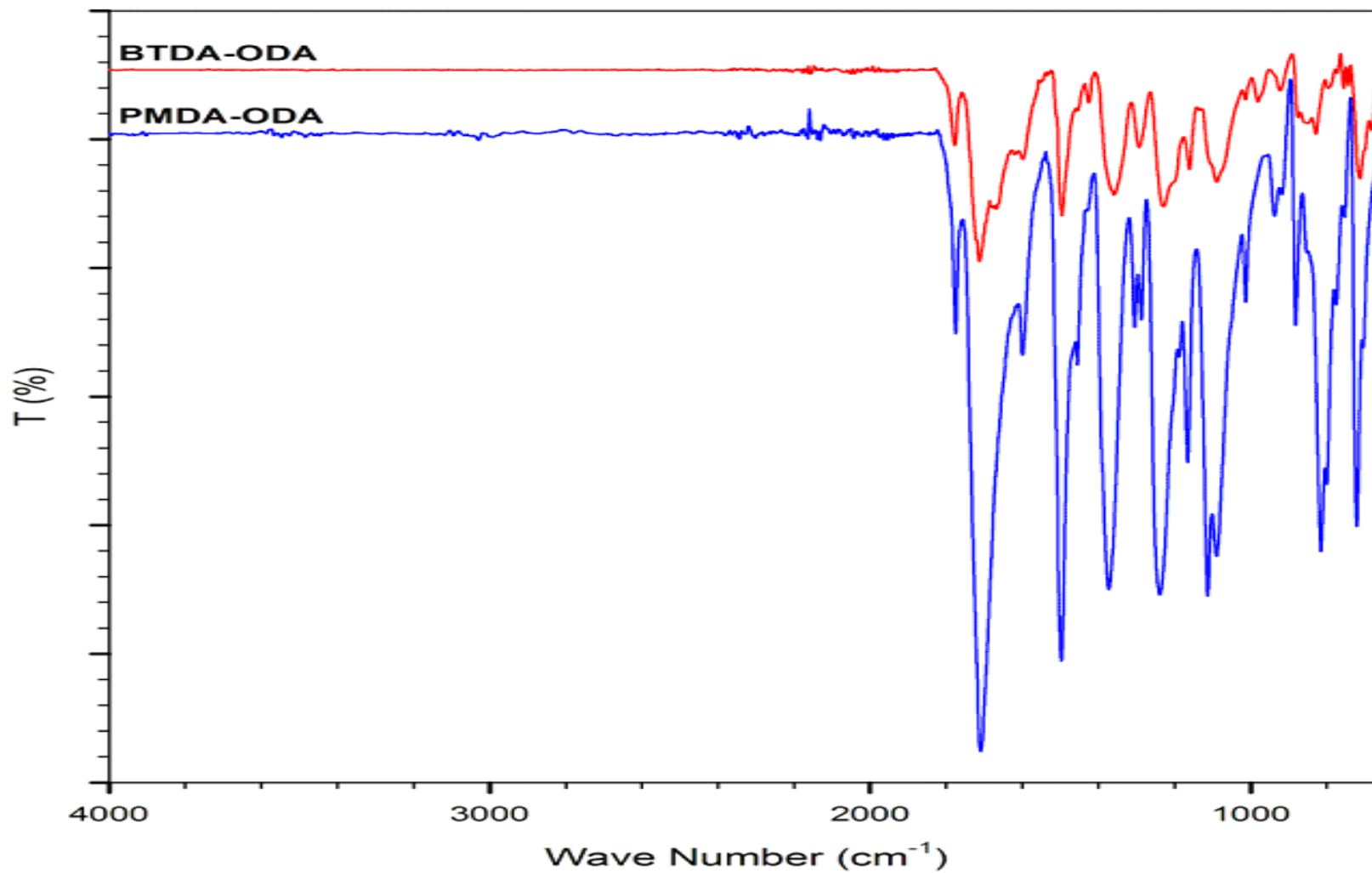


Figure 3.3 (a): FTIR spectra of pristine PMDA-ODA and BTDA-ODA: range 4000-650 cm⁻¹.

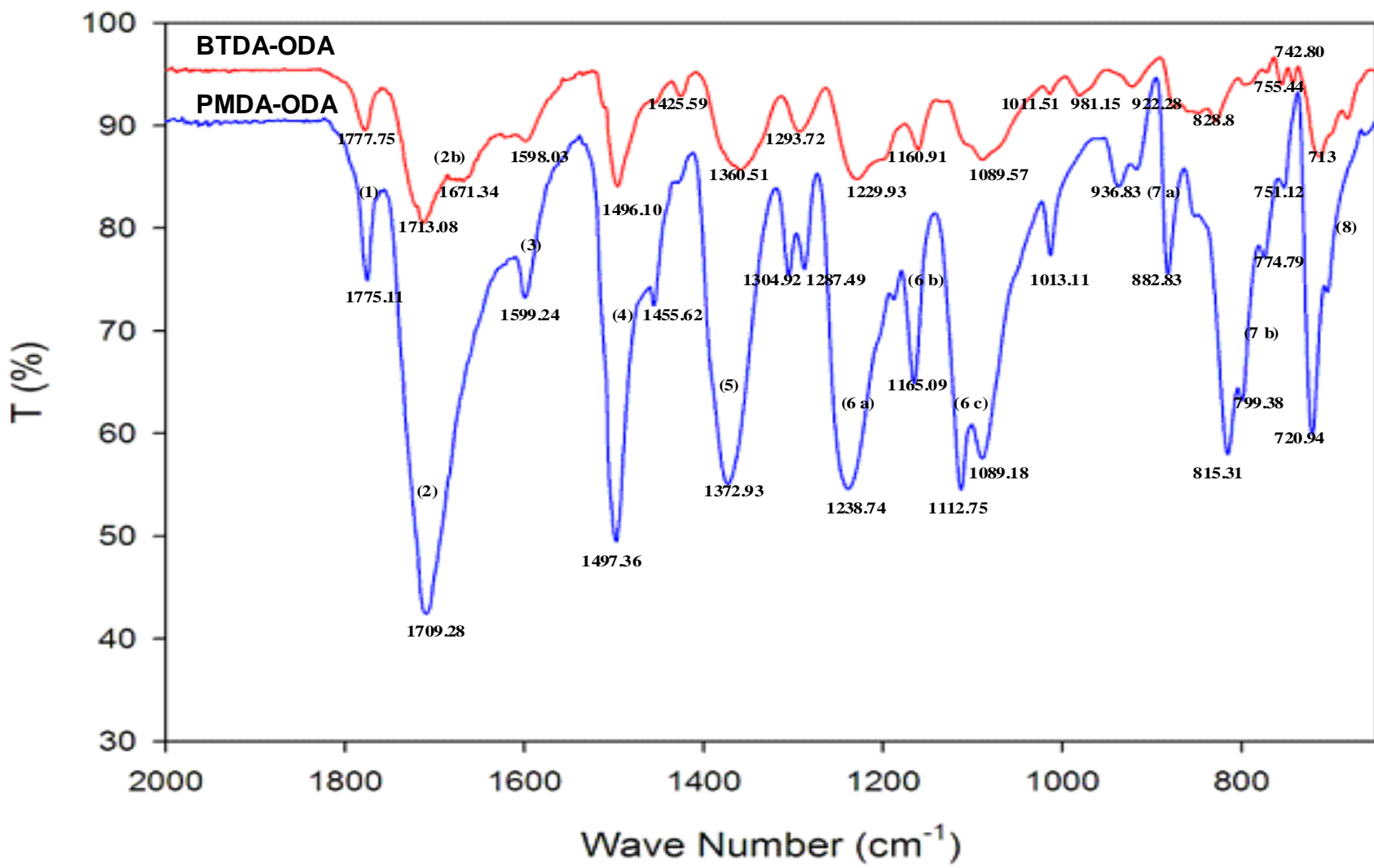


Figure 3.3 (b): FTIR spectra of pristine PMDA-ODA and BTDA-ODA: expanded view of the range 2000-650 cm⁻¹.

3.3.2 Ion-beam irradiation induced molecular structure changes in the polyimide films

Common changes observed after Irradiation in both PMDA-ODA and BTDA-ODA

ATR-FTIR spectra of PMDA-ODA and BTDA-ODA films irradiated with a 5.5 MeV Cu^{3+} ion-beam at a fluence of 1×10^{14} to 5×10^{14} ions cm^{-2} were obtained. Figure 3.4 (for PMDA-ODA) and Figure 3.5 (for BTDA-ODA) show the spectra of the pristine and the high fluence polyimides. In both sets of spectra a broad X-H stretching band appeared from 3100 to 2400 cm^{-1} characteristic of N-H, C-H or O-H. During the irradiation, gases such as CO, CO_2 , HCN, C_2H_2 and trace amounts of methane, ammonia, ethylene and water have been reported to be emitted from the PI films [7, 23, 29, 31-38]. Assuming that the band at 3100 to 2400 cm^{-1} is that of an O-H stretch, then it may have originated from adsorbed moisture on the surface of the irradiated PI film [41] as a result of exposure to the atmosphere after irradiation. Free radical formation has been reported to occur in irradiated PI films [39,40] and these chemically reactive sites would rapidly react with moisture from the atmosphere. This is supported by the observation that irradiated polyethylene exhibits a similar broad O-H band at 3100 to 2800 cm^{-1} , attributed to moisture adsorbed on the exposed surface after treatment [41]. To investigate whether the O-H group arose due to moisture adsorption, the irradiated films were subjected to an annealing process as detailed in Section 3.3.4.

The region of spectrum from 1700-1300 cm^{-1} contained many bands corresponding to different functional groups in the polymer (Figure 3.4b and Figure 3.5b). In the BTDA-ODA most of the band intensities in this region of the spectra were observed to diminish and broaden as the ion fluence increased. However the C=C bands at 1679 cm^{-1} to 1597 cm^{-1} showed small increases in intensities. In the PMDA-ODA spectra the band intensities in the 1700-1300 cm^{-1} region were observed to increase, broaden and shift to lower

frequencies, with the exception of the band at 1360 cm^{-1} which decreased in intensity. In particular the C=C bands at 1667 and 1605 cm^{-1} appeared to increase in intensity, in comparison with the bands in the unirradiated spectra. The C=C bands at 1597 to 1455 cm^{-1} displayed even more marked increases in intensities and band shifts at high fluence ($5 \times 10^{14}\text{ ions cm}^{-2}$). This indicates that carbonization of the radiation exposed films occurred, which was also accompanied by a visual discoloration of the film surface. Both the changes in physical appearance, and the variation in the infrared sensitive bands, are evidence of molecular degradation in the irradiated films.

Decrease in the intensities of other bands (as illustrated in Figure 3.4 and Figure 3.5), were indicative of significant bond cleavage occurring at the carbonyl, imide, ether and C-H bonds. At low fluence the C=O remains broad as they were in the pristine polymer and their intensity decreased. At higher fluence, the broad band in the pristine PMDA-ODA resolved into two bands at 1701 cm^{-1} and 1667 cm^{-1} . Although these were more intense than the broad C=O obtained at low fluence ($1 \times 10^{14}\text{ ions cm}^{-2}$ (spectrum not shown)) they were still less intense than the broad C=O band in the pristine polymer. Overall these changes suggest loss of C=O group, and or changes to their environment in the irradiated PMDA-ODA PI films. This suggests disintegration of the imide carbonyl and the five-membered imide ring, consistent with the proposals of Tretinnikov et al. and Virk et al.[37, 47].

The imide stretch band observed at 1373 , 1305 , 1089 - 1013 cm^{-1} in the pristine PMDA-ODA spectra were observed to shift to 1360 and 1029 cm^{-1} . The band at 1360 cm^{-1} was observed to initially decrease in the intensity at the low fluence and increase in intensity at the highest fluence and also the band narrowed. However, compared to the pristine PMDA-ODA spectra displayed a decrease in the width and intensity. Also the band at 1305 cm^{-1} was completely removed, whilst the bands at 1089 - 1013 cm^{-1} showed shift to 1029 cm^{-1} and an increase in the band intensity compared both to the low fluence and

pristine PMDA-ODA spectra. There was very strong band at 801 cm^{-1} this is representative of the imide ring deformation. The change observed in these spectra is indicative of changes to the PMDA-ODA molecular chain and surrounding environment.

The imide groups then form as an interim system, and simultaneous breakage of some ether bonds (of the phenyl group link) releases aromatic carbon moieties (of multi-substituted benzene rings) which may then condense to form PAH's and graphitic-type structures. The degradation of the BTDA-ODA films essentially follows the same chain of events as the disintegration of the PMDA-ODA film, with the exception that the benzophenone carbonyl does not readily decompose, due to its placement between the benzophenone aromatic rings in an inner plane orientation. Figures 3.6 (b) to (d) illustrate the sites in the polyimide molecular structure where the radiation induced decomposition has occurred.

The ether linkage band at 1239 cm^{-1} of the pristine PMDA-ODA films was observed at appears as a very weak shoulder at the low fluence. At highest fluence this ether band (1239 cm^{-1}) was observed to be broader, with decrease intensity compared to the pristine PMDA-ODA. As well as a shift in the band at $1239\text{-}1200\text{ cm}^{-1}$ in the pristine PMDA-ODA appeared resolved into two bands, this new bands are 1228 and 1214 cm^{-1} . These changes in the bands are indicative of damages and loss of the ether linkage and some deformation and possible cleaving occurring at this site.

The pristine PMDA-ODA aromatic C-H bending at 937 , 883 , 815 and 799 cm^{-1} were observed to be sharp narrow intensity bands. After irradiation this bands were observed to be very broad and stretched from $986\text{-}958\text{ cm}^{-1}$ and 775 cm^{-1} . In the low fluence film spectra one broad band was observed, however at the highest fluence this band appeared to be broad, with shoulder like bands.

Most importantly the intensity of the C=C band at approximately 1600 cm^{-1} increased compared to C=O. In the BTDA-ODA, low fluence, the aromatic bands between $1600\text{--}1500\text{ cm}^{-1}$ show increase in the intensities compared to the aromatic bands in the unirradiated. As for the PMDA-ODA films, the aromatic carbon band appeared at frequency from 1667 cm^{-1} to 1455 cm^{-1} , with a strong band at 1597 cm^{-1} indicating increased aromaticity [23, 46, 47]. Here, the increase in aromaticity indicated by an increase of C=C bonds, demonstrates carbonization of the polyimide films via elimination and the creation of bonds between carbon atoms. That is, the elimination of imide nitrogen and aromatic hydrogen groups resulted in an increase in carbon-rich structures. This leads to graphite-like formation of aromatic crystallites in PMDA-ODA and BTDA-ODA films.

In contrast, the BTDA-ODA band before irradiation was at band 1775 cm^{-1} , had shifted to 1784 cm^{-1} when the BTDA-ODA was irradiated, which showed that there was still a considerable amount of the carbonyl moiety between the benzophenone phenyl rings in the BTDA-ODA molecular structure. Therefore, in the irradiated BTDA-ODA, the benzophenone carbonyl in the BTDA molecular structure was not significantly affected by irradiation because it was wedged between the two aromatic rings of the benzophenone, which acted as protective shields.

Although the formation of fused rings was observed, it was not indicative of complete conversion to a graphitic fused-aromatic structure over the entire irradiated surface area. Irradiation at high fluence resulted in the elimination of C-H bands, partial elimination of imide linkages and significant changes in the aromatic characteristic of the polyimides [48]. In the irradiated BTDA-ODA the phenyl ether band appears as a weak shoulder in bands at 1100 cm^{-1} , 1030 cm^{-1} , and 1092 cm^{-1} , at ion fluences of (1×10^{14} , 3×10^{14} spectra not shown) and 5×10^{14} ions cm^{-2} respectively, therefore it was affected by irradiation, as clearly shown by the reduction in peak intensity indicating degradation of the phenyl ether

during irradiation. Observation of the phenyl ether peaks at lower ion fluences (spectra not shown), indicated that this group was not removed at a fluence lower than 3×10^{14} ions cm^{-2} . However in BTDA-ODA the carbonyl band was observed to shift to 1784 cm^{-1} from the initial position of 1775 cm^{-1} . Such a shift to higher frequency for BTDA-ODA, is distinctive of the symmetric vibration of a carbonyl band [49].

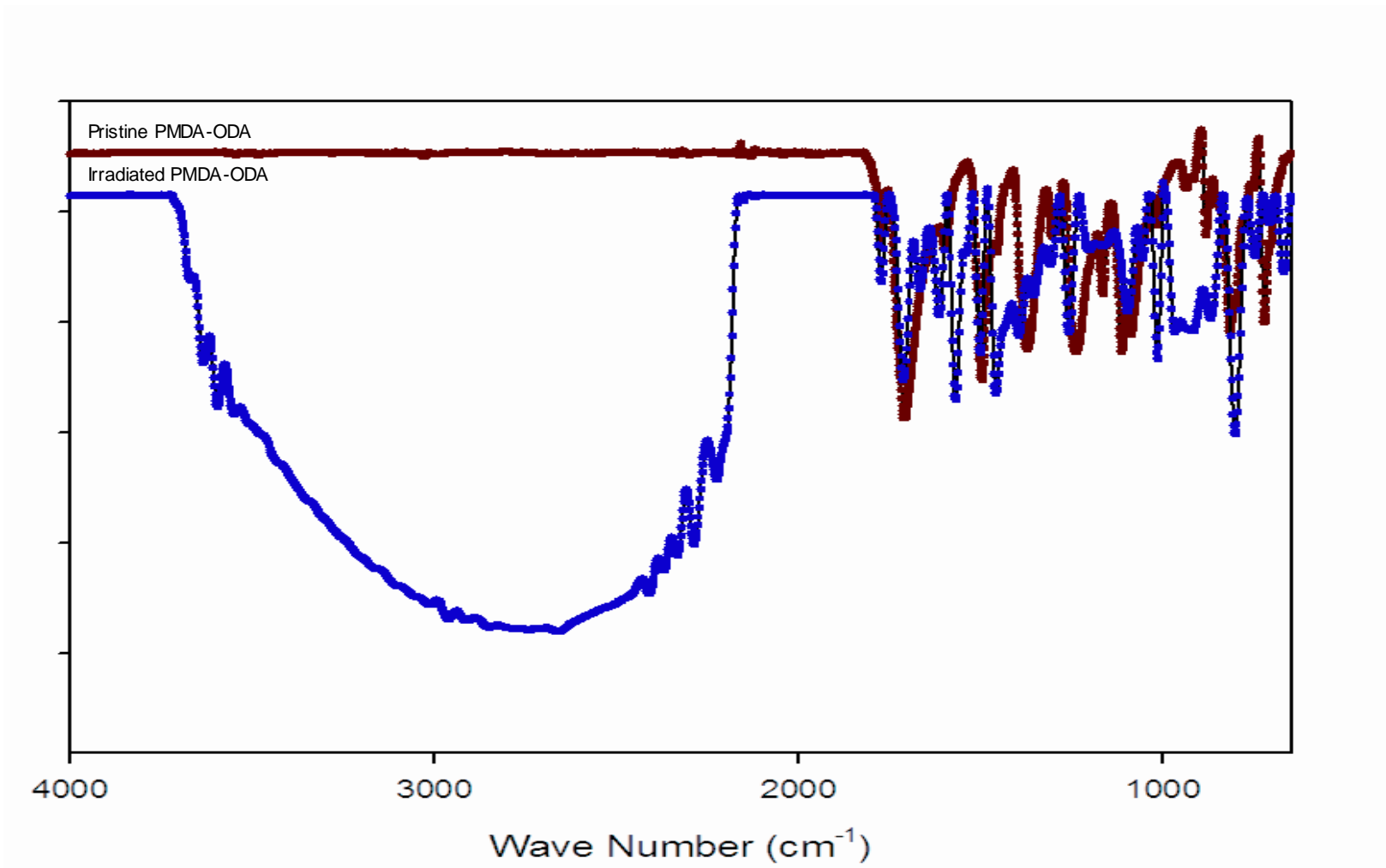


Figure 3.4 (a): ATR-FTIR spectra region of 4000-650 cm⁻¹ of pristine and irradiated PMDA-ODA (5×10^{14} ions cm⁻²) films.

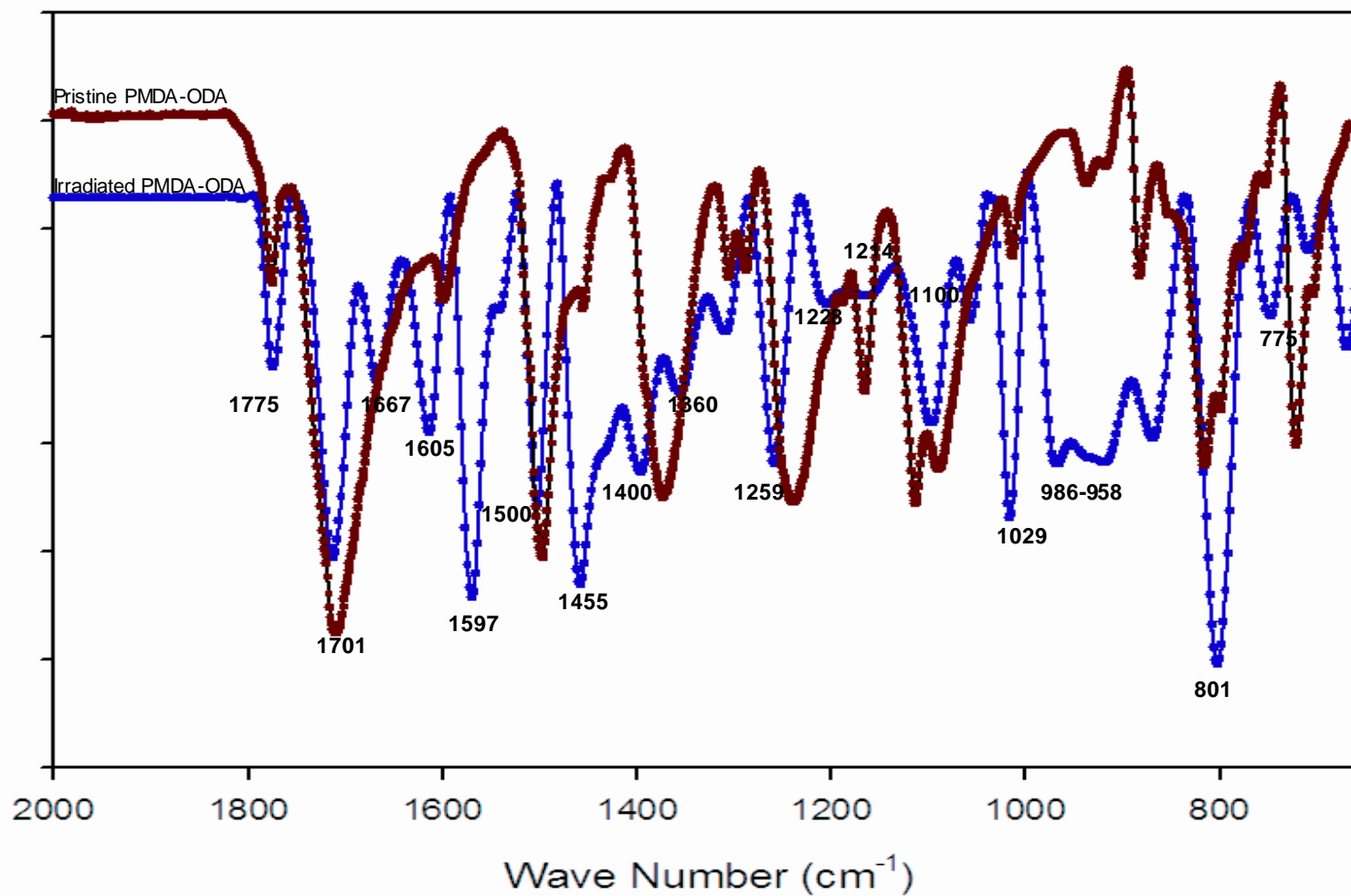


Figure 3.4 (b): ATR-FTIR spectra region of 2000-650 cm^{-1} of pristine and irradiated PMDA-ODA (5×10^{14} ions cm^{-2}) films.

Implications of the Observed Changes in the ATR-FTIR Spectra

In PMDA-ODA spectra, shifts in the characteristic bands and the reduction in their intensities may also be attributed to the displacement and /or elimination of imide and aromatic C-H groups [16, 42]. The backbone cleavage that occurred between the nitrogen of the imide group and the ether of the phenyl group, is indicative of partial breakdown of the linkage at the imide site. Considering the diminished intensities of the imide bands, it is reasonable to suspect that the backbone is cleaved between the imide nitrogen and the adjacent phenyl rings at either end of the repeat unit, consistent with the proposal of Steckenreiter et al [43]. This, together with the increases of aromatic carbon band intensity at 1597 cm^{-1} of the PMDA-ODA, the para-disubstituted phenyl at 1501 and 1455 cm^{-1} , and the out-of-plane imide C-H deformation at about 801 cm^{-1} , are all indicative of carbon rich structures forming in the irradiated films.

Upon examination of the carbonyl bands after irradiation of the PMDA-ODA films a variation in the bands was observed. The initial band at 1775 cm^{-1} in the pristine PMDA-ODA shifted to 1775 cm^{-1} , however the strong band at 1709 cm^{-1} had most changes which include the splitting, narrowing of, broaden and decrease in bands intensities. Also this pristine band at 1709 cm^{-1} was observed to have shifted slightly to about 1710 cm^{-1} and the smaller band shifted to 1708 cm^{-1} . Although the shift to higher frequency is indicative of presence of carbonyl, the decrease in the band intensity and the presence of the other carbonyl band at lower frequency are indicative of weakening of the bond between carbonyl and the phenyl rings. A study of polycarbonate (PC) films by Hirata et al. reported similar behaviour, where the carbonyl stretching band at 1770 cm^{-1} was reported to shift to a lower frequency after ion-beam irradiation [35]. This was shown to occur in PC due to decomposition of the weak carbonyl bonds between the phenyl rings in the irradiated PC.

In the spectra of the PMDA-ODA films, the increase in the aromatic carbon band intensity indicates that the aromatic carbon rings were resistant to irradiation damage and that the

relative concentrations of aromatic carbons increased. Mohammad et al. [36] reported that the intensity of the (C=C) stretch at 1610 cm^{-1} gradually increased with increase of irradiating fluence. The aromatic carbons in the pristine PMDA-ODA spectra were observed at band 1599 , 1497 and 1456 cm^{-1} , after irradiation of PMDA-ODA the aromatic carbon band were observed to extend from 1605 cm^{-1} to 1460 cm^{-1} . the band at 1599 cm^{-1} was sharp and low intensity band, however the band shifted to slightly lower frequency 1597 cm^{-1} and was strong band, whereas the band at 1497 cm^{-1} shifted to about 1500 cm^{-1} and the band at 1456 cm^{-1} move also slightly to 1460 cm^{-1} . The band at 1605 and 1597 cm^{-1} are indicative of aromatic carbons in general, whereas those at 1500 cm^{-1} and 1460 cm^{-1} are indicative of benzene rings in particular [31-38].

The band characteristic of the imide ring appeared in the pristine spectra at about 1373 and 1305 cm^{-1} , bands of C-N bonding appeared at 1089 and 1013 cm^{-1} . After irradiation of the PMDA-ODA there was a band at about 1374 cm^{-1} , this band had half the intensity of the band at 1373 cm^{-1} , also there was a shift in the position of the original band at 1305 cm^{-1} to about 1350 cm^{-1} . The band at 1089 and 1013 cm^{-1} were also observed to shift to 1100 and about 1050 cm^{-1} . This compared with the shift of band and the decrease in intensities as well as the strong new band at 801 cm^{-1} (which is indicative of imide ring deformation) is due to bond scission [50]. Svorcik et al. [36, 51] found that the bands at 1386 cm^{-1} and 730 cm^{-1} were due to imide ring deformation. This was associated with a thermally induced structural change of the PMDA-ODA films, consistent with the four stage mechanism shown in Figure 3.6. Primarily, the PMDA-ODA chain disintegrates via breakage of imide bonds to give a para-disubstituted phenyl and a symmetric stretching carbonyl.

Changes in the relative intensities and the shift of the carbonyl, aromatic carbon, and ether linkage bands suggest the surface chemistry change involves partial elimination of molecules in the repeat unit of the polyimide via chain scission. The phenyl ether bands appeared at 1239 cm^{-1} - 1200 cm^{-1} and at 1165 and 1113 cm^{-1} in the spectra of the pristine PMDA-ODA films, these bands were observed to shift to 1228 - 1214 cm^{-1} after irradiation. The bands were broad and not well defined (figure 3.4 (a)).

In addition, the aromatic carbon atoms were able to cluster together and bond to create stable fused rings, arising from imidic and carbonyl loss [7, 44]. Feurer et al. have reported that an increase in peak intensity for the aromatic carbons observed at 1605 cm^{-1} , results from a decrease in the intensity of imidic and carbonyl peaks [23]. This mechanism is reported to involve the formation of a graphite-like fused ring structure. The possibility of this occurring in the present case is supported by the broadening of the aromatic carbon band at 1597 cm^{-1} [7, 45] as seen in the expanded spectra in Figure 3.4 (b).

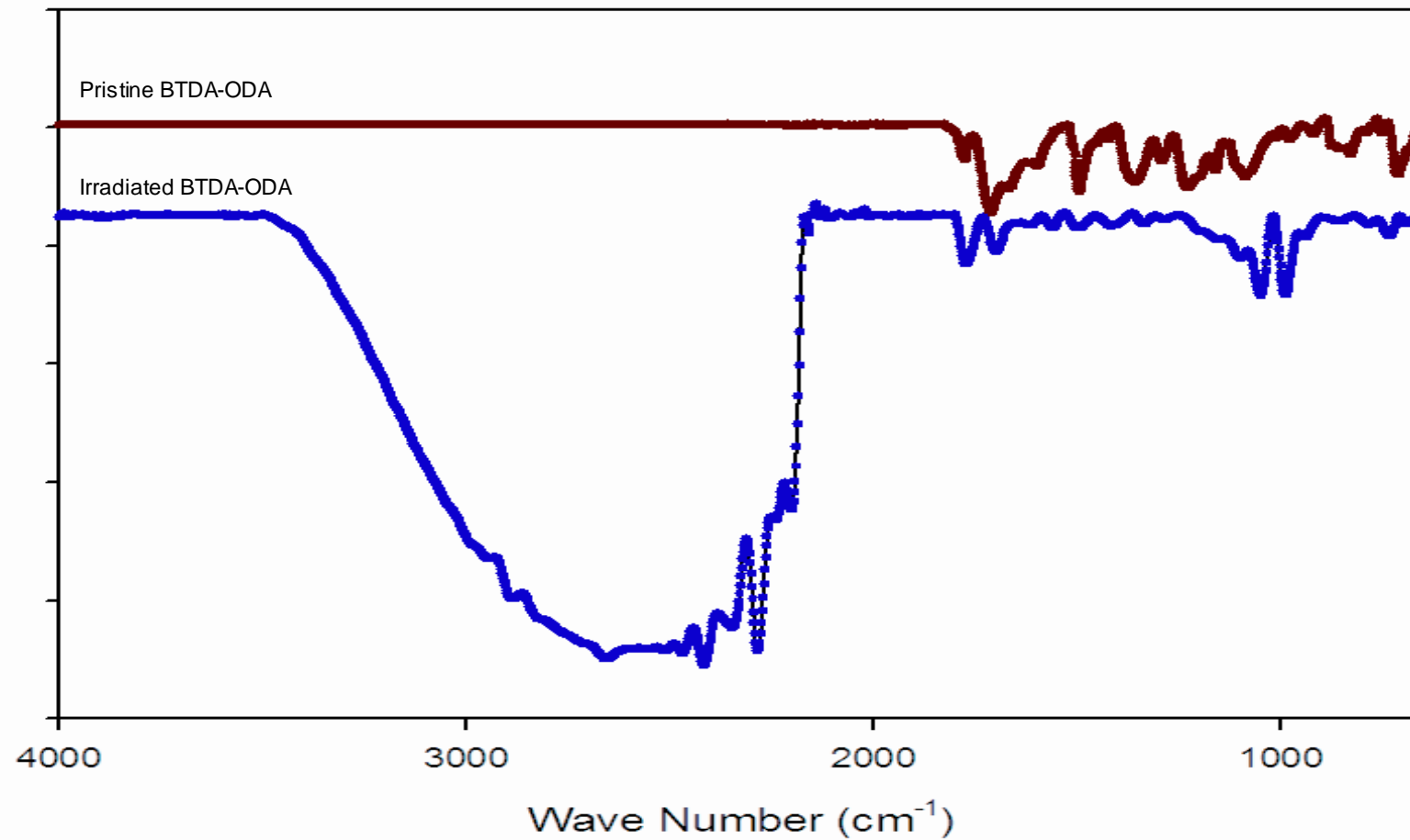


Figure 3.5 (a): ATR-FTIR spectra region of 4000-650 cm⁻¹ of pristine and irradiated BTDA-ODA (5×10^{14} ions cm⁻²) films

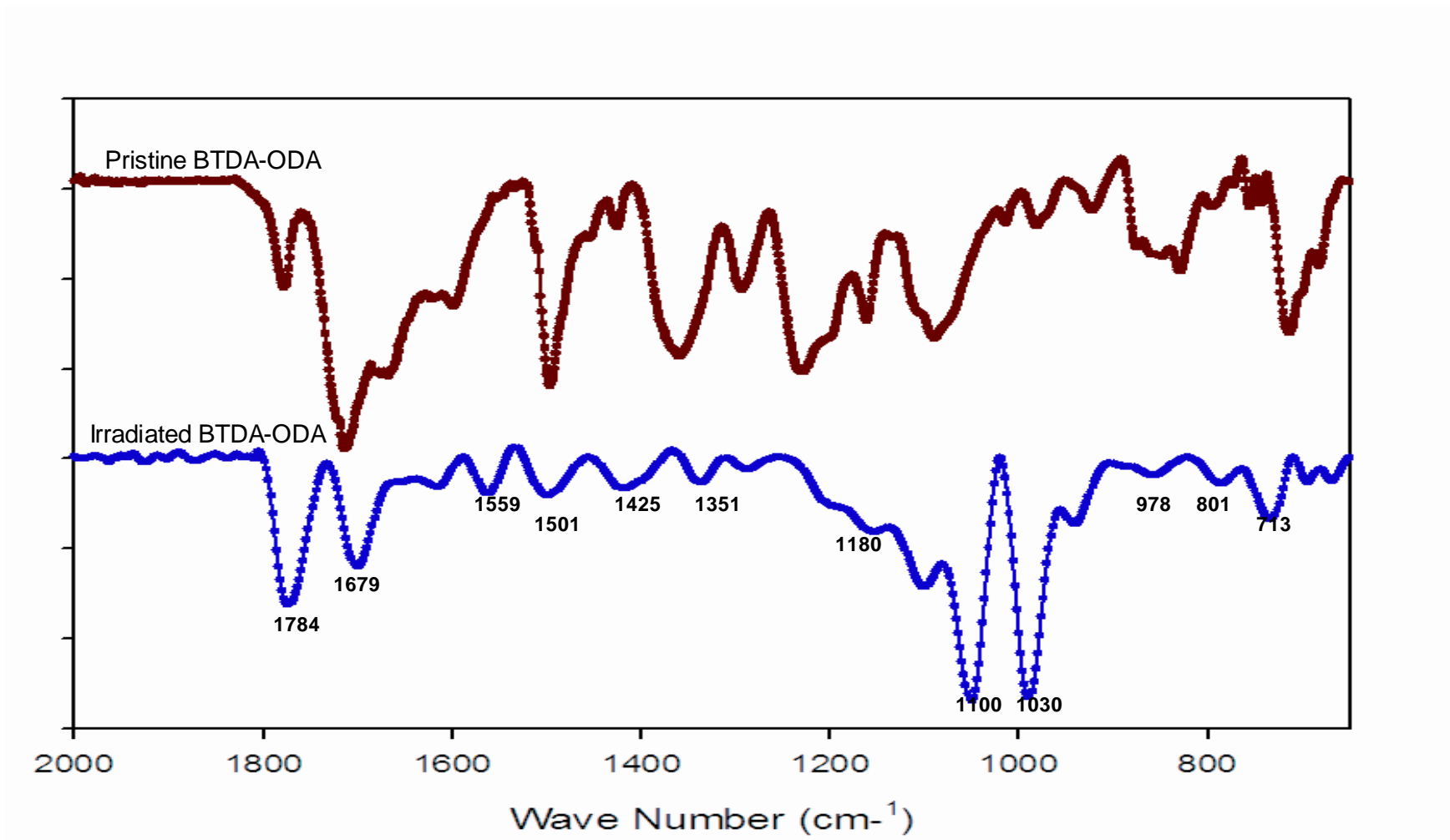


Figure 3.5 (b): ATR-FTIR spectra region of 2000-650 cm⁻¹ of pristine and irradiated BTDA-ODA (5×10^{14} ions cm⁻²) films.

The first three stages in the change in molecular structure of a PI after irradiation are represented in Figure 3.6.

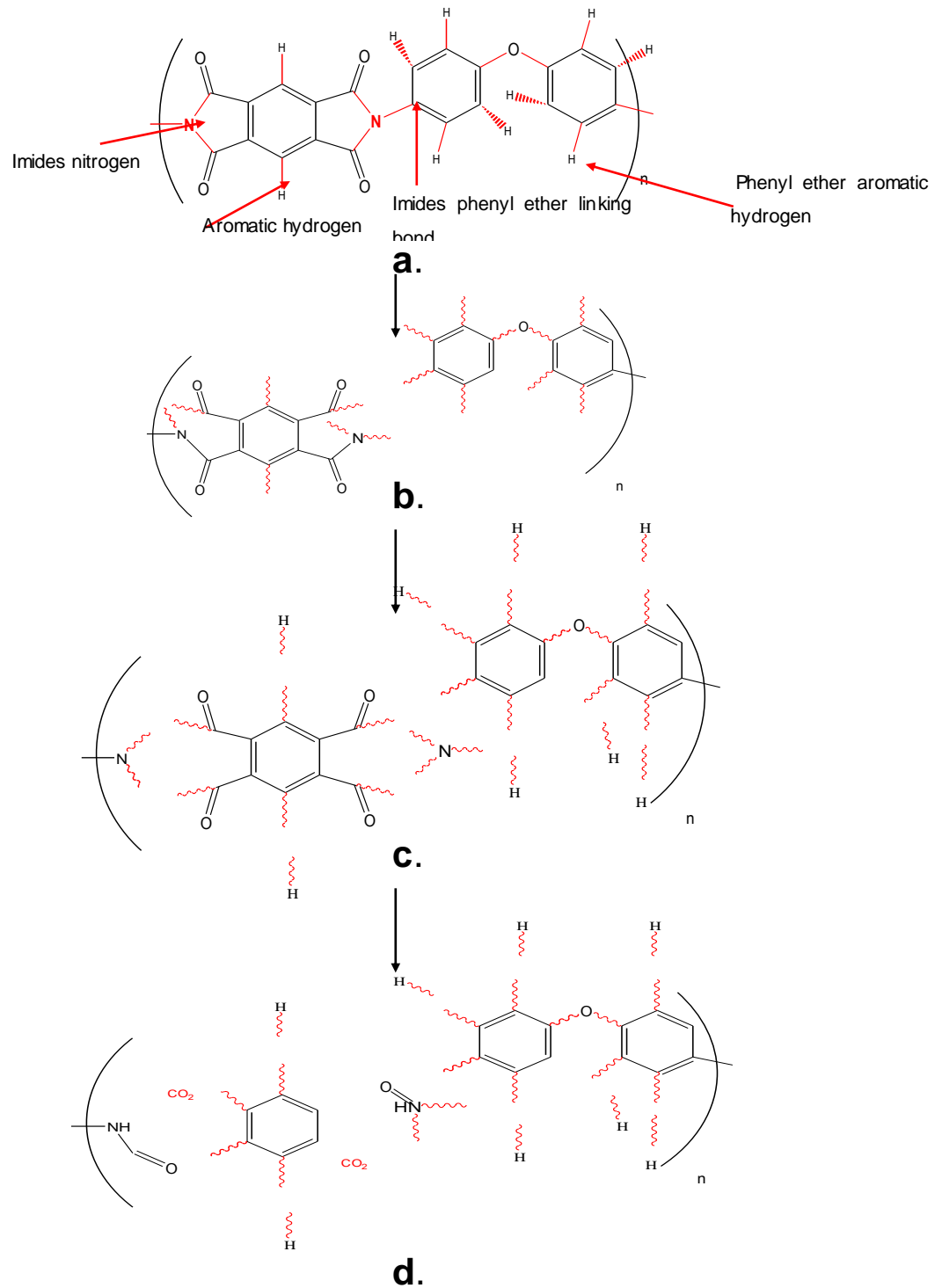


Figure 3.6: Decomposition and formation of unsaturated bonds and the formation of free radicals such as H atoms, adapted from literature [7]. (a) PI film before ion beam irradiation, (b & c) PI during irradiation and (d) PI films after irradiation.

Following the fragmentation illustrated in Figure 3.6 (d), it is expected that the aromatic moieties would condense to form fused rings, PAH's and ultimately carbonisation to give graphitic-like structures.

3.3.3 Effect of Annealing on the Molecular Characteristics of the irradiated Polyimide Films

Common Changes after Irradiation and Annealing in both PMDA-ODA and BTDA-ODA

In the PMDA-ODA and BTDA-ODA high frequency region of the spectra ($3100-2400\text{ cm}^{-1}$) a broad moisture absorbance band was observed. The following discussion specifically targets efforts to remove moisture and identify any structural changes associated with annealing of pristine and irradiated films of PMDA-ODA and BTDA-ODA prior to FTIR analysis. The annealing process enabled the spatial rearrangement of the polyimide molecular chains to give a more tightly packed and stronger interchain interaction. After drying, careful avoidance of exposure to moisture was taken, and the films were stored in a dry cabinet. In the initial ATR-FTIR examination of the annealed and irradiated PMDA-ODA and BTDA-ODA films, significant differences were observed when compared to the spectra of the non-annealed irradiated films.

The spectra of the pristine films (Figure 3.3) compared to the spectra of the irradiated films in Figures 3.4 and 3.5 after drying at 80°C , show a significant reduction in the width and intensity of the moisture band . The ATR-FTIR of films annealed at temperatures of 180°C and 280°C are shown in Figures 3.7 (a) and (b), where it is clear that any moisture adsorbed on the films has been eliminated . Watamori.et al. [18], in a study of the annealing effect on irradiated polyimide films, found that there was a significant depletion of hydrogen after annealing between 100°C and 300°C when the film was progressively held for five minute intervals at each temperature. Hydrogen desorption was reported when kapton films were annealed at 300°C ; however, other elements such as oxygen, nitrogen and carbon were not affected [18]. The effects of annealing on the band positions and intensities of the characteristic functional groups in PMDA-ODA and BTDA-ODA are shown in Figures 3.7 (a) and (b).

In the spectra of PMDA-ODA and BTDA-ODA, characteristic imide deformation bands were observed at 805 and 801 cm^{-1} respectively. As shown in Figure 3.7, after drying at 80°C, the imide deformation band increased in intensity. Annealing of both PMDA-ODA and BTDA-ODA at 180°C and 280°C reveals that the imide bands at 1371, 1305 and 1166 were diminished and/or eliminated, whilst the imide band at 1089-1013 cm^{-1} shows minor changes which indicate that there is a presence of the imide in some form, but the imide deformation bands at 805 and 801 cm^{-1} increased in intensity. These changes suggest that the imide rings were unstable after irradiation and are more unstable after annealing, which was indicated by further decomposition of the imide when heat treatment was applied.

The asymmetric ether bands of the irradiated PMDA-ODA and BTDA-ODA were observed at 1239 and 1229 cm^{-1} respectively. After drying at 80°C, the ether band shifted to 1200 cm^{-1} and the symmetric ether stretch, which increased in intensity, appeared at 1092 cm^{-1} .

However the PMDA-ODA film annealed at 180°C, and the BTDA-ODA film annealed at 280°C, both reveal a slight increase in intensity of the C-H bands at 713 and 680 cm^{-1} . This finding is consistent with the recovery of hydrogen that was reported by Watamori et al.[42], and attributed to the thickness of the irradiated film's surface.

The drying and annealing processes at temperatures of 80°C, 180°C and 280°C were selected for this analysis to understand, and identify, the changes that occur in the irradiated PI films as a result of thermal treatment.

Changes in the Spectra of PMDA-ODA Polyimide films After Annealing

In the previous section, the low frequency ATR-FTIR data for the un-annealed pristine and irradiated polyimide films, (PMDA-ODA and BTDA-ODA) were discussed. For PMDA-ODA the symmetric stretching mode of the carbonyl group, coupled through the five-membered imide ring, was at 1709-1701 cm^{-1} in the irradiated and dried PMDA-ODA. The carbonyl appeared as a shoulder at 1700 cm^{-1} , and although weak, it suggested that there was still some carbonyl functionality remaining in the films [52, 53]. In the dried and annealed PMDA-ODA, the carbonyl band shifted from 1765 cm^{-1} to 1756 cm^{-1} after annealing at 180°C and 280°C, exhibiting slow but gradual thermal decomposition of the PMDA-ODA carbonyl. Simultaneously, the shift of the band at 1765 to 1756 cm^{-1} toward the benzene ring band position suggests that annealing assists in the orientation and elimination of unstable bonds as well as an increase in aromaticity.

Drying and annealing affected the aromatic structure of both PI's (Figure 3.6). The PMDA-ODA films exhibited a shift in the benzene ring band position from 1559 cm^{-1} to 1593 cm^{-1} . The phenyl band positions were also observed to shift from 1600 cm^{-1} and 1455 cm^{-1} to 1599 cm^{-1} and 1588 cm^{-1} . Aromatic carbon groups were no longer observed as single peaks but rather as part of a larger peak. The shift of the aromatic carbon ring peak to a slightly higher frequency meant it became part of several different bands of the aromatic rings in the infrared spectrum, one of the vibrations in the spectrum being in the 1700 cm^{-1} region. This again suggests that there are relatively more aromatic carbon groups than there were before irradiation.

These changes included the shift of the imide carbonyl stretching band towards the lower frequency of 1700 cm^{-1} , which was indicative of gradual decomposition of the PMDA-ODA carbonyl; the shift to a higher frequency for the band at 1557 cm^{-1} to 1592 cm^{-1} , signifying the formation of benzene rings; the shift in the phenyl band from 1600 cm^{-1} and 1455 cm^{-1} to 1599 cm^{-1} and 1588 cm^{-1} , which also demonstrated a shift towards the formation of aromatic

carbon rings; and finally, the elimination of the imide band represented by the increased intensity of the imide deformation band at 801 cm^{-1} .

Changes in the BTDA-ODA thin film spectra

In contrast to PMDA-ODA the BTDA-ODA the partially reduced intensity of the benzophenone carbonyl ($>\text{C}=\text{O}$) stretching mode at 1779 cm^{-1} was accompanied by a progressive increase in intensity of the imide. This was consistent with the observations of Sun et al., Hu et al., and Maneesha et al. [7, 42, 44].

In the BTDA-ODA film spectra, the benzene ring bands were also observed to shift from 1501 cm^{-1} and may have been incorporated into the band at 1779 cm^{-1} , which is a broad band stretching from approximately 1800 cm^{-1} to 1500 cm^{-1} . The spectra of the BTDA-ODA PI film, dried and annealed at 180°C , show that at high ion fluence, the intensity of the C-H peak at 680 cm^{-1} was reduced.

In the spectra of the BTDA-ODA irradiated films exhibited a shift in the carbonyl stretch to 1779 cm^{-1} along with an increase in the band intensity, which was indicative of the formation of a carboxylic group; this was accompanied by a slight recovery in intensity of the C-H bands at 713 cm^{-1} and 680 cm^{-1} at a temperature of 280°C .

To date, there have been very few literature reports on annealing studies after radiation exposure of polymer films. It was evident from the annealing studies that irradiated PMDA-ODA films were the more suitable for the measurements described in the subsequent Chapters of this thesis, due to their superior thermal stability.

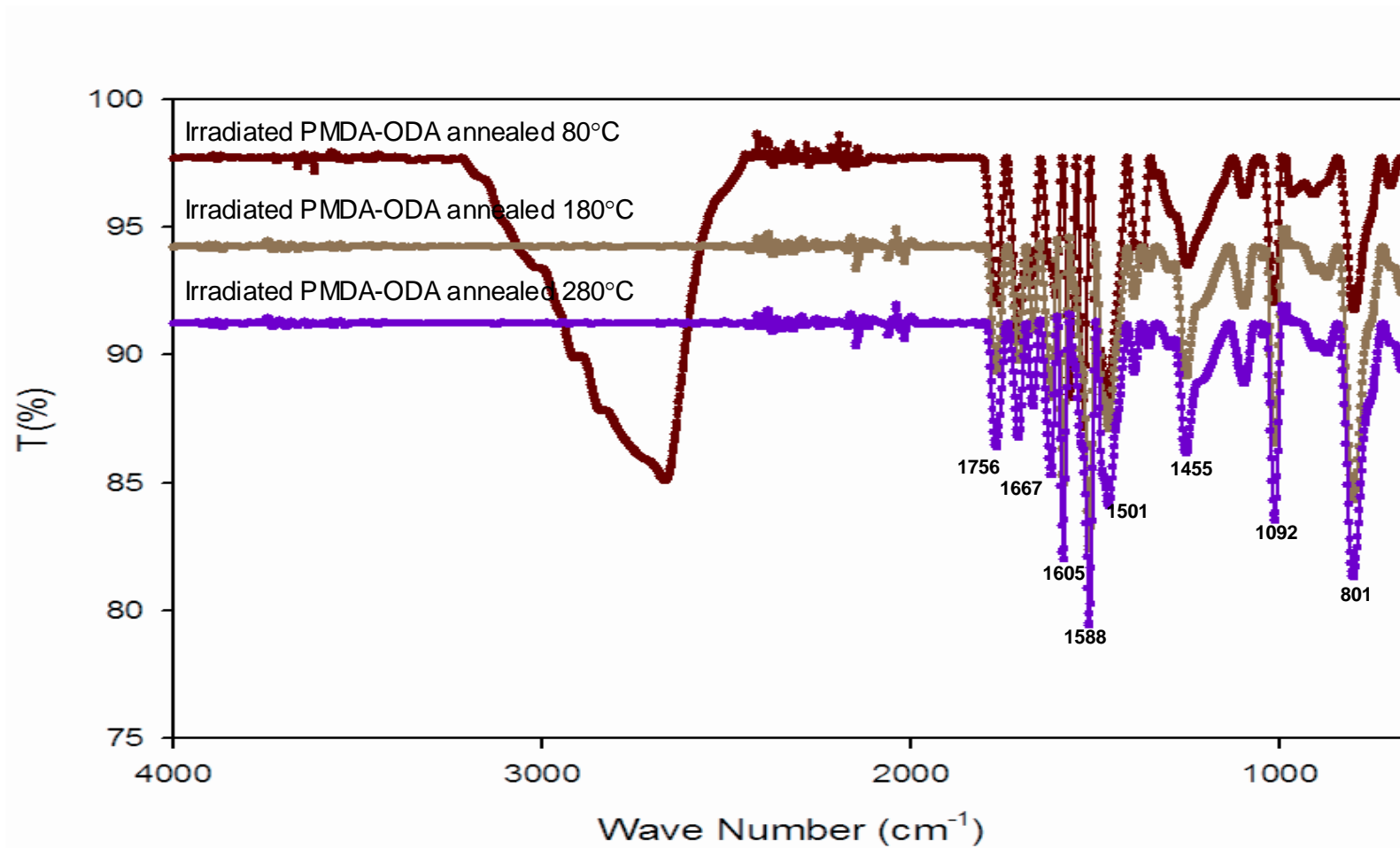


Figure 3.7 (a): The ATR-FTIR spectra of irradiated, pristine, dried and annealed films, PMDA-ODA with fluence values of 3×10^{14} ions cm^{-2} .

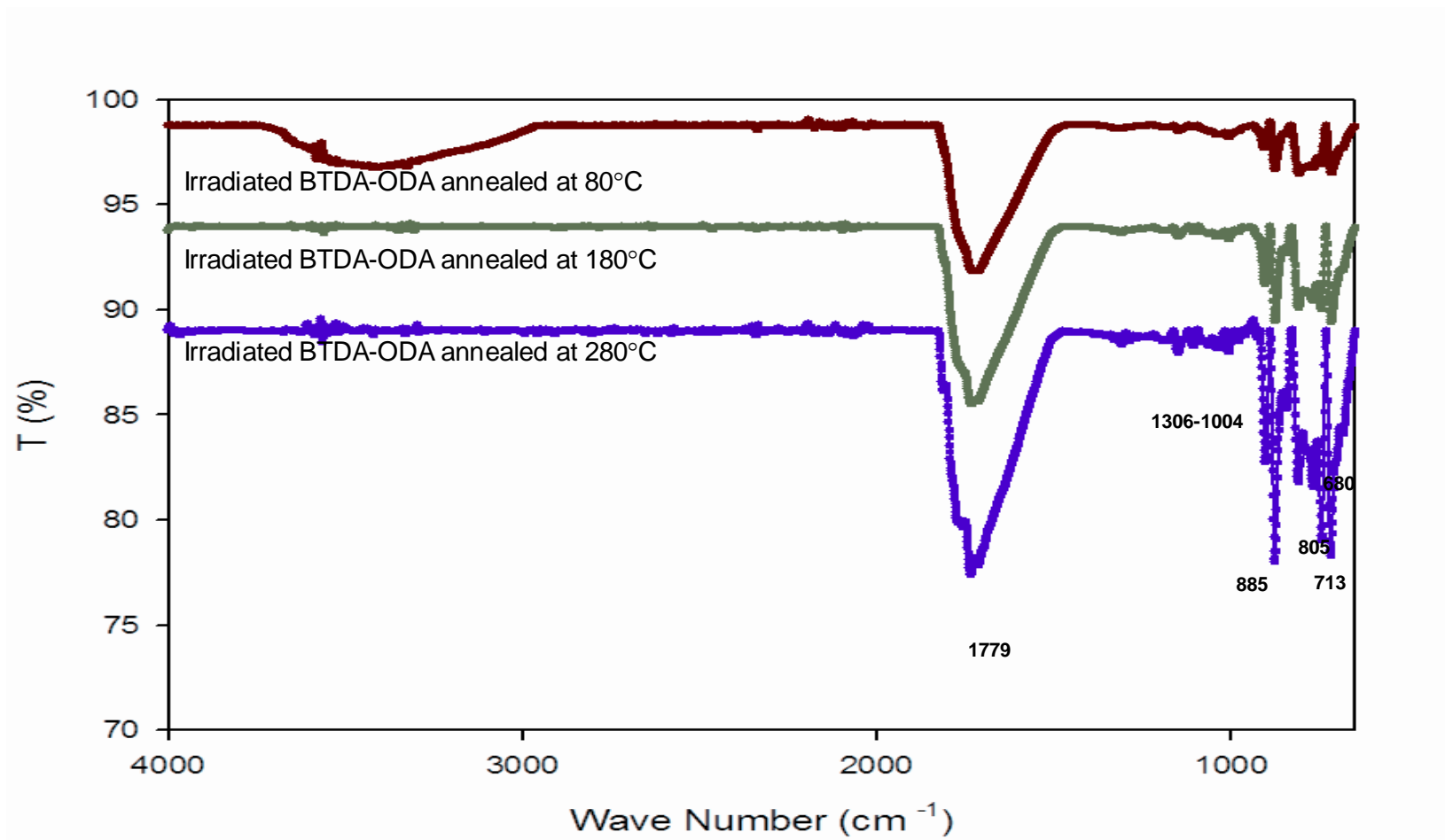


Figure 3.7 (b): The ATR-FTIR spectra of irradiated, pristine, dried and annealed films, BTDA, with fluence values of 3×10^{14} ions cm^{-2} .

3.3.4 X-Ray Photoelectron Spectroscopic studies of the PMDA-ODA films.

Although ATR-FTIR examination of the irradiated PI films showed variations in band position and intensity consistent with radiation induced chemical changes, a more sensitive method of analysis is desirable to confirm the presence of the increased aromatic carbon structure, indicative of the formation of carbon-rich regions in the surface of the PMDA-ODA PI films after Cu^{3+} ion-beam irradiation. Thus, X-ray photoelectron spectroscopy (XPS) was chosen as an appropriate technique which has been widely used for elemental analysis and chemical structure characterisation as it is a sensitive probe for the electronic environment around an atom, examining as it does, the ionisation (binding) energies of electrons in individual atomic orbitals [56].

Table 3.3 lists changes in the elemental concentrations in the PI films resulting from Cu^{3+} ion-beam irradiation. An average value of the binding energy was determined over three areas per film, with standard deviations of the order of 1%. Survey and high resolution XPS spectra of carbon, nitrogen and oxygen were acquired before, and after, Cu^{3+} ion-beam exposure for various fluences. The most significant changes in the irradiated surface layer occurred at the highest fluence of 5×10^{14} ions cm^{-2} . Clearly, the Cu^{3+} ion-beam irradiation has selectively depleted the oxygen and nitrogen content, and simultaneously increased the amount of carbon in the film.

Elemental ratios of the non-irradiated and irradiated PI films

The elemental composition and C/N, C/O ratios are presented in Table 3.3, where it is evident from the data for the film exposed to a fluence of 2×10^{14} ions cm^{-2} that the elemental composition of the irradiated PMDA-ODA films decreased for oxygen and nitrogen and increased for carbon. These results indicate that the oxygen and nitrogen atoms in the pristine PMDA-ODA were selectively ablated from the film's surface by the

Cu³⁺ ion-beam. This selective ablation not only reduced the relative ratio, but also caused the gradual formation of graphitic-carbon in the irradiated surface layer.

Table 3.3: The elemental composition ratios of the PI, pristine PMDA-ODA film surface, the irradiated film surface.

Samples	Elemental composition (wt %)			Elemental ratio (atom %)	
	C	N	O	C:N	C:O
Theoretical Values of PI	69.1	7.3	20.9	11:1	4.4:1
pristine PI	67.4	4.38	27.58	38:1	9:1
2x10 ¹⁴ ions cm ⁻²	85.81	2.96	11.23	29:1	7.6:1
3x10 ¹⁴ ions cm ⁻²	87.11	2.44	10.45	35:1	8.3:1
5x10 ¹⁴ ions cm ⁻²	89.9	0.89	9.21	101:1	9.7:1

PI = PMDA-ODA , Empirical formula C₂₂H₁₀O₅N₂ , molar mass = 382

The elemental composition is calculated automatically from the relative areas under the XPS bands.

Figure 3.8 presents the XPS survey spectra of PMDA-ODA PI films before, and after, Cu³⁺ ion-beam irradiation at a fluence of 5x10¹⁴ ions cm⁻². The peaks observed in these spectra can be assigned to the C 1s, O 1s and N 1s ionisation levels, and the C/N and C/O atomic ratios change significantly after irradiation when compared to the pristine ratio. The surface composition of the PI films before, and after, irradiation are listed in Table 3.3, where it can be seen that after the most intense irradiation the initial C/N atomic ratio of 38:1 increased to 101:1, and the initial C/O atomic ratio of 9:1 increased slightly to 9.7:1, suggesting a significant loss of N and a small decrease in O from the PI film, respectively. These results clearly indicate a progressive trend towards carbonisation of the PI film as the ion-beam fluence increases. Although the values of the pristine PI are different, the change that occurred after irradiation is very clear.

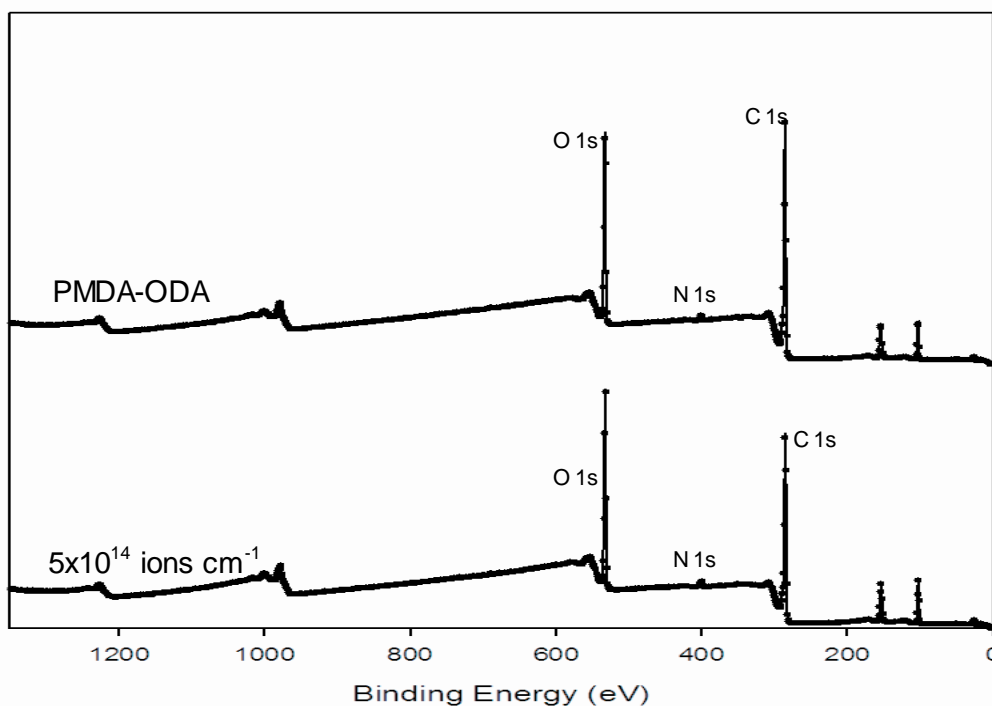


Figure 3.8 : XPS survey spectra of the pristine PMDA-ODA PI film and the film irradiated at a fluence of 5×10^{14} ions cm^{-1} .

The ratio of components in the XPS bands of the non-irradiated PI films

The molecular structure of pyromellitic dianhydride–4,4'-oxidianiline (PMDA-ODA) is presented in Figure 3.9.

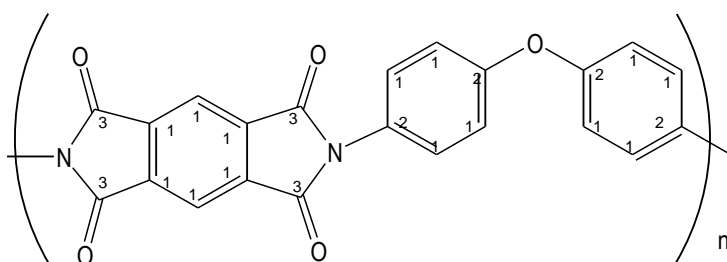
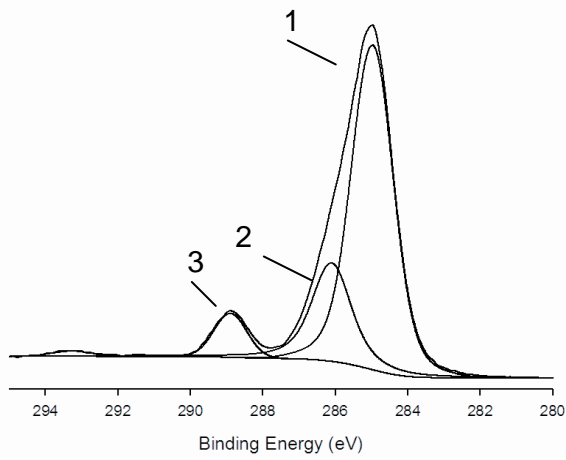
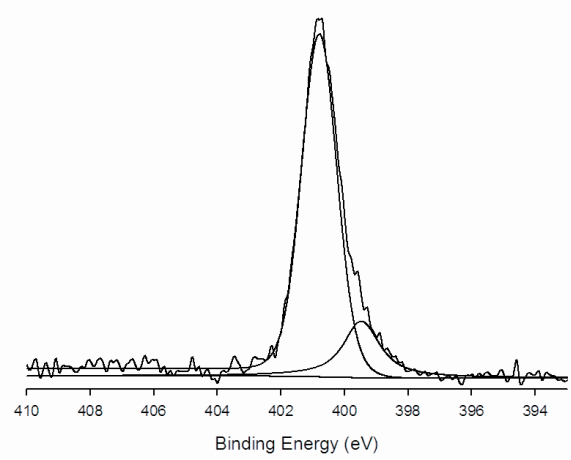


Figure 3.9: Molecular structure of pyromellitic dianhydride–4,4'-oxidianiline (PMDA-ODA). The numbers on the atoms in this structure refer to the numbers on the component peaks in Figure 3.10.

C1s



N1s



O1s

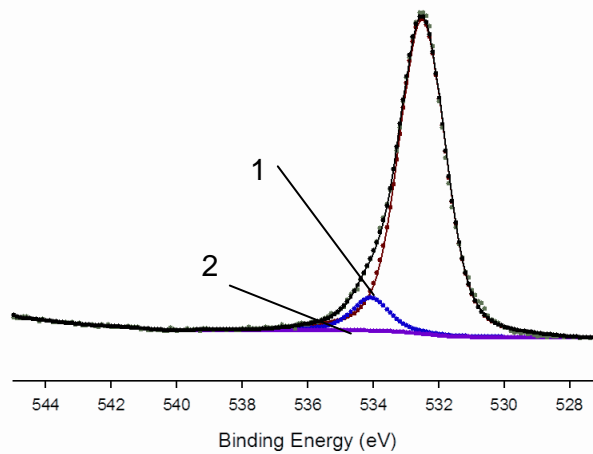


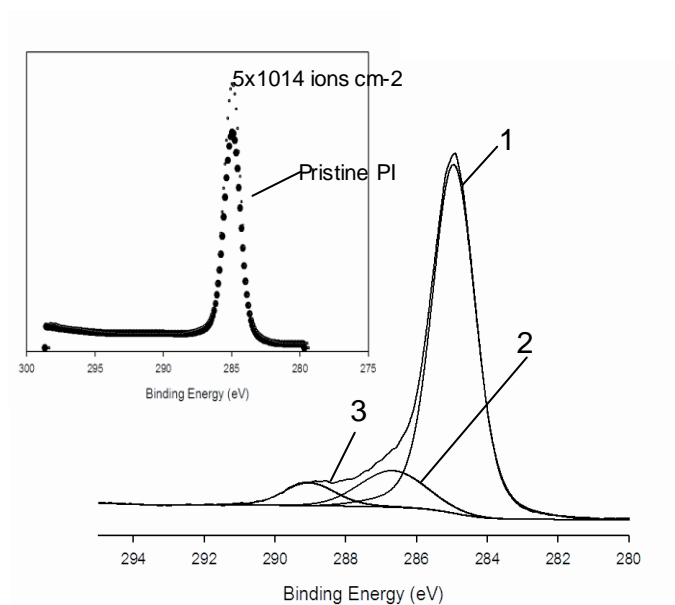
Figure 3.10: XPS spectra of the non-irradiated pristine PI films after curve-fitting; each curve was assigned to a corresponding bond in the PMDA-ODA polyimide.

Peak deconvolution of the XPS results for each element in the non-irradiated PMDA-ODA film are shown in Figure 3.10, where each component of all the element peaks was found to have a Full Width at Half-Maximum height (FWHM) in the range of 1.07 to 1.71 eV. The numbers attached to the component peaks correspond to the numbers indicated on the atoms in Figure 3.9.

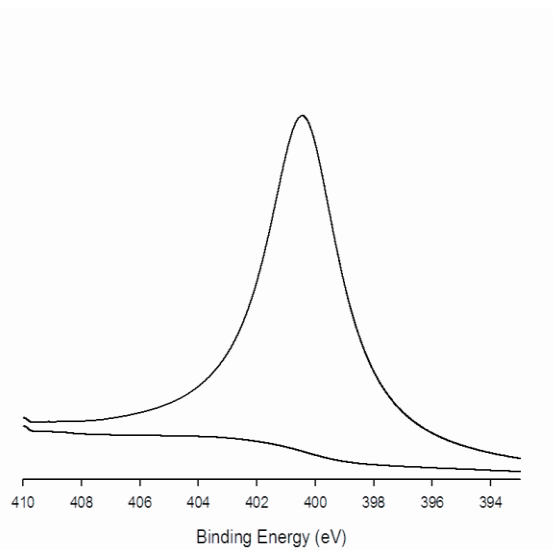
The C 1s band was deconvoluted into three different components, as reported by Hoffmann et al. [55]. Component peak 1, at a binding energy of 284.96 eV, is attributed to the sp^2 hybridised carbon atoms ($>C=C<$) of the three benzene rings in the PMDA-ODA structure.. Component peak 2, at a binding energy of 286.1 eV, was assigned to the sp^2 hybridised carbon atoms attached to a nitrogen single bond in the imide group and to the ethereal oxygen and component peak 3 at a binding energy of 288.89 eV, corresponds to the sp^2 hybridised carbon atom in the carbonyl group ($>C=O$) double bond. The C-O single bonds and the C-N single bond fall in the same region with very similar binding energies, hence it is difficult to separate the components, as the binding energy differences are very small.

Before irradiation, the O 1s band appears as two bands at binding energies of 532.51 and 534. eV , this is attributed to the oxygen of the C=O bond, and the ether oxygen of the ODA portion. Also, in the non-irradiated PMDA-ODA polyimide, the N 1s band, at a binding energy of 400.79 eV, was assigned to the imide nitrogen, and a very weak component at 399 eV was attributed to impurities in the film.

C 1s



N 1s



O 1s

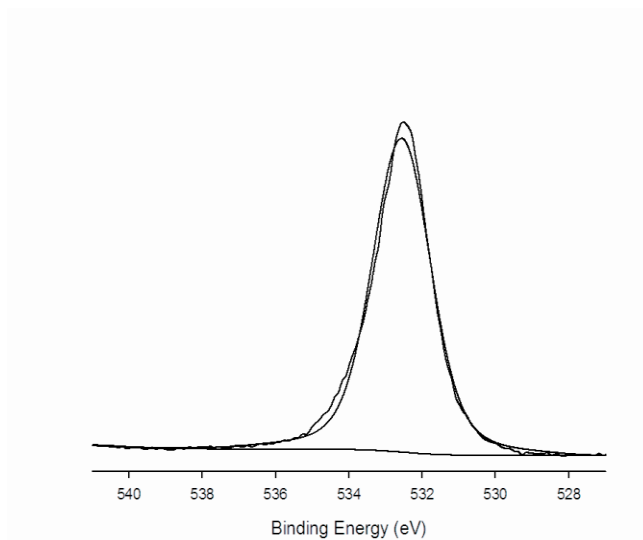


Figure 3.11: presents the deconvoluted XPS spectra for the irradiated PI films, from which the data in Tables 3.4 and 3.5 have been compiled.

The ratio of components in the XPS bands of the Cu³⁺ ion-beam irradiated PI films

Table 3.4: below, presents a summary of the deconvoluted XPS data for both the pristine and irradiated PMDA-ODA films.

Component peaks	Binding Energy (eV)					
	C 1s			N 1s		O 1s
	1	2	3	1	2	1
Samples						
Pristine PI film	284.96	286.1	288.89	400.79	399.46	532.51
Fluence 5x10 ¹⁴ ions cm ⁻²	284.95	286.68	289.01	400.42	---	532.56

Table 3.5 provides a summary of the component ratios, including the theoretical values for PMDA-ODA and samples of a pristine PMDA-ODA film surface, the irradiated films, and graphite, as determined from deconvolution of the XPS bands shown in Figures 3.12 & 3.13.

Table 3.5: The XPS component ratios for the C 1s, N 1s and O 1s binding energy bands for the theoretical PI, pristine PMDA-ODA film surface, the irradiated films, and graphite.

Samples	Component atomic ratio							
	Carbon			Nitrogen		Oxygen		
	1	2	3	1	2	1	2	
Non-irradiated PI	47.1	15.28	5.02	3.64	0.74	27.53		
2x10 ¹⁴ ions cm ⁻²	53.36	4.12	6.09	3.27	25.76			
3x10 ¹⁴ ions cm ⁻²	57.13	4.3	3.77	2.67	32.24			
5x10 ¹⁴ ions cm ⁻²	58.72	8.84	4.56	2.11	31.14			

Component peak 1 for C 1s at a binding energy of 284.95 eV (previously assigned to the benzenoid >C=C< bonds) increased in the component ratio from it's original value of 47.1 to 57.1 after irradiation. This increase in component peak 1 was indicative of an increase

in the number of sp^2 hybridised carbons, implying an increase in carbon-rich structure along the ion path in the PI. This C=C structure formed due to chain scission and molecular rearrangements. After superimposing component peak 1 of the irradiated PI and the corresponding peak of the pristine PI film, an increase in the irradiated PIs' component peak 1 ratio was noted which is attributed to the decrease in the ratio of component peak 2 (=C-N) from 15.28 to 4.3. These results suggest the carbon atoms in component peak 1 in the PMDA structure before irradiation have rearranged after irradiation, and formed C=C bonds, consistent with the observations reported in the XPS studies of Ektessabi et al. [57].

In the irradiated sample, the C 1s component peak 2 was slightly broader than the corresponding peak in the pristine film, which is attributed to the presence of three different bonds; one was the aromatic ring bonds of the PMDA-ODA structure, the other was the C-N bonds of the imide in the PMDA structure, and the third was created by the redistribution of carbon and nitrogen atoms that occurred due to chain scission and rearrangements of the molecular structure after ion-beam irradiation. The decrease in the C 1s component 3 ratio from 5.02 to 3.77 is suggested to arise from the loss of the ether oxygen bonds. This loss of oxygen is only marginal, and not supported by the data from the O 1s binding energy spectra shown in Figures 3.12 and 3.13, where the component ratios of the C=O plus C-O-C bonds changed from 27.53 to 25.76 (or 31.1 at higher fluence) before and after irradiation, respectively, although the small increase may be indicative of post-irradiation reactions of the films with ambient oxygen.

Prior to irradiation, the FWHM of component 2 in the C 1s peak of the non-irradiated PMDA-ODA was 1.29eV, and after irradiation the value changed to 2.22eV. The change in the FWHM indicates broadening of the peak (previously assigned to the imide =C-N bond) which was reported by Ektessabi et al. [57] and attributed to the random collision of the incident ions (i.e nitrogen ions) with the neighbouring C=O structure.

Such a broadening in the binding energy was reported Ektessabi et al. [57] to arise from the adjacent molecular structure directly affecting the variation in binding energy of the atom analysed. For instance, component peak 2 of the C 1s band in Figure 3.12, assigned to the sp^2 C of the aromatic ring attached to the imidic N of the PMDA structure, may have been affected by the proximity of the C=O during irradiation as was reported by Ektessabi et al. [57]. A similar effect is believed to operate in the broadening of component peak 3 in the C 1s spectra, which was found to have a FWHM variation from 1.07eV, pristine, to 1.75eV after irradiation. Moreover, the change in the FWHM of component peak 1 of the C 1s binding energy spectra was relatively large in comparison to the FWHM of component peaks 2 and 3 before irradiation, and relatively smaller after irradiation, with FWHM's ranging from 1.44eV to 2.22eV. This is attributed to bond breaking and deformation of the molecular structure causing a redistribution and scattering of hydrogen, oxygen and nitrogen atoms as a consequence of ion-beam irradiation. These changes are consistent with radiation induced carbonisation of the PI film surface.

3.5 CONCLUSION

The two polyimide films studied here using ATR-FTIR and XPS, PMDA-ODA and BTDA-ODA, were found to exhibit structural changes and molecular modification in direct response to ion-beam irradiation, and the impact of the surrounding atmosphere on the irradiated films. Both bond scission and cross-linking reactions, and an increase in the size of the aromatic crystallites, accompanied by a decrease in imidic and hydrogen atoms was observed. The presence of aromatic crystallites was suggested by the increase in intensity, and the shift in band position, of aromatic carbon in fused rings. The evidence presented suggests that chain-scission reactions gave rise to the formation of graphite-like structures in the area where the ion-beam penetrated the PI surface, consistent with reported observations [54-56].

Following ion-beam irradiation, the surface reactivity of the PI films was enhanced which caused them to become susceptible to their surrounding atmosphere, especially toward the facile absorption of moisture. This was evident from the broad moisture-related band that stretched from 3100 to 2400 cm^{-1} . Drying and annealing after the films were irradiated was found to result in the reduction and eventual elimination of this band. As such, all future PI films were treated to remove any adsorbed moisture before measurement.

The ATR-FTIR spectra in the low frequency region revealed that the modification which occurred to the carbonyl bonded imide nitrogen, directly affected the carbonyl functionality. The breakdown of the backbone imide linkage, and the elimination of hydrogen from the PI molecular structure, resulted in the formation of graphitic-like fused rings along the ion-paths in the modified surface of the PI, and this was supported by the XPS results. This was found to be consistent with the proposed mechanism for the pyrolytic conversion of a polyimide insulator to a semi-conductor and the laser induced permanent electrical conductivity, reported in the literature [23, 46]. It is concluded that the degradation of a polyimide film subjected to ion-beam irradiation was the consequence of chain scission reactions. The changes that were observed to occur in the molecular structure of these PIs suggested that the etched channels in the penetrated surface have been modified both chemically and physically. These changes have an impact on certain physical properties including electrical conductivity, micromechanical and electromechanical behaviour, as will be discussed in Chapters 4, 5 and 6.

A further important effect of annealing at the elevated temperatures of 180°C and 280°C, which completely removed moisture, was the increase in the intensity of the bands that represent the deformation of imide rings, along with a decrease in the intensity of bands that were characteristic of carbonyl and C-H. The BTDA-ODA benzophenone carbonyl band was only slightly affected. At these higher temperatures, the intensity of the PMDA-ODA ether bands was slightly affected, while the peaks of the aromatic carbons were observed to increase in intensity as the imide carbonyl peaks diminished in intensity [17, 23, 34, 37]. For BTDA-ODA the

change in hydrogen content was found to be dependent on the thickness of the film and the depth of irradiation. From the ATR-FTIR analysis of the two different polyimide films, the PMDA-ODA films have been found to have superior properties with regard to thermal degradation and structural stability.

In Chapters 4 and 5 extensive studies on the PMDA-ODA irradiated films will be described. Chapter 4 discusses the electrical conductivity properties of the irradiated films, concentrating on the aromatic crystallites that originate as a result of irradiation, since they are an essential requirement for the attainment of semiconducting properties. Chapter 5 describes a micromechanical study of the irradiated films, particularly with regard to their structural integrity. In addition, it includes a study of the electromechanical behaviour of the irradiated films.

3.6 References

1. Lambert, J.B., Shurvell; H.F., Lightner; D.A., Cooks., R.G. *Organic Structural Spectroscopy*. New Jersey United States of America: Prentice-Hall, Inc. 1998.
2. Long, J.E.R. Long, S.A.T. *Spectroscopic Analysis of Radiation-Generated Changes in Tensile Properties of Polyetherimide Film*. Technical Paper (NASA Langley Research Centre).2429. 1985.
3. Davenas, J., Xu, X.L., Boiteux, G. Sage, D., *Relation Between Structure and Electronic Properties of Ion Irradiated Polymers*. Nuclear Instruments and Method in Physics Research B, 1989. 39:p. 754. doi: [10.1016/0168-583X\(89\)90891-4](https://doi.org/10.1016/0168-583X(89)90891-4)
4. Xu, X.L., Xu, D., Xu, H.L., Wang, R., Zou, S.C., Du, G.D., Xia, G.Q. Existence of Structural Inhomogeneity in Ion - Beam - Modified Polyimide Films. *Journal of Vacuum Science and Technology A: Vacuum, Surfaces and Films* 1994. 12:p. 3200.
5. Sun, Y., Zheng. Z., Changlin Li, *Correlation Between the Structure Modification and Conductivity of 3 MeV Si Ion-Irradiated Polyimide*. Nuclear Instruments and Method in Physics Research B, 2002. 191:p. 805
6. Watamon, M., *Change of Hydrogen Concentration After Ion Beam Irradiation on Polyimide Films with 100-400C Annealing*. Nuclear Instruments and Method in Physics Research B, 2006. 249:p. 158.
7. Garg, M., Quamara, J.K., *Electrical Conduction Behaviour of High energy Ion Irradiated Kapton-H Polyimide Film*. Nuclear Instruments and Methods in Physics Research B, 2001. 179:p. 389.
8. El-Sayed A., Hegazy, T.S., Nishii, M., Seguchi, T. *Irradiation Effect on Aromatic Polymers: 2. Gas Evolution During Electron-Beam Irradiation*. *Polymer*. 1992. 33:p. 2904.
9. Fink, D., Omichi, H. Sasuga, T. Amaral, L. *Infrared Transmission of Ion Irradiated Polymers*. *Radiation Effect and Defects in Solids*. 1994. 132:p. 313.
10. Virk, H.S., *Physical and Chemical Response of 70 MeV Carbon Ion Irradiated Kapton-H Polymer*. Nuclear Instruments and Methods in Physics Research B. 2002. 191:p. 739.
11. Davenas, J., Boiteux. G., Fallavier, M., *Speculations on a Mechanism for The Ion Beam Induced Degradation of Polyimide*. Nuclear Instruments and Methods in Physics Research B. 1989. 39:p. 796.
12. Hnatowicz, V., Perina, V., Havránek,V., Vosecek, V., Novotný, J., Vacík, J. Svorcik, V., Rybka, V., Kluge, A. *Degradation of Polyimide and Polyethyleneterephthalate Irradiated with 150 and 200 keV Ar+ Ions, Studied by RBS and ERD Techniques*. Nuclear Instruments and Methods in Physics Research B. 2000. 161-163:p. 1099.
13. Lewis, M.B., Lee, E.H. *Residual Gas and Ion-Beam Analysis of Ion-Irradiated Polymers*. Nuclear Instruments and Methods in Physics Research B. 1991. 61:p. 457.

14. Wang, Y.Q., *Hydrogen Standards in Elastic Recoil Detection Analysis*. Nuclear Instruments and Methods in Physics Research B. 2004. 219-220:p. 115.
15. Kaneko, T., Watamori, M., Makita, H., Araujo, C., Kano, G. *Damage Evaluation After Ion Beam Irradiation on Polyimide Films Using ERD and RBS Techniques Simultaneously*. Nuclear Instruments and Methods in Physics Research B. 2004. 219-220:p. 236.
16. Terai, T., Kobayashi, T. *Properties of Carbon Films Produced From Polyimide by High-Energy Ion Irradiation*. Nuclear Instruments and Methods in Physics Research B. 2000. 166-167:p. 627-631.
17. Devasahayam, S., *FT-Raman Studies of a Range of Polyimide Subjected to High-Energy Radiation at Room and Elevated Temperatures*. Journal of Applied Polymer Science. 2006. 101:p. 1575-1582.
18. Watamori, M., *Change of Hydrogen Concentration After Ion Beam Irradiation on Polyimide Films with 100-400C Annealing*. Nuclear Instruments and Methods in Physics Research B. 2006. 249:p. 158.
19. Megusar, J., *Low Temperature Fast-Neutron and Gamma Irradiation of Kapton Polyimide Films*. Journal of Nuclear Materials. 1997. 32:p. 185.
20. O'Donnell, J.H., Sangster, D.S. *Principals of Radiation Chemistry*. Edward Arnold. New York. 1970.
21. Rasoul, F.A.; Hill, D.J., Forsythe, T., O'Donnell, J.S., Pomery, J.H., George, G. A., Young, P. R., Connell, J.W., *Aspects of the Radiation Chemistry of Some Transparent Polyimides*. Journal of Applied Polymer Science. 1995. 54:p. 1857.
22. Guide, P.E.U., *Universal ATR Sampling Accessory*. Perkin Elmer, Inc. 2005.
23. Feurer, T., R. Sauerbery, M.C. Smayling, B.J.Story, *Ultraviolet-Laser-Induced Permanent Electrical Conductivity in Polyimide*. Applied Physics A. 1993. 56:p. 275.
24. Bos, A., *High Pressure CO₂/CH₄ Separation with Glass Polymer Membrane-Aspects of CO₂-Induced Plasticisation in Membrane*. Technology Group. The University of Twente. 1996.
25. Cornelius, C.J., Marand, E., *Hybrid Inorganic-Organic Materials Based on a 6FDA-6FpDA-DABA Polyimide and Silica: Physical Characterization Studies*. Polymer. 2002. 43:p. 2385.
26. Pethybridge, G.D., Dobson, P.J., Brook, R.J., *Supercritical Drying Of Barium Titanate Alcolgels*. Applications of Ferroelectrics, 1994.ISAF '94., Proceedings of the Ninth IEEE International Symposium 1995:p. 562.
27. Tauc, J., Grigorovici, R., Vancu, A., *RF-Plasma Polymerization and Characterization of Polyaniline*. Physical state solution. 1966. 14:p. 627.
28. Makuuchi, K., Asano, M., Abe, T. *Effect of Evolved Hydrogen Fluoride on radiation-Induced Crosslinking and Dehydrofluorination of Poly(vinylidene fluoride)*. Journal of Polymer Science: Polymer Chemistry 1976. A14:p. 617.

29. Chiang, P-C., Whang, W-T., *The Synthesis and Morphology Characteristic Study of BAO-ODPA Polyimide/TiO₂ Nano Hybrid Films*. Polymer. 2003. 44:p. 2249.
30. Chapiro, A., *Chemical Modifications in Irradiation Polymers*. Nuclear Instruments and Method in Physics Research B. 1988. 32:p. 111.
31. Rajulu, A.V., Reddy, R.L., Raju, K.M., Avasthi, D.K., Asokan, K., *Infrared Spectroscopic Investigation of Polymethyl Methacrylate/Polvinyl Chloride Blends Films Irradiated by a ²⁸Si Ion Beam*. Nuclear Instruments and Method in Physics Research B. 1999. 156:p. 195.
32. Picq, V., Ramillon, J.M., Balanzat, E., *Swift Heavy Ions Irradiation on Polymers: Hydrocarbon Gas Release*. Nuclear Instruments and Methods in Physics Research B. 2000. 146:p. 496.
33. Costantini, J.M., Couverur, F., Salvetal, J.P. Bouffard, S., *Micro-Raman Study of the Carbonization of Polyimide Induced by Swift Heavy Ion Irradiations*. Nuclear Instruments and Methods in Physics Research B. 2002. 194:p. 132.
34. Hirata, K., Saitoh, Y., Narumi, K., Nakajima, Y. Kobayashi, Y., *Non-Linear Effect of Cluster Irradiation on Chemical Modification of Polycarbonate*. Nuclear Instruments and Method in Physics Research B. 2002. 193:p. 816.
35. Mohammad A. Wahab, I.K., Ha, C-S., *Microstructure and Properties of Polyimide/Poly(vinylsilsesquioxane) Hybrid Composite Films*. Polymer. 2003. 44:p. 4705.
36. Tretinnikov, O. N., Ikada. Y., *Surface Characterization of Ion-Implanted Polyethylene*. Journal of Polymer Science, Polymer Physics. 1998. 36:p. 715.
37. Svorcik, V., K. Prošková, V. Hnatowicz, E. Arenholz, A. Kluge, *Polyimide Modified by Irradiation with C⁺ and N⁺ Ion Beams*. Polymer Degradation and Stability. 1999. 65:p. 131.
38. Srinivasan, R., Hall, R.R., Wilson, W.D., Loehle, W.D., Allbee, D.C, *Formation of a Porous, Patternable, Electrically Conducting Carbon Network by the Ultraviolet Laser Irradiation of the Polyimide PMDA-ODA*. Chemistry of Materials. 1994. 6:p. 888.
39. Srinivasan, R., Hall, R.R., Wilson, W.D., Loehle, W.D., Allbee, D.C, *Ultraviolet Laser Irradiation of the Polyimide, PMDA-ODA (Kapton™), to Yield a Patternable, Porous, Electrically Conducting Carbon Network*. Synthesis Metal, 1994. 66:p. 301.
40. Chengxiang, Z., L.Q., Yin Jie, *Photochemical Surface Modification of Polyimide Containing Benzophenone Unit by UV Source*. Polymer Engineering, 2001. 3:p. 54.
41. Watamori, M., *Change of Hydrogen Concentration After Ion Beam Irradiation on Polyimide Films with 100-400C Annealing*. Nuclear Instruments and Methods in Physics Research B. 2006. 249:p. 158.
42. Steckenreiter, T., Balanzat, E. Fuess, H. Trautmann, C., *Chemical Degradation of Polyimide and Polysulfone Films Under the Irradiation with Heavy Ion of Sveral Hundred Mev*. Journal of Polymer Science: Part A Polymer Chemistry. 1999. 37:p. 4318.

43. Ree, M., Kim, K., Woo, S.H., Chang, H., *Structure, Chain Orientation, and Properties in Thin Films of Aromatic Polyimides with Various Chain Rigidities*. Journal Applied Physics. 1996. 81:p. 698.
44. Davenas, J., Boiteux, G., *Ion Beam Modified Polyimide*. Advanced Materials, 1990. 2:p. 521.
45. Bruck, S.D., *Thermal Degradation of Piperazine Polyamide II-Poly(terephthaloyl piperazine), Poly(terephthaloyl 2-methylpiperazine) and Poly(isophthaloyl trans-2,5-dimethylpiperazine)*. Polymer. 1996. 7:p. 231.
46. Virk, H.S., *Physical and Chemical Response of 70 MeV Carbon Ion Irradiated Kapton -H Polymer*. Material Science. 2001. 24:p. 529.
47. Svorcik, V., Proskova, K., Hnатовicz, V., Arenholz, E., Kluge, A., *Polyimide Modified by Irradiation with C⁺ and N⁺ Ion Beams*. Polymer Degradation and Stability. 1999. 65:p. 131.
48. Hu, L., *Evolution in Chemical Structure and Gas Permeation Properties of Polyimide Induced by Ion Beam Irradiation*, in *Chemical and Environmental Engineering*. 2004. Toledo: United States. p. 222.
49. Guenther, M., Gerlach, G., Suchaneck, G., Share, K., Eichhorn, K-J., Wolf, B., Deinka, A., Jastrabik, L., *Ion-beam Induced Chemical and Structural Modification in Polymers*. Surface and Coating Technology. 2002. 158-159:p. 108.
50. Tyan, H.L., Lui, Y.C., Wei, K.W., *Enhancement of Imidization of Poly(amic acid) Through Forming Poly(amic acid)/organoclay Nanocomposites*. Polymer. 1999. 40:p. 4877.
51. Hu, Q., Marand, E., *In Situ Formation of Nanosized TiO₂ Domains within Poly(amide-imide) by a Sol-Gel Process*. Polymer. 1999. 40:p. 4833.
52. Davenas, J., Boiteux, G., XU, X.L., *Role of the Modifications Induced by Ion Beam Irradiation in the Optical and Conducting Properties of Polyimide*. Nuclear Instruments and Methods in Physics Research B. 1988. 32:p. 136.
53. Davenas, J., Boiteux, G., *Photon, Beam and Plasma Enhanced Processing*. Les Edition de Physique 1987.
54. Faguy, P.W., Lucas, R.A., Ma, W. *An FT-IR-ATR Spectroscopic Study of the Spontaneous Polymerization of Pyrrole in Iron-Exchanged Montmorillonite*. Colloids and Surfaces A: Physicochemical and Engineering Aspects. 1995. 105:p.105
55. Hoffmann, E.A., Kortvelyesi, T., Wilusz, E., Korugic-Karasz, L.S., Karasz, F.E., Fekete, Z.A. *Relation Between C1s XPS Binding Energy and the Partial Charge of Carbon Atoms in Polymers*. Journal of Molecular Structure: THEOCHEM. 2005. 725:p. 5.
56. Zeng, D.W., Young, K.C., Xie, C.S. *XPS Investigation of the Chemical Characteristics of Kapton Films Ablated by a Pulsed TEA CO₂ Laser*. Surface and Coatings Technology. 2002. 153:p. 210.
57. Ektessabi, A.M, Hakamata, S. *XPS Study of Ion Beam Modified Polyimide Films*. Thin Solid Films. 2000. 377-378:p. 621.

4

TEMPERATURE DEPENDENT ELECTRICAL BEHAVIOUR of IRRADIATED POLYIMIDE FILMS

4.1. Introduction

As discussed in Chapter 1 irradiation is an efficient route to promoting the formation of conducting sites as well as the introduction of other substantial modifications to polymer properties. Use of the irradiation process is attractive as there are a range of different ions which have the ability to change materials at the molecular level. This structural modification of PI films has been described in Chapter 3, where it was found that graphitic-fused ring structures were formed along the path etched by the ion-beam in the insulating PMDA-ODA films. The carbon-rich clusters were found to be well dispersed in the surface penetrated by radiation in the PMDA-ODA film, forming carbon composites similar to those of the conventional carbon nanotube and carbon nanocomposite films investigated by Mora-Huertas et al. [17] The carbon-black nanoparticles used in the study by Mora-Huertas et al. [18] possessed a microstructure of many overlapping graphitic layers well dispersed in a PI matrix.

Wolszczak et al. [4] investigated the behaviour of both conducting and insulating polymers after γ -ray or electron-beam irradiation, and found that the electrical properties of the materials changed significantly [4]. The changes to the conducting polymers, polyaniline, polypyrrole and polythiophene, included two variations of their properties. Firstly, the

conductivity decreased with increasing dose when the irradiation was performed in a vacuum; and secondly, the conductivity increased with irradiation under a dopant atmosphere [4]. For the non-conducting polymers, polyaniline, polypyrrole and polythiophene, the conductivity was reported to increase with increasing radiation dosage [4].

The introduction of this type of electrical conductivity in an insulating material has been studied extensively over the years. For example, Yuguang et al. [5] studied polyethylene terephthalate (PET) modified by Ag, Cr, Cu and Si ion implantations at doses ranging from 1×10^{16} to 2×10^{17} ions cm^{-2} . These workers found that at a dose of 2×10^{17} ions cm^{-2} the resistivity was less than 10 Ohm cm for all irradiation ions with the exception Si ion, which was several hundred Ohm cm. This change was related to the effect of the different ions on the molecular structure of PET [5].

Other studies, such as that reported by Fitzer et al. [1] in the review article, "The chemistry of the pyrolytic conversion of organic compound to carbon" [1] emphasises the pyrolytic conversion of organic compounds into carbonaceous materials. For example, in the 1980s, Kaplan used heavy ion irradiation, to induce conductivity in organic insulating materials by degradation processes, which involved the nucleation and growth of conducting clusters [2]. In addition, Feurer et al. [6] reported that the electrical conductivity of a polyimide increased by 16 orders of magnitude after UV-laser irradiation, and that the activation energy for electron transfer was 3.9 eV after 300 pulses which decreased to 5 meV after 1000 pulses, at a fluence of 80 mJ cm^{-2} [6]. The study of electrically conducting structures reported by Philips et al. [7], found that polyimide films evolved into electrical conductors as a result of laser irradiation to produce electrically conductive localised clusters of carbonaceous materials after a sufficient accumulation of clusters, dependent on the extent of exposure to the laser beam.

The temperature dependent electrical conductivity of the irradiated materials and/or polymers was used to determine the charge transport mechanism. Davenas et al. [14] have reported that the irradiation of PI films at both liquid nitrogen and room temperature resulted in a conducting phase that was thermally assisted in accordance with the reported large dose effect. This conductivity was also reported to be inhibited when the PI films were heated to 400°C. The UV-laser irradiation study by Phillips et al. [7] discovered that the functional dependence of the resistivity resulting from temperature changes was consistent with the so-called Variable Range Hopping (VRH) electrical conduction mechanism. Similar VRH conduction mechanisms were also observed by Feurer et al. [6] to be associated with heat treatment of the irradiated polyimide.

The hopping conduction between two localised electronic states was reported to be the result of an electron-lattice interaction. The atomic vibrational motion resulting from the hop varies with the relative energy between the localised states [3]. If the hopping is adiabatic, this implies that the electron transfer energy between the two sites that take part in the hop is larger than the phonon energy, thus the electronic carriers follow the changing atomic configuration. If the hopping is non-adiabatic, then it suggests that the electron transfer energy between the two sites is smaller than the phonon energy. The hopping rate of the non-adiabatic jump depends on the relative distance between hopping centres.

Since ion-beam irradiation can modify the electrical conductivity properties of very small areas of polymer, it is possible to reduce the size of devices used in various industries, as the irradiation process allows for targeted atomic molecular structure change. This technology is particularly applicable in the nuclear power, defence electronics and space industries [3]. Other examples of micro-devices include flexible circuits, semiconductor pads, microprocessor chip carriers, coil insulation, magnetic wire insulation and solar arrays [8]. It is evident from the study carried out by Svorok et al.[8] among others, that

polyimides provide the ultimate, unique and superior chemical, mechanical and thermal properties for irradiation investigations [8].

In this chapter, the conversion of insulating polyimide into conducting polyimide films is examined with respect to conductivity and charge transport mechanisms. In the previous Chapter, the effect of irradiation on the molecular structure and thermal stability were discussed. In this Chapter the relationship between the molecular structure changes and the electrical conductivity will be addressed, as well as the effect of heat on electrical conductivity, in terms of charge transport and moisture absorption post-irradiation.

4.2 Sample Preparation and Characterisation

Several irradiated PMDA-ODA films were used depending upon the analysis method. Here, the PMDA-ODA films were prepared according to the process shown in Figure 2.12 of Chapter 2. PMDA-ODA films exposed to an ion-beam fluence of 1×10^{14} to 5×10^{14} ions cm^{-2} were used for electrical conductivity studies. The dimensions of the film strips were, length 2 mm and width 1.56 mm, and conductive silver contacts [9, 21] were painted on each end of the irradiated films.

The temperature dependent electrical conductivity was performed in a chamber filled with nitrogen. The standard 'two probe method' was used for PMDA-ODA films with low resistance. The "two probe method" involved two probes placed in direct contact with the silver painted area of the films. Further details of the contact arrangement are available in Section 2.3.3.2 of Chapter 2.

The ohmic contact of the silver paint was confirmed by impedance and current-voltage (I-V) measurements as discussed in Chapter 2. The room temperature electrical conductivity measurements were performed as described in Section 2.2.1 of Chapter 2, and involved the films being held at 25°C in a nitrogen atmosphere for 30 minutes before data collection.

4.3 Electrical Resistance Behaviour of Irradiated Films

4.3.1 Ambient Temperature Electrical Properties of Irradiated Polyimide Films

The room temperature Current (I)-Voltage (V) measurements were performed by applying a voltage ranging from 0 to 28 Volt to the PI films which had been irradiated at various fluences.

When a voltage (V) is applied across a material, a current of magnitude (I) flows, and in accordance with Ohm's law, the current is proportional to the voltage at low applied voltages :

$$\text{So, } I \propto V \text{ ; and Ohm's law gives } I = \frac{V}{R} \quad (4.1)$$

Where I (ampere = coulomb/sec) is the current flow, V (Joule/coulomb) is the voltage applied and R (ohm) is the electrical resistance.

In addition to illustrating ohmic conduction, the I-V curves can also be used to obtain information about the nature of the conduction processes occurring, such as, ionic hopping, tunnelling, Schottky and Poole-Frankel mechanisms [25-28].

Figure 4.1 illustrates a typical I/V curve demonstrating ohmic behaviour.

From the I-V plot the electrical resistivity of the irradiated films was calculated using the following equation:

$$\rho = \frac{RA}{L} \quad (4.2)$$

Where ρ is the electrical resistivity, R is the electrical resistance of the specimen, A and L are the area and length of the specimen, respectively, through which the current passes.

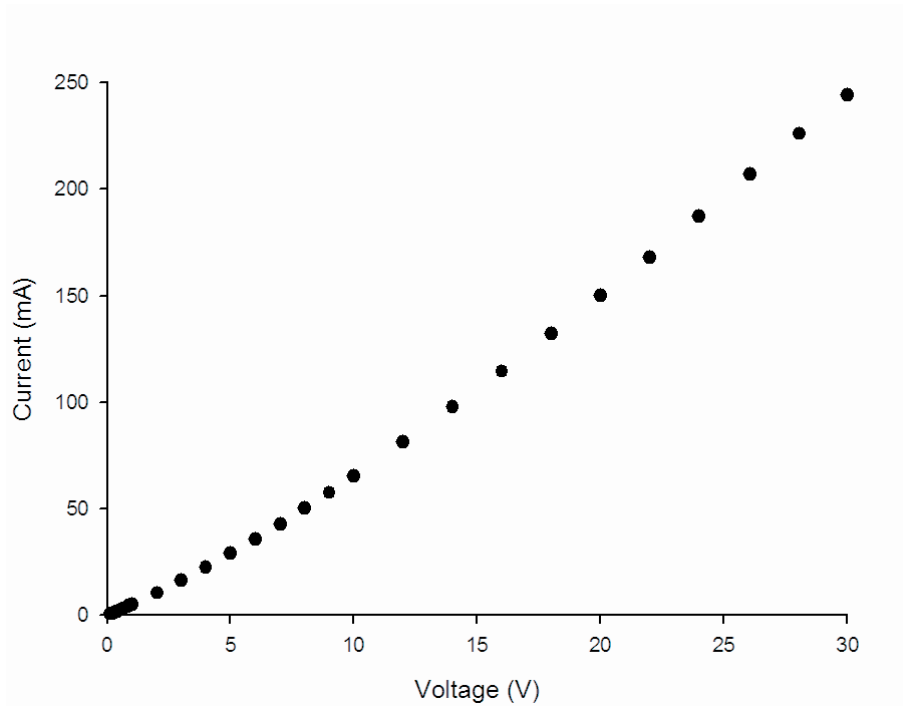


Figure 4.1: Current-Voltage graph confirming ohmic behaviour of the irradiated PI film fluence 5×10^{14} ions cm^{-2} .

Figure 4.2 illustrates the significant decrease in resistivity (ρ) (ie., an increase in electrical conductivity, σ) of the PI films with increased ion-beam fluences, ranging from 9×10^{13} to 5×10^{14} ions cm^{-2} . For example, the resistivity of a PMDA-ODA film was lowered by almost five orders of magnitude from a resistivity high of $10^5 \Omega \text{ cm}$ to approximately $10^1 \Omega \text{ cm}$. Likewise, in the study by Kaplan et al.[29] of the initially highly resistive organic thin films (3,4,9,10-perylenetetracarboxylic dianhydride (PTCDA), 1,4,5,8 naphthalenetetracarboxylic dianhydride (NTCDA), and Ni phthalocyanine (NiPc)) it was observed that the resistivity of the films decreased by 13 orders of magnitude, as the ion dose increased. A comparison of the behaviour of the two PIs examined in this study,

PMDA-ODA and BTDA-ODA, showed a significant compositional dependence. This was evident at a fluence of 3×10^{14} ions cm^{-2} , where the resistivity difference was nearly two orders of magnitude. The dependence of the electrical resistivity on the ion-beam fluence in these irradiated PMDA-ODA nanocomposite films was consistent with the reported results of CNT-polymer composites [14, 17, 21, 30].

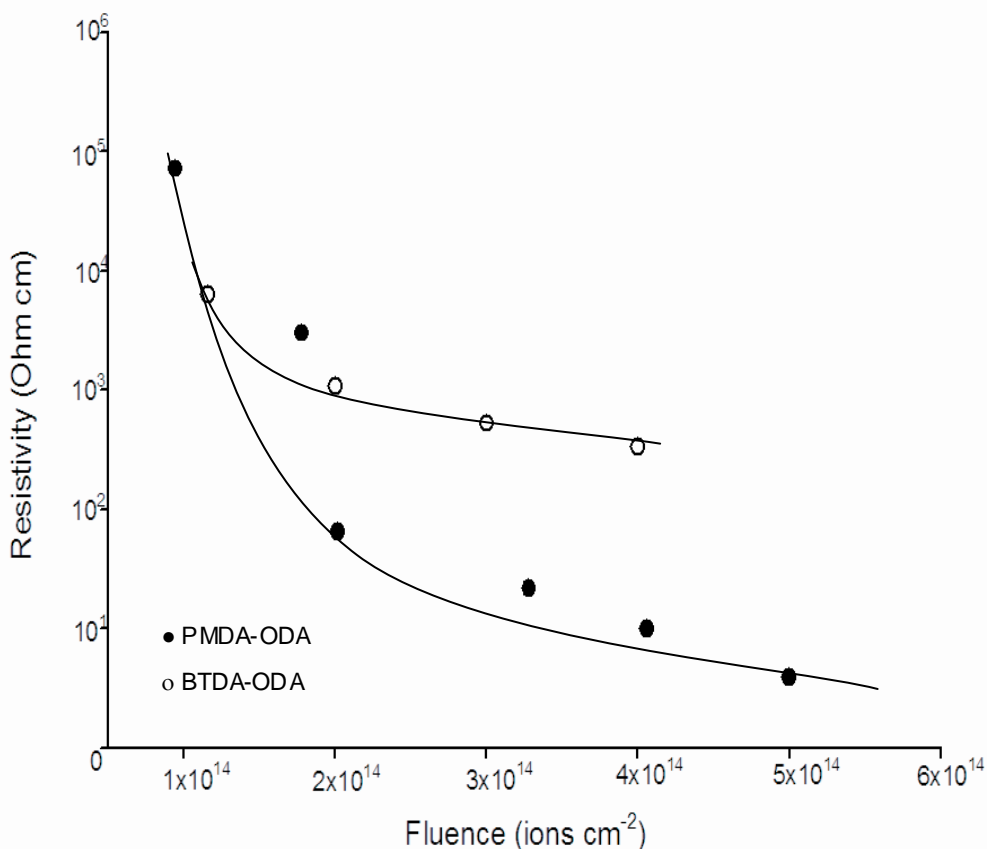


Figure 4.2: Electrical resistivity variation with fluence of irradiated PMDA-ODA and BTDA-ODA PI nanocomposite films.

4.3.2 Temperature Dependent Electrical Behaviour of Irradiated Polyimide Films

As reported in Chapter 3, the high energy Cu^{3+} ion-beam irradiation of PMDA-ODA polyimide films results in chain scission and bond cleavage along the ion path as the energy is dissipated into the surrounding polymer matrix. This gives rise to the formation of carbon-rich graphite-like tracks etched into the surface of the films.

The temperature dependent electrical resistivity of PMDA-ODA films over the temperature range of 298 to 328K, and exposed to ion-beam fluences of 9×10^{13} to 5×10^{14} ions cm^{-2} , are plotted in Figure 4.3. As can be seen, the resistivity (and hence, resistance) decreases with increasing temperature, which is consistent with the reported semiconducting behaviour of the films. During the first cycle of measurements, the residual stress and thermal history arising from irradiation of the PMDA-ODA films produced distorted data. However, the subsequent second and third cycles of electrical resistive behaviour were observed to be reproducible, reversible and free of hysteresis.

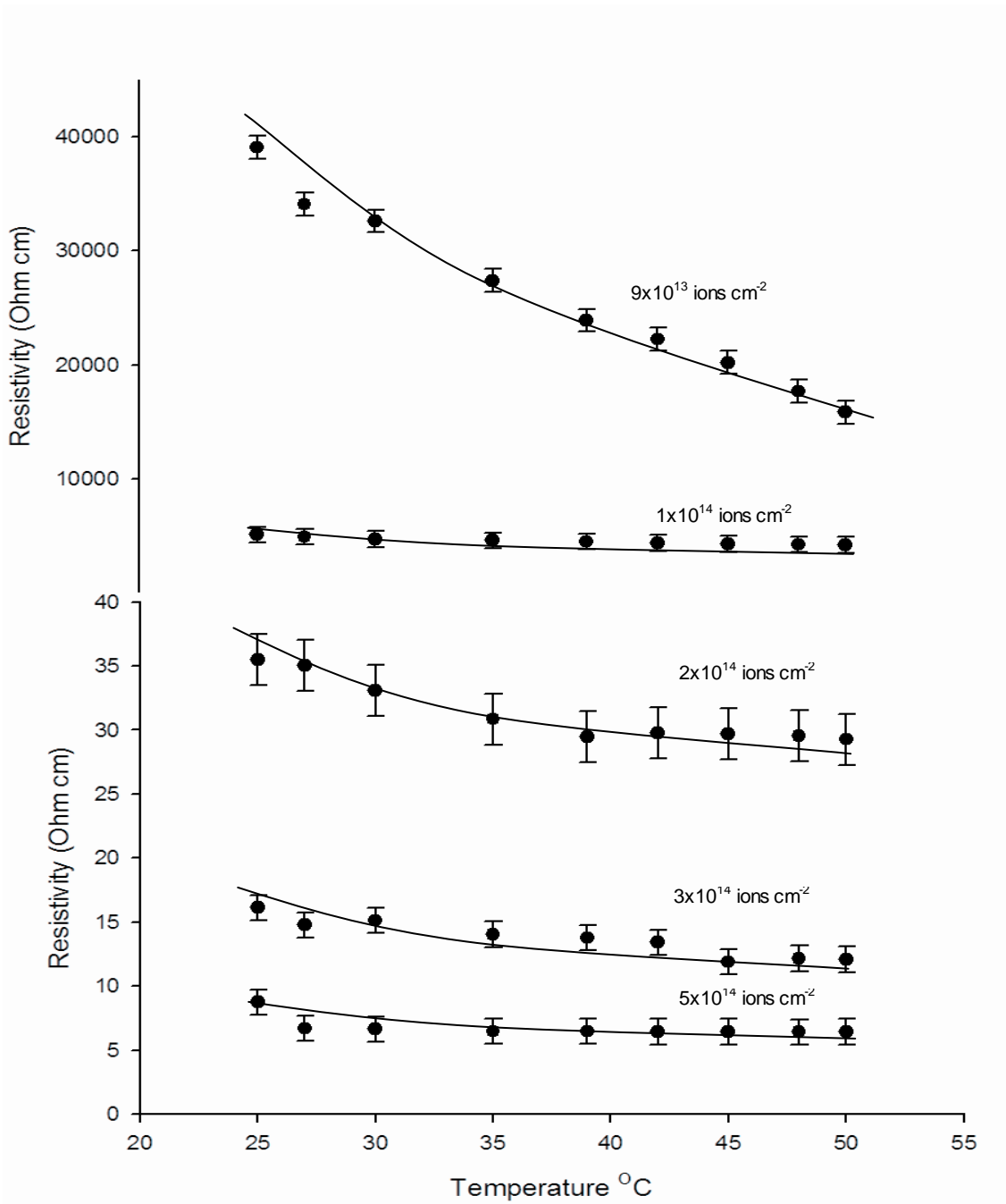


Figure 4.3: Temperature dependent electrical resistivity of the irradiated PMDA-ODA films with fluence values ranging from 9×10^{13} to 5×10^{14} ion cm^{-2} .

Because of the semiconducting behaviour of the irradiated PMDA-ODA films, the resistivity variation with temperature can be analysed in terms of an Arrhenius relationship of the form :

$$\rho = \rho_0 \exp[-(E_a / kT)^{-1}] \quad (4.3)$$

where ρ is the resistivity, ρ_0 is the pre-exponential factor, E_a is the activation energy (which in this case is expressed in electron-volts (eV)), k is the Boltzmann constant (8.6×10^{-5} eV / K), γ is the power law of the temperature exponent, and T is the absolute temperature in Kelvin .

The temperature exponent, γ , also defines the hopping dimension (as in Equation 1.5, Chapter 1).

$$\text{So } \ln(\rho/\rho_0) = -(\gamma Ea/kT) \text{ ie., } \ln(\rho) = \ln(\rho_0) - (\gamma Ea/kT) \quad (4.4)$$

For a 3-D charge hopping process, γ is 1,

$$\text{So, } \ln(\rho) = \ln(\rho_0) - (Ea/kT) \quad (4.5)$$

And so a plot of $\ln(\rho)$ [or $\ln(\sigma)$, since $\rho = 1/\sigma$] versus $1/T$ should be linear, from which the slope can be used to obtain a value of E_a .

Figure 4.4 illustrates how the calculated E_a values decrease with increasing fluence, with a value of 2.28 eV at a fluence of 0.9×10^{13} ions cm^{-2} , and 0.42 eV at a fluence of 5×10^{14} ions cm^{-2} . This observation is consistent with the fact that at higher fluences there will be many more overlapping graphitic tracks, arranged more densely, so the "hopping distances" should be shorter, with a lower activation barrier, allowing more ready charge movement.

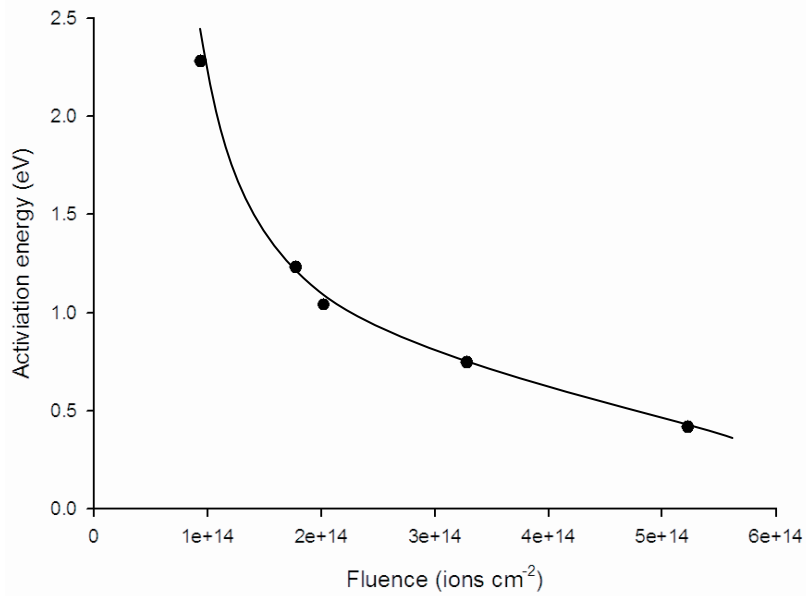


Figure 4.4: Variation in E_a for different fluences of the Cu^{3+} ion-beam irradiation of the PMDA-ODA films.

Electrical Transport Mechanism(s)

The electron transport properties of composites containing semiconductors have been extensively investigated in the past. For example, semiconducting irradiated films were studied by Salvetal [3], Klafter [23], Phillips [7] and Sheng, Abeles and Arie [24] who reported electrical transport via various hopping conduction mechanisms, including Nearest Neighbour Hopping (NNH), which involves charge hopping at close particle proximity, and Variable Range Hopping (VRH), which occurs at large particle separations. Sheng [22, 23] also reported Fluctuation Induced Tunneling (FIT), which involves thermally activated electron tunneling from one site to another.

The typical Arrhenius plot, based on Equations 4.4 and 4.5, $[\ln(\rho/\rho_0) = -(E_a/kT)^\gamma]$ i.e., $\ln(\rho) = \ln(\rho_0) - (E_a/kT)^\gamma$, allows the Arrhenius equation exponent of T (γ) to be evaluated. Studies reported by Cella et al., Magudapathy et al. and Quivy et al. [11,12,13] on polymer-graphite composite materials and Silver nanoclusters embedded in glass matrix indicate a variation of the power law exponent from 0.25 to 1 in complex composite

systems, suggesting more than one type of mechanism was involved in conduction [6,7,9, 11]. For example, the temperature dependence of the resistivity of granular metals was reported to exhibit a temperature exponent (γ) of -0.5, suggesting the operation of various transport mechanisms.

Yuguang et al. and Feurer et al. [5,6] reported the low temperature behaviour of metal implanted polymer and laser irradiated polyimide films fitted a $1/T^{0.25}$ relationship ($\gamma = 0.25 = 1/4$) which results from Mott's three dimensional (3D) Variable Range Hopping (VRH) mechanism, and at a higher temperature activated charge transport, which gave a $1/T$ relationship.

Figure 4.5 presents a plot of $\log(\sigma = \text{conductivity})$ versus ($1/T$, putting $\gamma = 1$) where it can be seen that an excellent linear correlation was observed over a wide temperature range, consistent with the variable range hopping theory reported by Mott, predicting a T^{-1} dependence.

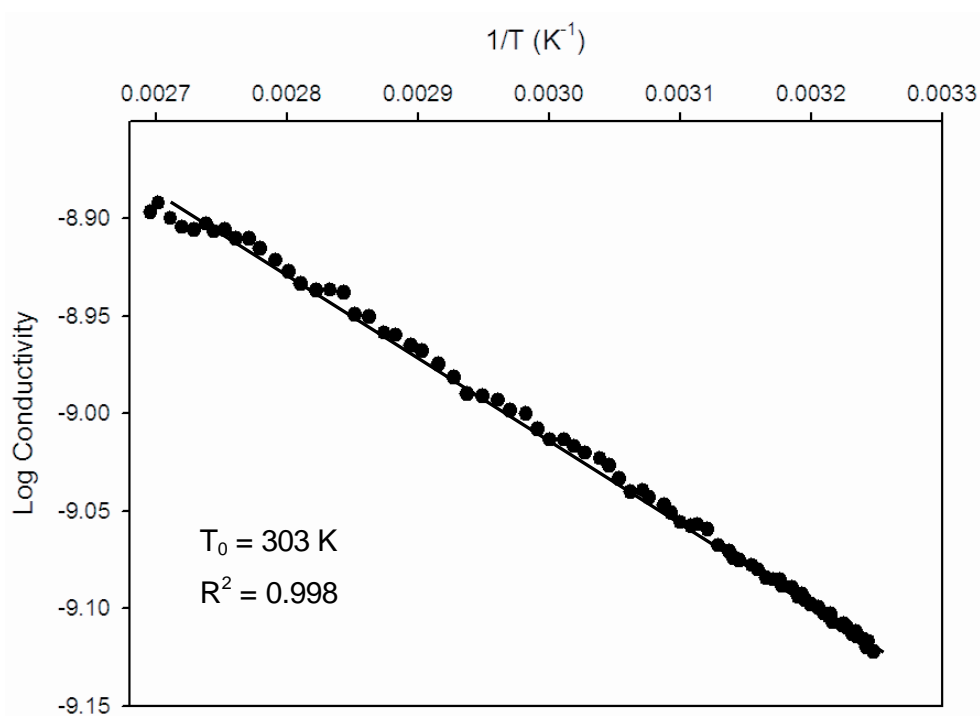
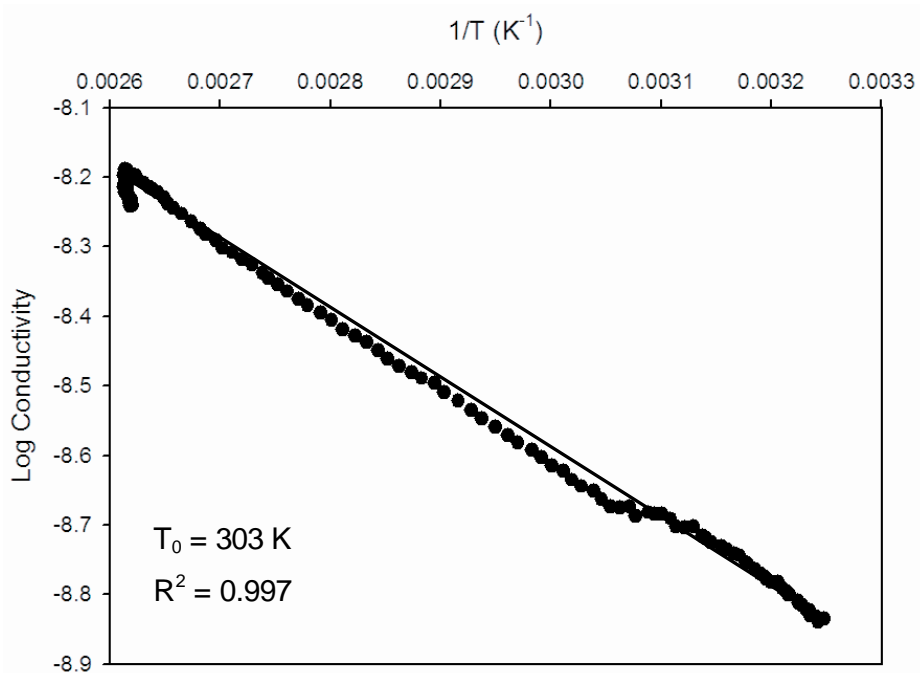


Figure 4.5: Plots of the natural logarithm of the conductivity versus $1/T$, (a) PMDA-ODA PI film fluence 2×10^{14} ions cm^{-2} and (b) PMDA-ODA PI film fluence 5×10^{14} ions cm^{-2} , over the temperature range 25°C (298 K) to 55°C (328 K).

This behaviour of the conductivity can thus be ascribed to the hopping of carriers between conducting sites that were separated by an insulating barrier, as suggested by Sheng and Abeles [24, 20,19,15].

Hence, the results presented here suggest that the electron transport mechanism in the irradiated PMDA-ODA PI films arises from three dimensional (3D) hopping within the ion tracks and charge transport tunnelling between the ion tracks [28]. This mechanism is similar to the electron charge transport reported to occur between carbon nanotubes (CNT) in a CNT-PI composite [31,32].

Evidence to support this model comes from work performed for this thesis, where a HRTEM of the cross sectional image of the irradiated films has revealed the formation of dense ion tracks whose paths criss-cross and overlap one another, as shown in Figure 4.6-a. The SAED diffraction pattern presented in Figure 4.6-b confirmed the ion-tracks were carbon-rich with a graphitic-like structure (as discussed earlier, in Chapter 3) so this microstructure has similarities to a carbon nanotube composite as in CNT-PI composite [31, 32].

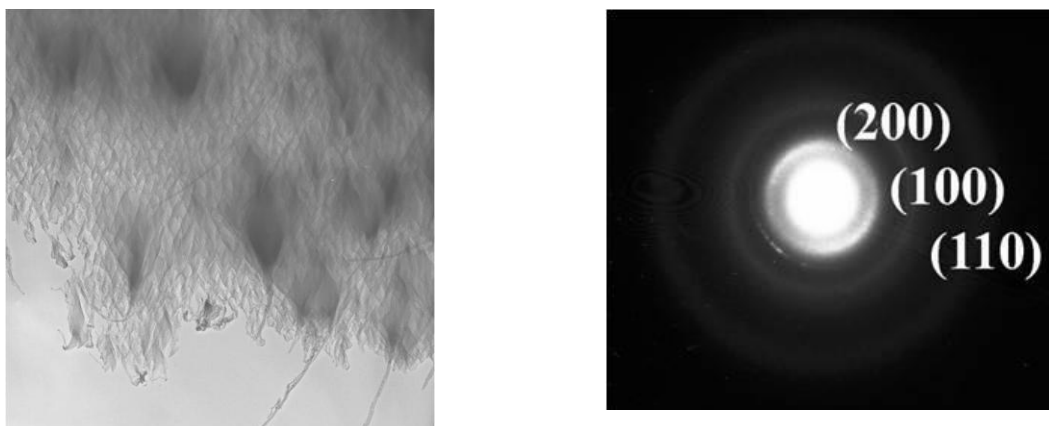


Figure 4.6: (a) HRTEM of the cross sectional image of the irradiated films (b) The SAED diffraction pattern.

4.3.4 Moisture Effect on Electrical Properties

There has been great interest in the conductive behaviour of polymers exposed to various gases for application as gas sensors in industry. For example, the temperature dependent conductivity of PMDA-ODA polyimide was reported to increase when exposed to water vapour [34]. Polyimide materials benefit from aromatic chain layering, and are expected to have good mechanical properties, such as thermal stability and easy processability. However, polyimide materials may not be ideal sensor materials due to the inherent time dependence of their response and susceptibility to moisture-induced stress relaxation. Increased absorption of moisture uptake in the irradiated polyimide films as compared to their pristine counterpart is reported in the literature [35]. In the present work, the electrical behaviour of the irradiated PI films was investigated when they were exposed to moisture with nitrogen as carrier gas. All the polyimide films irradiated in the fluence range from 1×10^{14} to 5×10^{14} ions cm^{-2} exhibited increased electrical resistance when exposed to moisture as compared to corresponding dried and moisture free samples. The sensitivity to moisture was higher at high fluences consistent with increased moisture uptake in high fluence irradiated films. Moisture sensitive characteristics of polyimide film irradiated at a fluence of 5×10^{14} ions cm^{-2} were investigated by subjecting the film to a range of environmental conditions as presented below.

The PMDA-ODA film irradiated at a fluence of 5×10^{14} ions cm^{-2} was used in the study of the moisture effect on electrical properties. Under air-conditioned situations, the film was found to have a resistance value of 0.174 M ohms (Figure 4.7 (a)). When subjected to dry nitrogen and left for 30 minutes, the measurement of the electrical resistance of the film was found to increase to 0.189 M ohms (Figure 4.7 (b)). Whilst under the same conditions, the film was subjected to slow heat treatment in temperature ranging from 25 °C to 50 °C. The temperature was then cycled back to 25 °C. This assisted in the alignment and relaxation of the polymer molecular structure. After the thermal cycle, the

resistance value was found to be stable at 0.189 M ohms (Figure 4.7 (b)). This indicates that electrons can easily flow between conducting sites under these conditions.

The film was again subjected to an air conditioned atmosphere and the electrical resistance was found to decrease to 0.176 M ohm (Figure 4.7 (c)). When the film was subjected to water-saturated nitrogen at room temperature there was an increase in electrical resistance to 0.4 M ohm (Figure 4.7 (d)). The films were then subjected to heat treatment whilst under this condition, and this resulted in a small decrease in the electrical resistance to 0.35 M ohm (Figure 4.7 (e)).

The film was again subjected to air and the electrical resistance was found to drop to 0.30 Mohms (Figure 4.7 (f)).

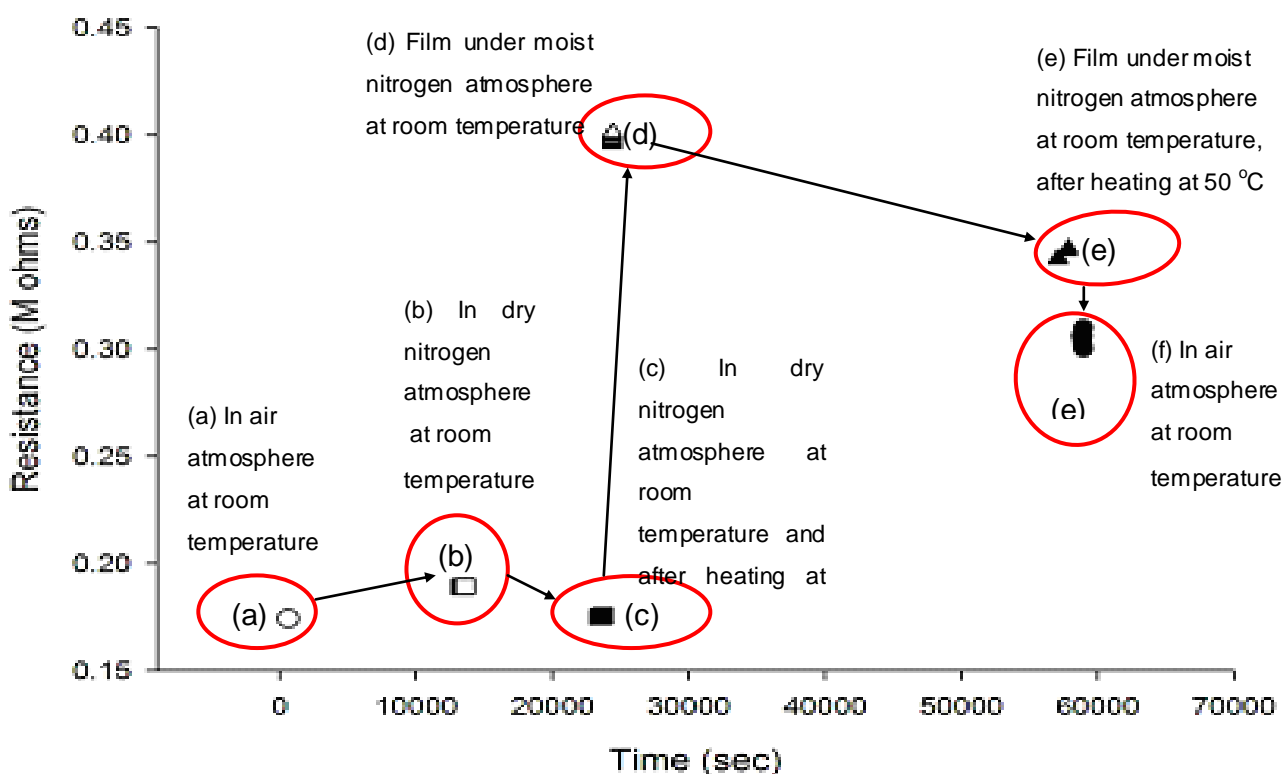


Figure 4.7: Irradiated PMDA-ODA film fluence 5×10^{14} ions cm^{-2} resistance change over time, atmosphere and temperature.

Similar behaviour was observed for PMDA-ODA PI films irradiated at fluence values of 1×10^{14} and 3×10^{14} ions cm^{-2} .

The observed behaviour of the PMDA-ODA PI film irradiated at fluence range of 1×10^{14} to 5×10^{14} ions cm^{-2} (possessing substantial room temperature electrical conductivity), indicates that exposing the irradiated polyimide to water vapour affects their charge transport characteristics. The D.C. resistance increase in these irradiated films may be due to the influence of space charges and charge trapping phenomena at the functional groups present in the irradiation altered portion of the polyimide film (the mechanism has not been investigated yet). In contrary, in un-irradiated polyimide films (unaltered polyimide films possessing very high electrical resistance $> 10^{14}$ Ohms), the electrical resistance decreases by orders of magnitude as compared to dry films [36].

4.4 Conclusion

The effect of ion-beam irradiation on the electrical conductivity of PMDA-ODA PI films has been described in this chapter, where it was found that the electrical conductivity of the irradiated films increased as a function of increasing fluence value. For example, the electrical conductivity of a film exposed to a fluence of 5×10^{14} ions cm^{-2} was found to be more than 4 orders of magnitude higher, when compared to that of a film irradiated at a fluence of 1×10^{14} ions cm^{-2} .

The temperature dependent electrical conductivity characteristics of PMDA-ODA films irradiated over the fluence range of 9×10^{13} to 5×10^{14} ions cm^{-2} , established that they behaved as typical semiconductor films. The temperature dependent behaviour of the electrical conductivity was also exploited to establish the effective charge transport mechanism.

An examination of the relationship between electrical conductivity and temperature was modelled on the granular metal films reported by Salvetat et al. [3], and the multiwall carbon nanotube composites reported by Kim et al. [10], in order to determine the temperature exponent of the irradiated PMDA-ODA films, which provides information about the charge transport mechanism. The films were found to exhibit a thermally activated characteristic of $(1/T^1)$ in the temperature range 298 K to 328 K (Figure 4.5). The linear relationship observed suggests that while other mechanisms were available for charge transfer to occur through fluctuation induced tunnelling (exponents of 0.5), the dominant mechanism for electrical conduction in the irradiated films occurs through electron hopping from one site to the next, in a three dimensional manner (exponent of 1).

It was also found that the irradiated films had a higher activation energy of 2.28 ± 0.05 eV to 0.42 ± 0.05 eV for electron transfer, compared to that required in the CNT-PI composite films studied by Mora-Huretas et al., which were found to be 23 ± 0.05 meV [21].

The effect of gases on the electrical behaviour of the irradiated films was evident by the increase and decrease of resistance in response to changes in the atmosphere bathing the film. Water vapour was found to weaken the temperature dependence of the films, whilst the mere retention of water vapour was found to reduce the electrical conductivity.

4.5 References

1. Fitzer, K.M., Schaeffer, W., *In Situ X-ray Diffraction Performed on Mesophase Formation During the Carbonization of Acenaphthylene*. Chemistry and Physics of Carbon. 1971. 7:p. 237.
2. Brom, Y., Aviram, Am., Broers, A., Sun, B., *EPR Study on Star-Shaped Copolymers Containing C₆₀ Core*. Solid State communication. 1980. 35:p. 135.
3. Salvetat, J.-P., Costantini, J.-M., Brisard, F., Zuppiroli, L., *Onset and Growth of Conduction in Polyimide Kapton Induced by Swift Heavy-ion Irradiation*. Physical Review B. 1996. 55: p. 6238.
4. Wolszczak, M., Kroh, J., Abdel-Hamid, M.M., *Some Aspects of the Radiation Processing of Conducting Polymers*. Radiation Physics and Chemistry. 1995. 45: p. 1.
5. Wu, Y., Zhang, T., Zhang, H., Zhang, X., Deng, Z., Zhou, G., *Electrical Properties of Polymer Modified by Metal Ion Implantation*. Nuclear Instruments and Methods in Physics Research B. 2000. 169:p. 89. [doi: 10.1016/S0168-583X\(00\)00022-7](https://doi.org/10.1016/S0168-583X(00)00022-7)
6. Feurer, T., Sauerbrey, R., Samayling, M.C., Story, B.J., *Ultraviolet-Laser-Induced Permanent Electrical Conductivity in Polyimide*. Applied Physics A Solids and Surfaces. 1993. 56:p. 275.
7. Phillips, H.M., Wahl, S., Sauerbrey, R., *Submicron Electrically Conducting Wires Produced in Polyimide by Ultraviolet Laser Irradiation*. Applied Physics Letter. 1993. 62:p. 2572.
8. Svorok, V., Proskova, K., Hnatowicz, V., Arenholz, E., Kluge, A., *Polyimide Modified by Irradiation with C⁺ and N⁺ Ion Beams*. Polymer Degradation and Stability. 1998. 65:p. 131.
9. Odzhav, V.B., Popok, V.N., Kozlova, E.I., Jankovskij, O.N., Karpovich, I.A. *Electrical Properties of Polyethylene Modification by Ion Implantation and Diffusion*. Nuclear Instruments and Methods in Physics Research B. 2000. 166-167:p. 655.
10. Kim, H.M., Choi, M.S., Joo, J., *Complexity in Charge Transport for Multiwalled Carbon Nanotube and Poly(methyl methacrylate) Composites*. Physical Review B. 2006. 74:p. 54202.
11. Cella, J., *Degradation and Stability of Polyimide, Polyimide; Fundamentals and Application*. Ghosh, M.K. Mittal. M.L., ed. Marcel Dekker Inc: New York. 1996.
12. Quivy, A., Deltour, R., Jansen, A.G.M., Wyder, P., *Transport Phenomena in Polymer-Graphite Composite Materials*. Physical Review B. 1988. 39:p. 1026.
13. Magudapathy, P., Gangopadhyay, P., Panigrahi, B.K., Nair, K.G.M., Dhara, S., *Electrical Transport Studies of Ag Nanoclusters Embedded in Glass Matrix*. Physical Review B. 2001. 299:p. 142.

14. Davenas, J., Boiteux, G., Xu, X.L., *Role of the Modifications Induced by Ion Beam Irradiation in the Optical and Conducting Properties of Polyimide*. Nuclear Instruments and Methods in Physics Research B. 1988. 32:p. 136.
15. Aneli, J.N., *Effect of Temperature on Conductivity of Electrically Conducting Polymer Composite*, in *Aging of Polymers, Polymer Blends and Polymer Composites*. 2002. 64:p. 225.
16. Mott, N., *Metal Insulator Transitions*. Taylor & Francis, 2ed edit 1990.
17. Mora-Huertas, N.E., P. Murugaraj, and D.E. Mainwaring, *Temperature-Dependent Transport Properties in the Semiconducting Regime of Nanoparticles Carbon-Polyimide Composite Films*. Physica E. 2004. 24: p. 119.
18. Huertas, N.E.M., *Functional Thin Film Polyimide Nanocomposites*, Ph.D. thesis in *School of Applied Sciences. Science Engineering and Technology Portfolio*. RMIT University, Melbourne. 2005.
19. Xdkins, C., *Conduction in Granular Metals-Variable-Range Hopping in a Coulomb Gap*. Journal of Physics, 1998. 1:p. 1253.
20. Devenyi, A., Manaila-Devenyi, R., Hill, R.M., *Hopping Conduction Through Localized States in Nb/Al₂O₃*. Physical Review Letters. 1972. 29:p. 1738.
21. Mainwaring, D., Murugaraj, P., Jakubov, T., Khelil, N.A., Siegele, R. *Electron Transport in Semiconducting nanoparticle and nanocluster carbon-polymer composites*. Solid State Communications, 2006. 137:p. 422.
22. Sheng, P. *Fluctuation-Induced Tunneling Conduction in Disordered Materials*. Physical Review B. 1979. 21:p.2180.
23. Klafter, J., Sheng, P. *Hydrostatic Pressure Effect on Switching Phenomena in Copper-Containing Plasma Thin Films*. Journal of Applied Physics. 1984. 17: p: L93.
24. Sheng, P., Abeles, B., Arie, Y. *Transition Metal- Nonmetal in Conductivity of Ceramic Hole-Doped Cobaltites*. Physical Review Letters. 1973. 31:p. 44.
25. Vanderschueren, J., Linkens, A. *Nature of Transient Currents in Polymers*. Journal of Applied Physics. 1978. 49:p. 4195.
26. Sessler, G. M., Hahn, B., Yoon, D. Y. *Electrical Conduction in Polyimide Films*. Journal of Applied Physics. 1986. 61:p. 318.
27. Shuhei, N., Goro's, Masayuki, I., *Electrical Conduction of Nylon 6 at High Temperature*. Japanese Journal of Applied Physics. 1981. 20:p. 47
28. Luo. S., Wong. C.P., *Study on Effect of Carbon Black on Behaviour of Conductive Polymer Composites with Positive Temperature Coefficient*. IEEE, Transaction on Components and Packing Technologies. 2000. 22:p. 151.
29. Kaplan, M.L., Forrest, S.R., Schmidt, P.H. and Venkatesan, T. *Optical and Electrical Properties of Ion Beam Irradiation Films of Organic Molecular Solid and Polymers*. Journal of Applied Physics. 1983. 55:p. 732.

30. Murugaraj, P., Mainwaring, D.E., Jakubov, T., Mora-Huertas, N.E., Ali Khelil, N., Rainer Siegele. *Electron transport in semiconducting nanoparticle and nanocluster carbon-polymer composites* Solid State Communications. 2006,137 p:422
31. Smith, R.C, Carey, J.D., *Charge Transport Effects in Field Emission From Carbon Nanotube-Polymer Composites*. Applied Physics Letters. 2005. 87:p. 263105.
32. Foygel, M., Morris, R.D., Anez, D., French, S., Sobolev, V.L., *Theoretical and Computational Studies of Carbon Nanotube Composites and Suspensions: Electrical and Thermal Conductivity*. Physical Review B. 2005. 71:p. 104201.
33. Mott, D.B., Buchner, S.P., *Comparison of Interface Positive Charge Generated in Metal Oxide Silicon Devices by High Field Electron Injection and X-ray Irradiation*. Applied Physics Letters. 1987, 51:p. 1643.
34. Russell, J.D., Kardos, J.L. *Crosslinking Characterization of a Polyimide AFR700B*. Polymer Composites. 1997. 18:p. 595.
35. Guenther, M., Sahre, K., Suchaneck, G., Gerlach, G., Eichhorn, K.-J., *Influence of ion-beam induced chemical and structural modification in polymers on moisture uptake* Surface and Coatings Technology 142144 Ž2001. 482488
36. Bellucci, F., Khamis, I., Senturia S. D. and Latanision, R. M. *Moisture Effects on the Electrical Conductivity of Kapton Polyimide*. J. Electrochem. Soc. 1990, 137, , 1778-1784

5

MICROMECHANICAL and ELECTROMECHANICAL BEHAVIOUR of IRRADIATED POLYIMIDE THIN FILMS

5.1 Introduction

The irradiation of PI materials was intended to produce substantial changes in the polymers' micro-structure, with a view to enhancing their mechanical properties. Currently, modified PI's are used in nuclear power plants and for the manufacture of military aircraft as well as space shuttles [1]. The mechanical properties of the PI films were found by Chen *et al.* to improve as a result of irradiation, and this may allow them to be used for a much wider range of applications, especially where other materials are eroded and fatigued as a result of their environment [1]. Indeed, it has been found that after irradiation of PI films with light ions such as ^1H , ^4He , ^5B and ^{13}C at various energies, the mechanical properties, such as elongation at break, show improvement, as reported by Kucheyev *et al.* [2] and Guenther *et al.* [3].

Crosslinking and degradation caused by irradiation considerably changes the microstructure of the material, and this can, in turn, result in a change to the mechanical properties of the PI films. Thomas *et al.* [4] reported in the study of irradiated blends of polypropylene and ethylene-vinyl acetate rubber, that there was a decrease in the tensile strength, elongation at break, modulus of elasticity and hardening and softening temperatures as a result of chain scission, whereas crosslinking caused an increase in these respective properties in the study of Charge Transfer in Aromatic Polyimide [5]. A

study into the effect of γ -ray irradiation of polypropylene (PP), polyethylene (PE), polyvinyl chloride (PVC), ethylene propylene copolymers and other polymeric materials revealed that oxygen was incorporated during the irradiation process, resulting in a change in the mechanical properties of the films [6-12]. Other findings, such as that by Yoda *et al.* [13] on intermediately crosslinked polymers, reported a linear relationship between the irradiation dose and the logarithm for volume swelling. In addition, the study by Gillen and Clough [14] reported the degradation of cable elastomeric materials after polymer irradiation in oxygen under pressure.

Additionally, it has been reported that the competing chain scission and crosslinking reactions that occur in polyamide (PA) due to irradiation, result in a reduction in the modulus, tensile strength and yield stress of the PA films [66]. Irradiation of the polymers generally caused one or more of the following changes in the irradiated material, a decrease in the length of molecular chains, an increase in crosslinking between molecular chains and/or other modifications in the crystalline structure [67].

Moreover, several other studies have been carried out on the mechanical properties of polymer composites irradiated at low temperatures [6,7,15-17]. Research into the mechanical properties of composites such as E-glass-PI/epoxy or carbon fibre-PI/epoxy after electron irradiation, has illustrated a reduction in the ultimate strength and the shear modulus. This suggests degradation in the mechanical properties of the electron irradiated composites [18]. It was reported that the decrease in the capacity of the load transferred from matrix to the fibre was due to radiation damage at the interface [18]. The efficiency of the irradiation induced degradation generally depends on the aromaticity of the polymer used. Fast neutron irradiation was reported to be several times more efficient than γ -rays in inducing the change, but the degradation was dependant on the type of polymer and its susceptibility to irradiation[19].

With the use of PIs in various applications, in particular, in thermal blankets, electric insulators, satellite antenna covers, array substrates and as a polymeric membrane for solar sail systems [20,21], it is vital that the PI is able to retain good tensile and optical properties [22]. In electron beam irradiation investigations, PIs were reported to have maintained good optical and tensile properties at temperatures below 177 °C. However, above this temperature the modulus began to deteriorate and the transmittance of the exposed films decreased [22].

In the work described in this thesis, the pristine PI, as well as irradiated PI films, were examined in relation to their mechanical properties as a function of different temperatures and fluences. Molecular structural changes corresponding to changes in mechanical properties discussed in this Chapter have been discussed in Chapter 3.

In a study of composite films as strain gauge materials, electromechanical characterisation was reported to demonstrate the adaptability and correct functioning of the sensor as a strain gauge [50]. In the work described in this thesis, irradiation of the PI films resulted in carbon-rich fused-ring cylindrical-like molecular structures, with electrical conductivity in the semiconducting range. The change in an irradiated film's electrical resistance, in response to the mechanical strain applied, is investigated in this study. A change in electrical resistance of the composites can be expected when modification occurs due to the deformation and damage resulting from mechanical loading. This change in resistance as a result of external loading has also been reported for a carbon black-elastomer composite [51]. The electromechanical behaviour of single-walled carbon nano-tube composites was reported to elicit detailed information on the localised structural behaviour: this can be extracted by measuring the component-level and structural response resulting from external loading [51].

The studies of thin film composites for strain gauge materials have been extensive due to their suitability for various commercial and industrial applications. Dynamic strain measurements of materials refers to the measurement of the strain rate of change, where the strain rate of change is larger than the temperature rate of change [52]. If the gauge factor is higher as a result of the deformation factors, then the change in resistance under an applied static strain and the changes in the dimensions of the films would both be due to microstructure change.

The effect of mechanical strain on the electrical resistance of cermet -based composites filled with nano-phase carbon black has been examined, due to their potential use as strain sensor materials [53,54,60]. Conductive carbon black-polymer composite films were found to behave reversibly when used as sensor materials for a wide variety of gases [55]. Advanced sensor materials require characterisation in aggressive environments to provide experimental verification [56] of their reliability.

The investigation on sensor development by Cochrane and co-workers [50] reported that the longitudinal extension of the sensor leads to a shrinking in the cross section area. This was also reported to decrease the electrical connection between the conductive particles in the conductive polymer composite.

In this chapter of the thesis, micromechanical and electromechanical characteristics of irradiated polyimide films were investigated and the results compared in terms of the radiation dose (fluence) given to each film. The observations in the previous Chapters, and the findings reported by Mora-Huertas *et al.* [41], initiated the electromechanical and micromechanical studies of irradiated PI films described in this Chapter, due to their possible application as flexible and simple sensors.

5.2 Sample Preparation and Characterisation

This section briefly describes the experimental methods used to characterise the mechanical properties of the polyimide thin films prior to, and following, ion-beam irradiation. The thin polyimide films were prepared via the process shown in Chapter 2, Section 2.5.2, and films exposed to a fluence ranging from 1×10^{14} ions cm^{-2} to 5×10^{14} ions cm^{-2} were used in the present study.

Mechanical, electromechanical and dynamic analysis experiments were performed on the polyimide (PMDA-ODA) thin films (length 2.00 mm and width 1.56 mm) having a thickness of 125 microns and irradiation depth of 10 microns. The study used a Perkin Elmer DMA7 linked to a Keithley multimeter and data acquisition system to determine each sample's Young's modulus, glass relaxation temperature and gauge factor. The dynamic mechanical thermal analysis was carried out in a nitrogen atmosphere with a 10 °C/min temperature ramp for temperatures from 25°C to 125°C. The mechanical load applied was between 110mN and 2000mN longitudinal tension applied at a rate of 100mN/min.

5.3.1 Room Temperature Mechanical Analysis

Static stress-strain curves were obtained for the pristine (unirradiated) and irradiated PMDA-ODA PI thin films exposed to ion-beam fluences between 1×10^{14} and 5×10^{14} ions cm^{-2} .

Figure 5.1 shows the initial mechanical analysis of an unirradiated PMDA-ODA film, illustrating, (a) static stress-strain measurements at room temperature, (b) Storage and loss modulus behaviour in the frequency range 1 to 30 Hz, and (c) storage and loss modulus behaviour over the temperature range 25 to 250 °C.

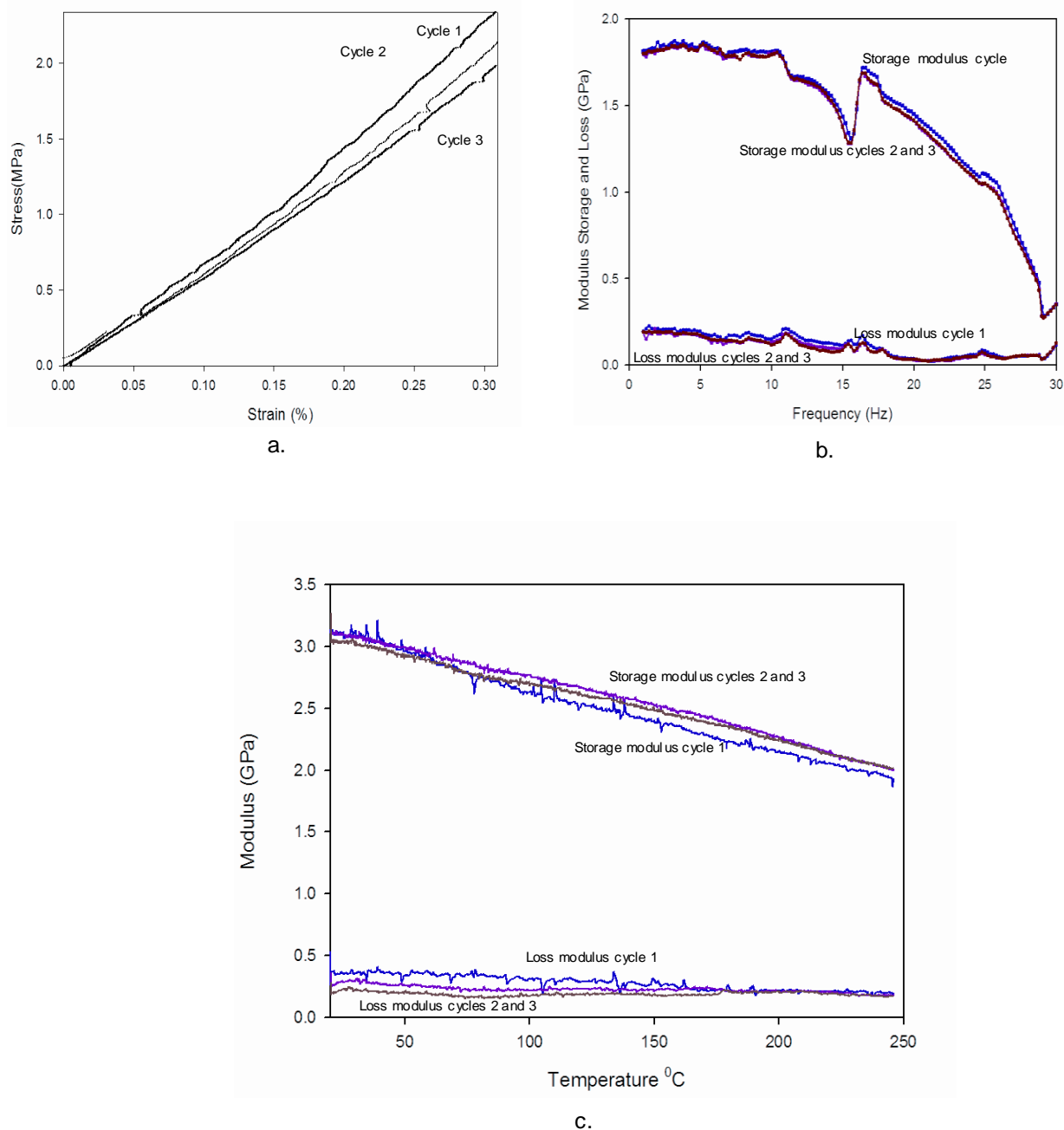


Figure 5.1: Initial mechanical analysis of unirradiated PMDA-ODA film, (a) static stress-strain measurements at room temperature, (b) storage and loss modulus, in frequency range 1 to 30 Hz and (c) storage and loss modulus, over temperature range 25 to 250 °C.

The static stress-strain curves for the pristine PI thin films exhibited elastic behaviour in the strain range studied. The reproducibility of the measurements is also evident from the repeated cycles on each plot.

Figure 5.2 illustrates Stress-Strain curves for unirradiated and irradiated PMDA-ODA films measured at ambient temperature. Young's modulus was calculated from the slope of the curves in Figure 5.2 for all the different films, and the results are shown in Table 5.1. The small degree of reduction observed with increased fluence was found to be similar to that reported for a CNT-polyimide composite [23,24], in which case it was attributed to the minimum interaction between the polyimide matrix and the filler. Although the nanochannels in this study are not foreign particles, the properties of these nanochannels, i.e. ion tracks, are similar to those of CNT's, as suggested by the ATR-FTIR spectra and electrical conductivity discussed in Chapters 3 and 4.

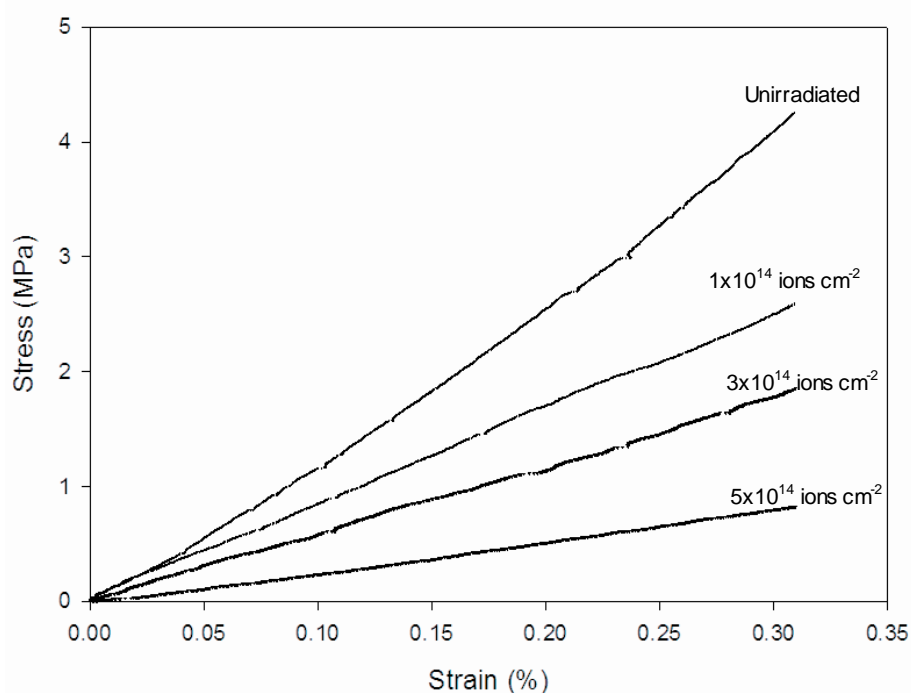


Figure 5.2: Stress Strain curves of unirradiated and irradiated PMDA-ODA films at ambient temperature.

5.3.2 Temperature Dependent Mechanical Analysis

Temperature dependent static mechanical analyses were performed on the unirradiated and irradiated PMDA-ODA films exposed to fluence values ranging from 1×10^{14} ions cm^{-2} to 5×10^{14} ions cm^{-2} , at temperatures ranging from 25 °C to 125 °C, and the results are presented in Figure 5.3 a-d. Both unirradiated and irradiated PMDA-ODA films were longitudinally pre-stretched at an ambient temperature of 25°C. The same stress measurements were applied to all the PMDA-ODA films at pre-stretching and throughout the test.

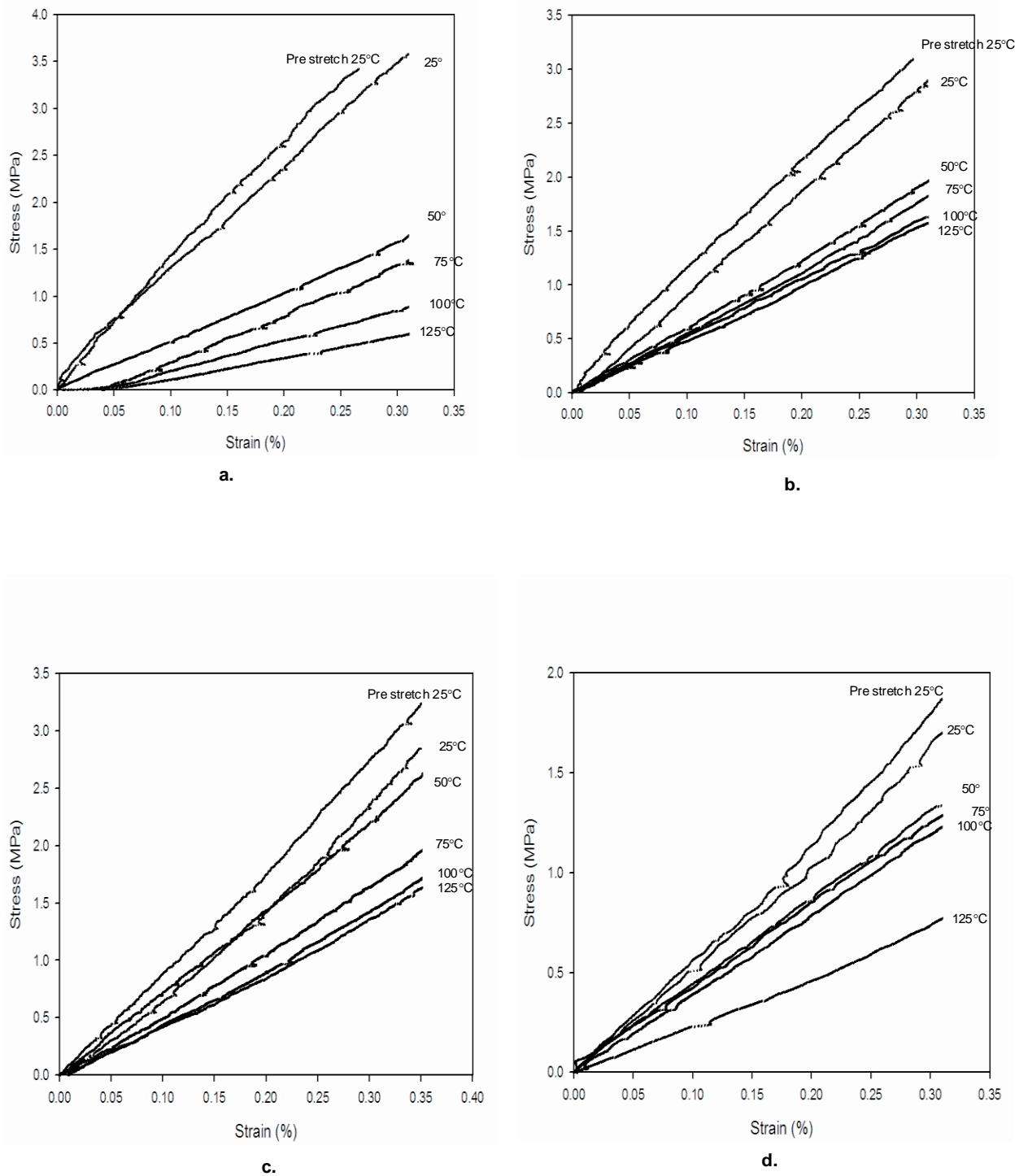


Figure 5.3: Temperature effect on the static mechanical analysis of PMDA-ODA films with fluence values of ; a) unirradiated, b) 1×10^{14} ions cm^{-2} , c) 3×10^{14} ions cm^{-2} , and d) 5×10^{14} ions cm^{-2} .

The PMDA-ODA films displayed in a linear decrease with increasing temperature. For example, a sample exposed to a fluence of 3×10^{14} ions cm^{-2} and subjected to a 0.25% strain, exhibited a stress of 2.35 MPa at 25 °C which decreased to 1.6 MPa at 50 °C, and continued to decrease to 1.45, 1.35 and 1.33 MPa at 75 °C, 100 °C, 125 °C respectively. This decrease in stress is attributed to molecular motion, leading to softening of the films due to the broad glass transition, such as a β_2 sub-glass transition. Fuming Li *et al.* [64] have described the glass transition processes as follows: the β_1 process is attributed to the local motion of the diamine constituents, while the β_2 process is caused by the local motion of the dianhydride constituents. The α process is associated with the glass transition. Hence, it is suggested that thermal activation of these motions softens the irradiated polyimide and decreases the stress and its modulus.

It is observed that the stiffness of the films decreased with increasing temperature, which resulted in a progressive decrease in Young's modulus, which is obtained from the slope of the stress-strain curves. The change arises from microstructure changes (fused ring formation, see Chapter 3) leading to increased mobility of the polymer materials in the composite films. The change in Young's modulus was most noticeable for the PMDA-ODA film exposed to a fluence of 3×10^{14} ion cm^{-2} , starting at 50°C. For the film exposed to a fluence of 5×10^{14} ions cm^{-2} the difference is more evident at 125°C.

This difference at 125 °C for the higher exposure film, appears to be less (0.23 MPa) than that for the room temperature value in the lower exposure film (0.36 MPa). In the study of composites by Huertas *et al.* [41] and Miwa *et al.* [40], similar decreases were evident in Young's modulus. Table 5.1 presents a list of Young's modulus values versus temperature, and the trend is indicative of some threshold of irradiation between fluence values of 1×10^{14} and 3×10^{14} ions cm^{-2} linked to a change in molecular structure.

Table 5.1. Young's Modulus of the irradiated PMDA-ODA films at different temperatures.

Temperature (°C)	Young's Modulus (GPa)			
	Unirradiated	1x10 ¹⁴ (ions cm ⁻²)	3x10 ¹⁴ (ions cm ⁻²)	5x10 ¹⁴ (ions cm ⁻²)
25	1.93	1.65	1.21	0.98
50	1.87	1.59	1.11	0.89
75	1.81	1.53	1.08	0.83
100	1.69	1.46	0.99	0.95
125	1.64	1.44	0.78	0.73

5.3.3 Temperature-Dependent Dynamic Mechanical Analysis

Polyimide, although considered a quality engineering polymer with high strength and heat resistance, does exhibit susceptibility to temperature after irradiation, as discussed in Chapter 3, due to the effect of radiation on functional groups and molecular structure. In the static stress-strain measurements, Young's modulus of the PMDA-ODA films (Table 5.1) shows a decrease as a result of structural modification with irradiation across ambient to elevated temperatures (25-125 °C). Whilst the irradiation induced changes have increased the aromatic content of the matrix, chain cleavage and decomposition have reduced the high temperature stability due to changes in glass relaxation processes in this PI composite thin film. PI thin films have been found to exhibit structural relaxations that are temperature dependent. In ²³⁸U ion irradiated PI samples, the carbonyl groups influenced the dipolar relaxation of free radicals, causing deep and shallow energy traps that affected the α -glass relaxation behaviour [42]. Proton beam irradiation was reported to create two relaxations, notably they were the β_2 -sub-glass relaxation at 100 °C and the main glass relaxation at about 400 °C [43], which were possibly due to crystallisation. Electron beam irradiation on the other hand, caused chain scission in PI's and resulted in a decrease in the β_2 -sub-glass relaxation temperature [22]. Irradiation by these various sources alter the relaxation and crystallisation processes, with the β_2 -sub-glass relaxation

being the most susceptible, while the main glass relaxation appears more stable. Artiaga et al. [42], noted two relaxations, the β_1 -sub-glass relaxation and β_2 -sub-glass relaxation at temperatures between 50 °C and 250 °C in the analysis of electron beam irradiated PI. According to those studies the aromatic ring structures present in the PI decreased the β_2 sub-glass relaxation temperature and therefore fluctuations in glass relaxation processes [11-14, 42, 43]. This is primarily due to aromatic groups protecting the imidic groups from radiation damage. In this work, the glass transition relaxation behaviour of PI films has been investigated to observe effects of ion beam irradiation.

Figure 5.4 shows the DMTA storage modulus and loss modulus of unirradiated and irradiated PI films. With increasing irradiation dosage, the PI's *storage modulus* increased over the temperature range of 25 °C and 150 °C. It can also be seen there is a gradual decrease in the storage modulus at each fluence between the temperatures of 25 °C and 150 °C. This indicated that structural change with irradiation has changed the elastic response of the PI (PMDA-ODA) films. It has been shown that increase of irradiation dose increases the graphitic structure, and this results in an increase in the rigidity within the films. This aromaticity increase protected the PI from any significant decomposition.

The *loss modulus* exhibited a continuous decrease with increasing temperature up to 350 °C, however, some very small increases (like little peaks) were also observed. This peak like increases indicated a reduction in stiffness of the molecular structure of the irradiated PMDA-ODA films. Similar results have been reported by Kang *et al.*, who observed two relaxation peaks at 100 °C and 420 °C in electron beam irradiated PI films [22], similar observations of small relaxation peak-like were reported in other literature [32-37]. In accordance with the properties listed by Du Pont for their pristine PI, it was reported that the high temperature this peak-like increases originated from glass relaxation. The lower temperature peaks originated from a contribution of adsorbed water molecules and/or β_2

sub-glass relaxations. The β_2 sub-glass relaxation was found to be associated with the rotation or oscillation of phenyl groups within the PI diamine moiety as reported by Pireaux *et al.* and Chern *et al.* [44,45]. The β_2 sub-glass relaxation peak in the PMDA-ODA films although broad, could arise from some overlap between the β_1 sub-glass relaxation and the β_2 sub-glass relaxation processes.

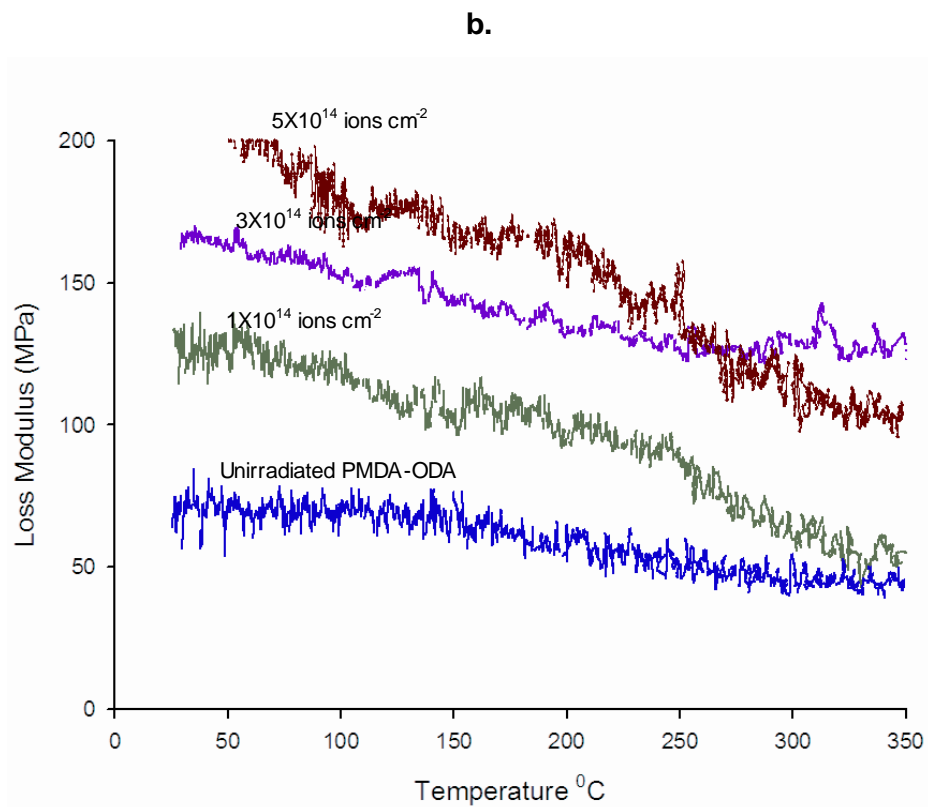
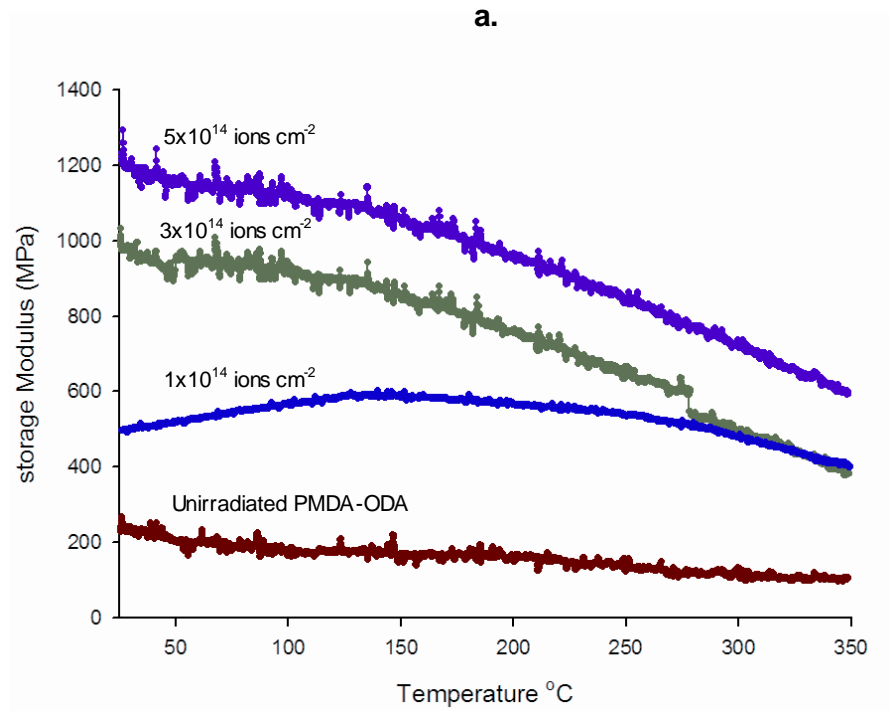


Figure 5.4: DMTA of unirradiated and irradiated PI films (a) storage modulus, (b) loss modulus.

c.

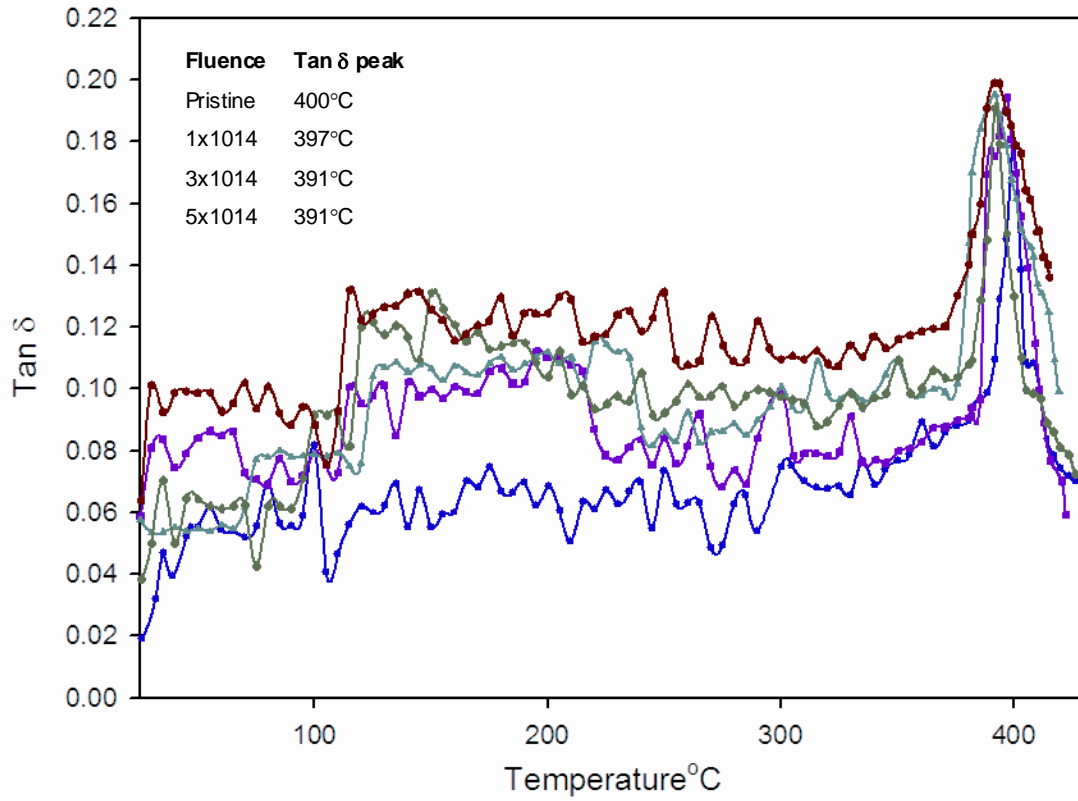


Figure 5.4: DMTA of unirradiated and irradiated PI films (c) Tan δ

5.4 Electromechanical Characterisation of PMDA-ODA

The sensitivity of a strain sensor is conventionally expressed as a gauge factor (GF) which relates the relative change in resistance ($\Delta R/R_0$, where R_0 is the resistance without any displacement or imposed strain ε ($\Delta L/L$) and ΔR is the change in resistance) to the relative change in length ($\Delta L/L$). The relative change in length equals the axial strain (ε), so we can write:

$$GF = \frac{\left(\frac{\Delta R}{R_0}\right)}{\varepsilon} \quad (5.1)$$

The changes in the electrical resistance of the irradiated PI films (fluences of 3×10^{14} and 5×10^{14} ions cm^{-2}) were monitored while the films were subjected to strain [Figure 5.5a].

The resistance of the film with fluence of 5×10^{14} ions cm^{-2} increased by 26% for an applied strain of 1000 micro-strain resulting in a gauge factor of about 290. This GF value was markedly greater than the GF values of 8-12 reported by Huertas [41]. Above 1000 micro-strain the resistance increased exponentially. This change in the behaviour is consistent with a tunnelling gap electron transport mechanism that occurs between the carbon nanoclusters along the conducting channels as discussed by Murugaraj *et al.* [68] and references cited therein.

In the exponential region, the resistance –strain measured fitted the following expression

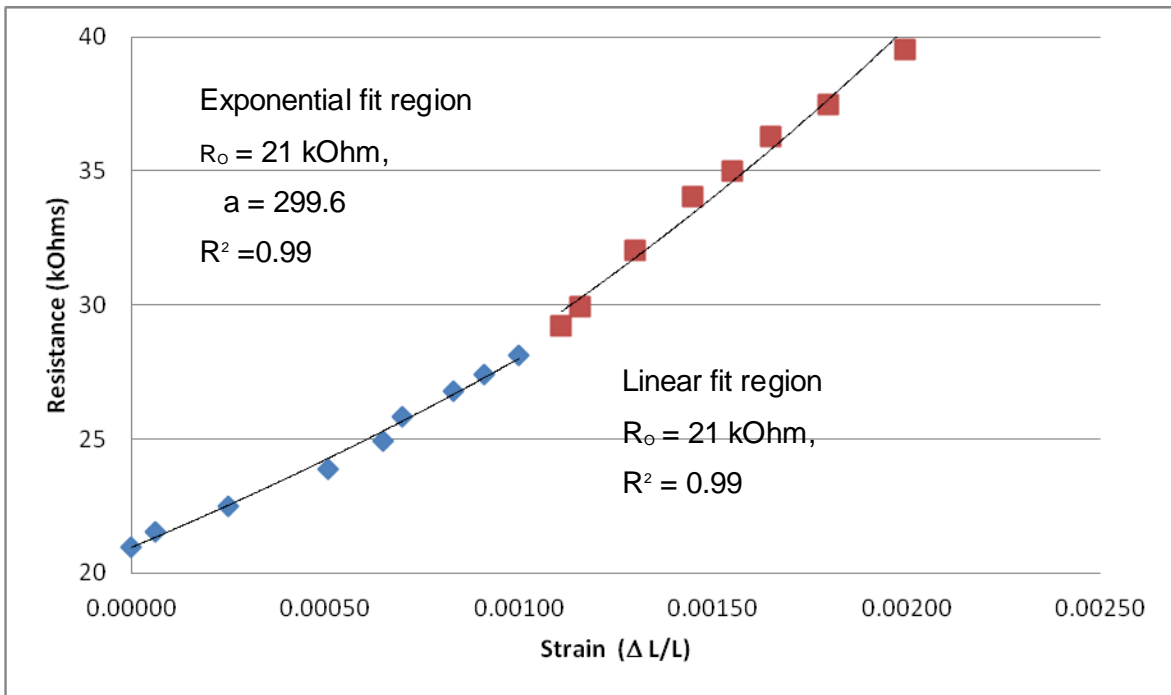
$$R_{\varepsilon} = R_0 e^{\alpha \varepsilon} \quad (5.2)$$

where R_{ε} is the electrical resistance for a given strain ε , R_0 is the resistance at zero strain [which was 21×10^3 Ohm for film irradiated at fluence of 5×10^{14} ions cm^{-2}]. By taking logs of each, this relationship becomes;

$$\ln(R_{\varepsilon}) = \ln(R_0) + \alpha \cdot \varepsilon \quad (5.3)$$

So a plot of $\ln(R_{\varepsilon})$ versus ε should yield a straight line of slope α . The calculated exponents (α) had a value of about 300 (with R^2 of 0.99) .

a.



b.

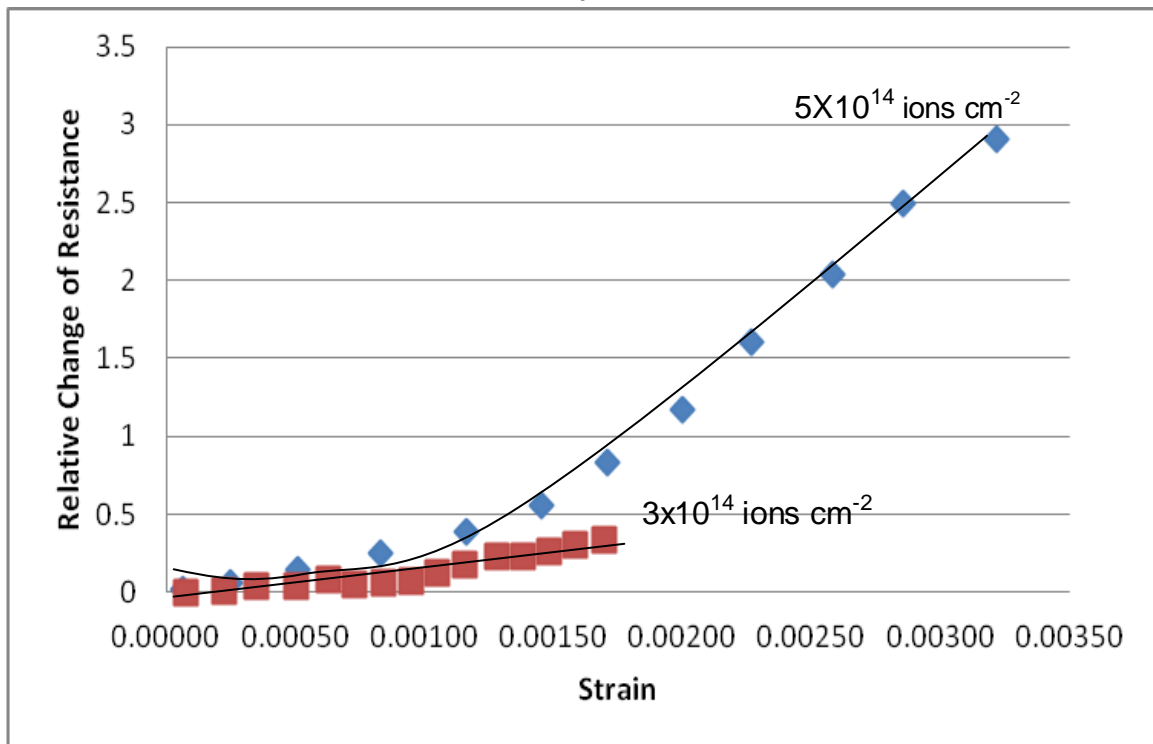


Figure 5.5: (a) Change in resistance with applied tensile strain for fluence $5 \times 10^{14} \text{ ions cm}^{-2}$; (b) Relative change in resistance in response to the application of strain on a PI film irradiated at fluence values of 3×10^{14} and $5 \times 10^{14} \text{ ions cm}^{-2}$ at ambient temperature.

The relative changes of resistance with applied strain for the irradiated films with fluence 3×10^{14} ions cm^{-2} and 5×10^{14} ions cm^{-2} are compared in Figure 5.5 (b). The relative change in resistance increased continuously with applied strain. In the linear regions, the Gauge Factor sensitivities obtained were 120 and 334 respectively. At higher tensile strain of about 300 micro-strain the electrical resistance increased, yielding a much higher Gauge Factor of about 1000.

The irradiated PI films were found to be free of hysteresis when subjected to strain over three cycles, with the resistance being observed to return to the initial value at the end of each cycle, suggesting reproducibility. The maximum strain to which the strain-sensing film is subjected is within the elastic limit of the irradiated PI film.

Previous work described in this thesis indicates that the microstructure of the irradiated PMDA-ODA films consists of overlapping ion tracks, with graphite-like structures within the ion irradiation channels originating at the surface, and propagating in a direction perpendicular to the planar surface of the film. These ion tracks contribute to the electrical conductivity via 3D hopping and tunnelling mechanisms in the irradiated PMDA-ODA films, as discussed in Chapter 4. The electron tunnelling occurs between the tracks which are separated by insulating dielectric polymeric medium.

The electromechanical behaviour of the irradiated PMDA-ODA films was found to be consistent with the electrical conduction mechanism in CNT (carbon nanotubes) - and carbon fibre- composites, as reported by Wang *et al.* [48]. In other studies on a continuous carbon fibre composite, the change in resistance in response to strain was attributed to the alignment of the fibre in the longitudinal direction of the strain [15,19, 57-63].

The Gauge Factor values for irradiated PMDA-ODA films were also observed to increase with increasing fluence values. This is possibly due to the existence of increased ion track density contributing to the tunnelling current.

5.5 Conclusion

The degradation of PMDA-ODA PI films during ion-beam irradiation results in changes in their mechanical properties. The increased radiation dosage broke down the original network structure of the PI molecular chain, and this was reflected in a decrease in Young's Modulus. The tensile strength measurements indicated that the PI films became slightly brittle at an irradiation fluence of 5×10^{14} ions cm^{-2} . In this study it was found that Cu^{3+} ion-beam irradiation was directly responsible for the destruction of the imidic groups in the PI molecular backbone. Thus, it can be concluded that PI films are, to a degree, non-resistant to ion-beam irradiation damage. Dynamic mechanical analysis indicated a decrease in the β_1 - and β_2 -sub-glass relaxation temperatures and the decomposition temperature. The PI used in the mechanical analysis study, while being generally stable, was not found to be sufficiently durable to survive reasonably high irradiation doses or temperature fluctuations.

The electromechanical properties of PMDA-ODA irradiated films were investigated as a function of fluence when placed under longitudinal strain. The behaviour of the irradiated films was found to be consistent with that of semiconducting strain gauges, and the PMDA-ODA irradiated films exhibited high Gauge Factor values, much higher than those reported for conventional composites. This illustrates that these irradiated PI films are suitable as strain sensitive gauges due to their desirable physical properties which include: a high strain sensitivity (for maximum electrical output for a given strain); a low and controllable temperature coefficient of resistance (for good temperature compensation); a wide operating temperature range (for widest range of applications); and a good fatigue life (for dynamic measurement) [2].

5.6 References

1. Chen, T., Yao, S., Wang, K., Wang, H. *The Modification of Mechanical Properties by 2MeV Si Ions Irradiated Polyimide*. Nuclear Instruments and Methods in Physics Research B. 2008. 266:p:3091.
2. Kucheyev, S. O., Felter, T.E., Anthamatten, M. *Deformation Behaviour of Ion-Irradiated Polyimide*. Applied Physics letter. 2004. 85:p:733.
3. Guenther, M., Gerlach, G., Suchaneck, G., Sahre, K., Eichhorn, K-J., Baturin, V., Duvanov, S., *Controlled Modifications in Electronic and Chemical Structures of a Nanoscale Region of Polystyrene by Fast Electrons*. Nuclear Instruments and Methods in Physics Research B. 2004. p:216.
4. Thomas, S., Gupta, B.R., De, S.K., *Mechanical Properties, Surface Morphology and Failure Mode of Gamma-Ray Irradiated Blends of Polypropylene and Ethylene-vinyl Acetate Rubber*. Polymer Degradation and Stability. 1987. 18:p. 189.
5. Salley, J. M., Frank, C.W., *Charge Transfer in Aromatic Polyimide, in, Polyimide: Fundamentals and Applications*. New York, Marcel Dekker Inc, 1996.
6. Seguchi, T., Hashimoto, S., Arakawa, K., Hayakawa, N., Kawakami, W., Kuriyama, I. *Mechanical Properties, Surface Morphology and Failure Mode of γ -Ray Irradiated Blends of Polypropylene and Ethylene-vinyl Acetate Rubber*. Radiation Physics and chemistry. 1981. 17:p. 195.
7. Seguchi, T., Arakawa, K., Hayakawa, N., Kuriyama, I., Watanabe, Y. *Degradation of Crosslinked Polyethylene in Water by Gamma-Irradiation*. Radiation Physics and Chemistry. 1982. 19:p. 321.
8. Seguchi, T., Arakawa, K., Hayakawa, N., Machi, S. *Effect of Film Draw Temperature (FDT) on Physical Properties of Polyethylene*. Radiation Physics and Chemistry. 1981. 18:p. 671.
9. Hegazy, E. A., Seguchi, T., Arakawa, K., Machi, S. *Irradiation Effects on Aromatic Polymers: 1. Gas Evolution by Gamma Irradiation*. Journal of Applied Polymer Science. 1981. 26:p.1361.
10. Hegazy, E. A., Seguchi, T., Arakawa, K., Machi, S., *Crosslinked Grafted PVC Obtained by Direct Radiation Grafting*. Journal of Applied Polymer Science. 1981. 26:p. 2947.
11. Arakawa, K., Seguchi, T., Watanabe, Y., Hayakawa, N. *Radiation-Induced Oxidation of Polyethylene, Ethylene-Butene Copolymer, and Ethylene-Propylene Copolymer*. Journal of Polymer Science. 1982. 20:p. 2681.
12. Arakawa, K., Seguchi, T., Hayakawa, N., Machi, S. *Stabilizer Additives in Ionizing Radiation Environments Under Oxidizing Conditions*. Journal of Polymer Science, Polymer Chemistry. 1983. 21:p. 1173.
13. Yoda, O. *Effect of Chain Scission Induced by Radiation on the Volume Swelling Ratio of Intermediately Crosslinked Amorphous Polymers*. Radiation Physics and Chemistry. 1983. 21:p. 467.

14. Gillen, K. T., Clough, R.L. *Radiation Induced Oxidative Degradation of Polymers—I: Oxidation Region in Polymer Films Irradiated in Oxygen Under Pressure Radiation* Physics and Chemistry. 1981. 18:p. 679.
15. DeVries, K.L. *Free-Radical Processes in Mechano-Chemical Degradation of Plastics and Rubber*. Journal of Polymer Science: Applied Polymer Symposium, 1979, p. 439.
16. Makhils, F.A., in, *Radiation physics and chemistry of polymers*. John Wiley and Sons: New York. 1975.
17. Bohm, G.G.A., Tveekrem, J.O., *Gamma-Ray Induced Deterioration of Natural Rubber Vulcanizates*. Rubber Chemistry Technology. 1982. 55:p. 575.
18. Seguchi, T., Arakawa, K., Ito, M., Hayakawa, N., Machi, S., *Radiochemical Oxidation of an Ethylene-Propylene-Hexadiene Terpolymer*. Radiation Physics and Chemistry. 1983. 21:p. 495.
19. Egusa, S., Kirk, M.A., Birtcher, R.C., *Neutron Irradiation Effects on the Mechanical Properties of Organic Composite Materials*. Journal of Nuclear Materials. 1984. 126:p. 152.
20. Banks, B.A., Snyder, A., Miller, S.K., De Groh, K.K., Demko, J., *Fast Three-Dimensional Modeling of Atomic Oxygen Undercutting of Protected Polymers*". Journal of Spacecraft Rockets. 2004. 41:p. 335.
21. Chipara, M., Benson, R., Chipara, M.D., Reyes, J.R., *Dynamical Mechanical Analysis of Proton Beam Irradiated Polyimide*. Nuclear Instruments and Methods in Physics Research B. 2005. 236:p. 432.
22. Kang, P.-H., Jeon, Y-K., Jeun, J-P., Shin, J-W., Nho, Y-C., *Effect of Electron Beam Irradiation on Polyimide Films*. Journal of Industrial and Engineering Chemistry. 2008. 14:p. 672.
23. Ogasawara, T., *Characterisation of Multi-Walled Carbon Nanotube/Phenylethynyl Terminated Polyimide*. Composites Part A. Applied Science and Manufacturing. 2004. 35:p. 67.
24. Ogasawara, T., Ishikawa, T., *Polyimide Composite Material Containing Carbon Nanotubes for Improving Heat Resistance*. Dokuritsu Gyosei Hojin Koku Uchu Gizyutsu Kenkyusho. 2004.
25. Chapiro, A., in, *Radiation Chemistry of Polymeric Systems*, High Polymers. Interscience Publishers, a Division of John Wiley & Sons, New York and London. 1962.
26. Charlesby, A., in, *Atomic radiation and polymers*. Pergamon press. London. 1959.
27. Dole, M., in, *The Radiation Chemistry of Macromolecules*., Academic Press. New York. 1972.
28. Makuuchi, K., Asano, M., Abe, T., *Effect of Evolved Hydrogen Fluoride on Radiation-Induced Crosslinking and Dehydrofluorination of Poly(vinylidene fluoride)*. Journal of Polymer Science Polymer Chemistry Edition. 1976.

29. Chapiro, A., *Chemical Modifications in Irradiated Polymers*. Nuclear Instruments and Methods in Physics Research, Section B: Beam Interactions with Materials and Atoms. 1988. 32:p. 111.
30. Rajulu, A.V., Reddy, R.L., Raju, K.M., Avasthi D.K., DK Asokan, *Handbook of Polymer Blends and Composites*. Nuclear Instruments and Methods in Physics Research B. 1999. 3:p. 195.
31. Hnatowicz, V., Peřina, V., Havránek, V., Voseček, V., Novotný, J., Vacík, J., Švorčík, V., Rybka, V., Kluge, A., *Degradation of Polyimide and Polyethyleneterephthalate Irradiated with 150 and 200 keV Ar⁺ Ions, Studied by RBS and ERD Techniques*. Nuclear Instruments and Methods in Physics Research, Section B: Beam Interactions with Materials and Atoms. 2000. 161-163 :p. 1099.
32. Costantini, J.M., Couverur, F., Salvetal, J.P., Bouffard, S., *Micro-Raman Study of the Carbonization of Polyimide Induced by Swift Heavy Ion Irradiations*. Nuclear Instruments and Method in Physics Research Section B. 2002. 194:p. 132.
33. Hirata, K., Saitoh, Y., Narumi, K., Nakajima, Y., Kobayashi, Y., *Non-Linear Effect of Cluster Irradiation on Chemical Modification of Polycarbonate*. Nuclear Instruments and Method in Physics Research Section B. 2002. 193:p. 816.
34. Garg, M., Quamara, J.K., *Electrical Conduction Behaviour of High Energy Ion Irradiated Kapton-H Polyimide Film*. Nuclear Instruments and Method in physics Research B. 2001. 179:p. 389.
35. Wahab, M.A., Kim, I.I., Ha, C.S., *Microstructure and Properties of Polyimide/poly(vinylsilsesquioxane) Hybrid Composite Films*. Polymer. 2003. 44:p. 4705.
36. Tretinnikov, O.N., Yoshito, I., *Surface Characterization of Ion-Implanted Polyethylene*. Journal of Polymer Science. Part B: Polymer Physics. 36:p. 715.
37. Feurer, T., Sauerbery, R., Smayling, M.C., Story, B.J., *Ultraviolet-Laser-Induced Permanent Electrical Conductivity in Polyimide*. Applied Physics A. 1993. 56:p. 275.
38. Svorcik, V., Proskova, K., Hnatowicz, V., Arenholz, E., Kluge, A., *Polyimide Modified by Irradiation with C⁺ and N⁺ Ion Beams*. Polymer Degradation and Stability. 1999. 65:p. 131.
39. Strumpler, R., Glatz-Reichenbach, J. *Feature Article, Conducting Polymer Composites*. Journal of Electroceramics, 1999, 3: p. 329. [doi:10.1023/A:1009909812823](https://doi.org/10.1023/A:1009909812823)
40. Miwa, M., Akiyoshi Takeno, A., Hara, K., Watanabe, A. *Volume Fraction and Temperature Dependence of Mechanical Properties of Silicone Rubber Particulate/Epoxy Blend*. Composites. 1995. 26:p. 371.
41. Huertas, N.E.M, Ph.D. Thesis, *Functional Thin Film Polyimide Nanocomposites*, in *School of Applied Sciences. Science Engineering and Technology Portfolio*. RMIT: Melbourne. 2005:p. 208.
42. Artiaga, R., Chipara, M., Stephens, C.P., Benson, R. *Dynamic Mechanical Analysis of Proton Beam Irradiated Polyimide*. Nuclear Instruments and Methods in Physics Research B. 2005. 236: p. 432. [doi: 10.1016/j.nimb.2005.04.013](https://doi.org/10.1016/j.nimb.2005.04.013).

43. Pireaux, J.J., Gregoire, C., Caudano, R., Rei, M., Vilar, R. Brinkhuis, A., Schouten, A. *Electron-Induced Vibrational Spectroscopy. A New and Unique Tool to Unravel the Molecular Structure of Polymer Surfaces*. Langmuir. 1991. 7:p. 2433.
44. Chern, Y.T., *Synthesis of Polyamides Derived From 4,9-bis(4-aminophenyl) Diamantine*. Polymer. 1998. 39:p. 4123.
45. Tschegg, E., Humer, K., Weber, H.W., *Mechanical Properties and Fracture Behaviour of Polyimide (SINTIMID) at Cryogenic Temperatures*. Cryogenics. 1991. 31:p. 878.
46. Zhang, M.J., Zhi, F.X., *Crack Growth Mechanism in Some Polyamides*. Polymer 1988. 29:p. 2152.
47. DeVries, K.L., Hornberger, L.E., *Macroscopic, Microscopic and Molecular Aspects of Fracture in Polymers*. Polymer Degradation and Stability. 1989. 24:p. 213.
48. Aalie, J., Rahmatpour, A., Maghami, S., Preparation and Characterization of Linear Low Density Polyethylene/Carbon Nanotube Nanocomposites. Journal of Macromolecular . 2007. 46:p:877.
49. Holister, G.S., Window, A.L., in, *Strain Gauge Technology*, Applied Science publishers. Barking, England 1982.
50. Kost, J., Narki, M., Fouux, A., *Effect of Axial Stretching on the Resistivity of Carbon Black Filled Silicone Rubber*. Polymer Engineering and Science. 1983. 23:p. 567.
51. Flandin, L., Chang, A., Nazarenko, S., Hiltner, A., Baer, E., *Effect of Strain on the Properties of an Ethylene-Octene Elastomer with Conductive Filler*. Journal of Applied Polymer Science. 2000. 76:p. 894.
52. Marioli, D., Rolla, P., Taroni, A., *Thick Film Strain Gauges on Insulated Metal Substrates for High Sensitivity Mechanical Sensors*. Instrumentation and Measurement Technology Conference, IMTC/94. Conference Proceedings. 10th Anniversary. Advanced Technologies in I & M, IEEE. 1994:p. 1245.
53. Song, C., Kerns, D.V., Davidson, J.L., Kang, W., Kerns, S., *Evaluation and Design Optimization of Piezoresistive Gauge Factor of Thick-Film Resistors*. IEEE, 1991. 2:p. 1106.
54. Harovat, M., Belavic, D., Samardzija, Z., Holc, J., *An Investigation of Thick Film Resistor Fired at Different Temperatures for Strain Sensors*. 24th International Spring Seminar on Electronics Technology. Concurrent Engineering in Electronic Packaging. 2001.
55. Holanda R. *Development of thin film Thermocouples on Ceramic Materials for Advanced Propulsion System Applications*, in 7th International Symposium on Temperature: It's Measurement and Control in Science and Industry. 1992. Toronto Canada.
56. Chung, X.W. *Continuous Carbon Fibre Epoxy-Matrix Composite as a Sensor of its Own Strain*. IPO Publishing Ltd, 1996: p. 796.

57. Wang, P., *Preparation and Characteristics of Flexible Carbon Composite Film*. Qinghua Daxue Xuebao, Ziran Kexueban. 2003. 43: p. 1480.
58. Jih-Fen, A.W., Herbert, L.C. Martin, *Microfabricated Thin-Film Physical Sensors for Hostile Environment*. 17th DASC, The AIAA/IEEE/SAE Digital Systems Conference. 1998. :p. 7803.
59. Zee, F., Judy, J., *MEMS Chemical Gas Sensor*. Thirteenth Biennial University/ Government/Industry Microelectronics Symposium, IEEE. 1999. 7803-5240: p. 150.
60. Xiao, H.g., Li, H., Ou, J.P., *Piezoresistance Property of Cermet-Based Composite Filled with Carbon Black and the Application of it for Strain Sensing*. Proceedings of SPIE. 2007. 6526.
61. Estada, H.V., Estrada-Vazquez, J.F., *A New Method for the Characterization of the Longitudinal and Transverse Strain Sensitivities of Conductive Thin Films for their Use in Microsensors*. Design of Mixed-Mode Integrated Circuits and Applications, Third International Workshop, IEEE. 1999: p. 73.
62. Loh K. J., Lynch, J.P., Kotov, N.A., *Mechanical-Electrical Characterisation of Carbon-Nanotube Thin Films for Structural Monitoring Applications*. The International Society for Optical Engineering. 2006,:p. 6174.
63. Cochrane, C., Koncar, V., Lewandowski, M. Dufour, C. *Design and Development of a Flexible Strain Sensor for Textile Structures Based on a Conductive Polymer Composite*. Sensor. 2007. 7: p. 473.
64. Fuming Li, F., Ge, J.J., Honigfort, P.S., Fang, S., Chen, J.C., Harris, F. W., Cheng, S.Z.D., *Di-anhydride Architectural Effects on the Relaxation Behaviours and Thermal and Optical Properties of Organo-Soluble Aromatic Polyimide Films*. Polymer. 1999. Vol 40 (18:p. 4987.
65. Zhang, X.-W., Pan, Y., Zheng, Q., Yi, X.S., *Piezoresistance of Conductor Filled Insulator Composites*. Polymer International. 2001. 50:p. 229.
66. Lopez-Quintana, S., Rosaes, C., Gobernado-Mitre, I., Merino, J.C., Pastor, J.M., *Effect of β -Irradiation on Mechanical Properties of Metallocene Elastomers/PA6 Blends*. Polymer. 2004, 45:p.8041.
67. Fintzou, A.T., Badeka, A.V., Kontominas, M.G., Stahl, M.R., Riganakos, K.A., *Changes in Physicochemical and Mechanical Properties of Electron-Beam Irradiation Polypropylene Syringes as a Function of Irradiation Dose*. Radiation Physics and Chemistry. 2007. 76:p.97.
68. Murugaraj, P., Mainwaring. D., Khelil, N.A., Peng, J.L., Siegele, R., Sawant, P., *The Improved Electromechanical Sensitivity of Polymer Thin Films Containing Carbon Clusters Produced In Situ by Irradiation with Metal Ions*. Carbon 2010. 48:p4230.

6

SUMMARY

The effect of Cu^{3+} ion-beam irradiation on the microstructure of two polyimide (PI) films (PMDA-ODA, Kapton[®] and BTDA-ODA) was examined using ATR-FTIR and XPS spectroscopy. The results indicated modifications to the molecular structure of both films, with the major reaction arising from chain scission accompanied by a decrease in the number of imidic and hydrogen atoms present. The ion-beam etched nanochannels in the polymer that were found to be lined with graphite-like aromatic fused rings, which formed along the full depth of the ion-beam, to the point where the ion-beam was completely absorbed, which corresponded to about 10% surface penetration.

There were a number of significant changes in the FTIR spectra of the irradiated PI films, most notably the appearance of a broad water band in the $3100\text{-}2400\text{ cm}^{-1}$ range indicating moisture absorption into the film, suggesting that irradiation enhanced the vulnerability of the film to atmospheric effects. In the low frequency region ($2000 - 600\text{ cm}^{-1}$) it was found that the carbonyl group attached to the imide nitrogen was chemically modified, thus affecting the carbonyl's functionality. In addition, the breakdown of the backbone linkages of the polymer, via cleavage of the nitrogen of the imide and elimination of hydrogen from the PI molecular structure, led to the formation of crystallites containing graphite-like fused rings. This latter observation was also supported by the XPS results, which clearly demonstrated the growth of π -type C-C bonding as the irradiation dose fluence increased.

ATR-FTIR spectroscopy was used to examine the temperature dependent changes in the films following irradiation. Drying at 80 °C led to a reduction in the intensity of the adsorbed water stretching band by approximately 90 to 95%. At higher "annealing" temperatures, 180 °C-280 °C, the water band was eliminated and the intensities of the imide ring deformation bands increased, while the characteristic carbonyl bands decreased in intensity and hydrogen was eliminated. In addition, the intensity of the backbone ether band was found to be slightly decreased. Similar changes were observed in the FTIR bands of both PI films, but in the BTDA-ODA sample the benzophenone keto-carbonyl band was found to be slightly increased. Also, the change in the hydrogen content of the BTDA-ODA film was found to be dependent on the film's thickness and the depth to which the ion-beam penetrated during irradiation. The experimental results demonstrate the potential use of PMDA-ODA films for high temperature sensor applications, in preference to BTDA-ODA films, as the former films were more thermally robust.

The electrical conductivity of the irradiated PMDA-ODA films was found to increase as a function of increasing fluence (ion-beam intensity). Indeed, the electrical conductivity of a film treated at a fluence of 5×10^{14} ions cm^{-2} was found to be more than 4 orders of magnitude higher, when compared to that of a film irradiated at a fluence of 1×10^{14} ions cm^{-2} . Hence ion-beam irradiation of the PI films can be manipulated to provide desirable electrical behaviour.

A study of the temperature dependent electrical conductivity characteristics of the PMDA-ODA films, irradiated at fluence values ranging from 0.9×10^{14} to 5×10^{14} ions cm^{-2} , revealed that their conductivity behaviour was typical of that of semiconductor films. Thus, the theoretical treatment of the temperature dependence of the electrical conductivity of the irradiated PMDA-ODA films was based on a standard semiconductor relationship, which enabled calculation of the temperature exponent, based on the granular metal film model

reported by Salvetat et al.[1] and the treatment of multiwalled carbon nanotube composites reported by Kim et al.[2]. The resistance of the irradiated films was found to be inversely proportional to temperature, confirming their semiconducting behaviour with a thermally sensitive activation barrier. The excellent linearity of this relationship suggests that while there were other mechanisms available for charge movement to occur through fluctuation-induced tunnelling, the dominant mechanism of dc conduction in the irradiated PI films occurs via three dimensional thermally activated electron hopping from one site to the next.

Previous work in the literature suggested that PI films are irradiation resistant due to the presence of the aromatic rings which protect the imidic groups in the main chain structure. However, in the present work it was found that Cu^{3+} ion-beam irradiation was directly responsible for the disruption of the imidic groups and this affected the tensile strength of the PI films, as evidenced by changes in Young's Modulus, and they became slightly brittle at an irradiation fluence of 5×10^{14} ions cm^{-2} . Thus, the degradation of PI films subjected to ion-beam irradiation consists of both chemical and physical modifications to the films. Hence, PI films are not appropriate for applications in unshielded space environments, since ion-beam degradation of their mechanical properties may engender deformation and rupture, and possibly result in failure.

The electromechanical properties of PMDA-ODA irradiated films were found to be consistent with those of semiconducting strain gauges. The "gauge factor" (GF) of a strain gauge indicates its strain sensitivity, which arises from changes in specific resistivity (or conductivity) of a material due to an applied strain. The PMDA-ODA irradiated films possessed GF values much higher than those of conventional composites and an order of magnitude higher than any previously reported. Thus, these high GF films are suitable as sensitive strain gauges due to their desirable features which include: a high strain sensitivity (for maximum electrical output for a given strain); a low and controllable

temperature coefficient of resistance (for good temperature compensation); a wide operating temperature range (for widest range of applications); and a good fatigue life (for dynamic measurement). Thus, these irradiated films have great potential as strain sensors for civil applications in bridges, roads, buildings and aircraft, and in technological devices used in medical research, submarines, nuclear power plants and space craft, provided they are protected from intense radiation sources.

6.1 References

1. Salvetat, J.-P., Costantini, J.-M., Brisard, F., Zuppiroli, L., *Onset and Growth of Conduction in Polyimide Kapton Induced by Swift Heavy-ion Irradiation*. Physical Review B. 1996. 55: p. 6238.
2. Kim, H.M., Choi, M.S., Joo, J., *Complexity in Charge Transport for Multiwalled Carbon Nanotube and Poly(methyl methacrylate) Composites*. Physical Review B. 2006. 74:p. 54202.